Chapter – VI

RESULTS AND DISCUSSIONS

The detailed discussion on the experimental results for the reduction of methyl parathion (MP), chlorpyrifos (CPF) and carbofuran (CF) from aqueous solution using various treatment technologies is presented in this chapter. The results for coagulation – flocculation, Fenton oxidation, coagulation coupled with Fenton oxidation and toxicity are presented and discussed in separate sections.

6.1 Coagulation – Flocculation

The results obtained on the treatment of pesticide bearing aqueous solution through coagulation-flocculation are presented and discussed below in detail.

6.1.1 Analysis of results of experiments

In this study, experiments have been designed by CCD of RSM. Using Design-Expert software, the polynomial equations on the basis of coded and actual values of the input parameters for the performance are obtained. The ANOVA regression analysis has been carried out to analyse the results with the help of software. Finally, optimization has been performed to find out the optimum value of process inputs for confirmation through experiments.

6.1.2 Data analysis and experimental design

RSM was used to assess the optimum values of the two parameters [X_1: pH] = 4–9 and [X_2: coagulant dose] = 12.3 × 10^{-5} to 74 × 10^{-5} M ($FeCl_3$) and 3 × 10^{-5} to 18 × 10^{-5} M (alum) for maximum removal efficiencies of COD and pesticide concentration. Relationship between these two factors with residual COD and absolute pesticide concentration were evaluated with the help of CCD of RSM.

Depending on these two factors, the CCD design required 13 runs including four tests as factorial points, four tests as axial points, and five repeated tests as center points. Table 6.1 shows the levels of coded and actual values of the controllable variables and Table 6.2 shows the design of experiment.

Table 6.1: Actual and coded values of independent variables used for experimental design.

Variable	**Symbol**	**Real value of coded levels**			
		-1		**0**	**+1**
Initial pH	X_1	4		6.5	9
Coagulant dose (M)	X_2	Alum $\times 10^5$	3	10.5	18
		$FeCl_3$ $\times 10^5$	12.3	43.15	74

Table 6.2: Experimental design matrix and response variables of CPF.

Run	**Experimental design**		**Response variable (% Reduction)**			
	pH (X_1)	**Coagulant dose (X_2) (M)**	**$FeCl_3$**		**Alum**	
			CPF concentration	**COD**	**CPF concentration**	**COD**
1	0.00	0.00	79	75	70	60
2	0.00	-1.41	30	24	26	21
3	-1.41	0.00	44	38	36	30
4	1.00	-1.00	27	19	23	12
5	-1.00	1.00	65	51	52	50
6	-1.00	-1.00	40	25	22	10
8	0.00	0.00	79	75	69.5	59
9	0.00	0.00	78	74	69	58
10	1.00	1.00	40	32	36	27
11	1.41	0.00	52	43	47	34
12	0.00	1.41	68	74	72	54
13	0.00	0.00	77	73	70	60

6.1.3 Analysis of variance for CPF reduction

The coefficients of quadratic model of the CCD Equations (6.1− 6.4) were estimated by ANOVA for CPF simulated wastewater and data are given in Table 6.3. The coefficients of determination (R^2) for CPF reduction were 0.971 and 0.981 with alum and $FeCl_3$, respectively. The predicted responses (Y) were obtained in terms of coded factors as:

$$Y_{COD\ (Alum)}\,(\%) = 59.00 - 12.80\,X_1 + 14.55\,X_2 - 23.50\,X_1^2 - 17.50\,X_2^2 - 10.00\,X_1X_2 \quad (6.1)$$

$$Y_{Conc\ (Alum)}\,(\%) = 69.50 - 15.61\,X_1 + 16.48\,X_2 - 27.87\,X_1^2 - 18.87\,X_2^2 - 7.50\,X_1X_2 \quad (6.2)$$

$$Y_{COD\ (FeCl_3)}\,(\%) = 74.20 - 16.22\,X_1 + 16.33\,X_2 - 29.85\,X_1^2 - 20.85\,X_2^2 - 6.50\,X_1X_2 \quad (6.3)$$

$$Y_{Conc\ (FeCl_3)}\,(\%) = 78.20 - 20.90\,X_1 + 15.15\,X_2 - 28.54\,X_1^2 - 22.54\,X_2^2 - 6.25\,X_1X_2 \quad (6.4)$$

The ANOVA in this case confirms the adequacy of the quadratic model (the Model Prob > F is less than 0.05). The p-values (probability > F) for each model are < 0.05, which show that these are statistically significant (Irani et al., 2015). Table 6.4 shows the ANOVA regression analysis for simulated wastewater. The Model F-values of 18.62 and 21.96 using alum and $FeCl_3$, respectively for CPF reduction implies that the model is significant. The "F-value" implies that the Lack of Fit is significant. The R^2 value was used to evaluate the accuracy of the quadratic model. Figures 6.1 and 6.2 show the comparison of experimental (actual) and predicted values of the responses and help to judge the model suitability. As seen from these plots, good agreements between experimental and predicted values are obtained.

Table 6.3: Coefficient of quadratic model equating using CCD for CPF.

Factors	Coefficient values	
	Alum	**$FeCl_3$**
b_0	69.50	78.20
b_1	-15.6	-20.90
b_2	16.48	15.15
b_{12}	-7.50	-6.25
b_{11}	-27.87	-28.54
b_{22}	-18.87	-22.54
Std. Dev.	11.06	11.15
Mean	40.73	46.77
C.V. %	27.16	23.85

* Std. Dev. stands for "square root of the error mean square".
** C.V. stands for "coefficient of variance".

Table 6.4: ANOVA regression analysis for CPF reduction using $FeCl_3$.

Source	Degree of freedom	Sum of Squares		Mean square		F value		p- value Prob>F	
		Alum	**$FeCl_3$**	**Alum**	**$FeCl_3$**	**Alum**	**$FeCl_3$**	**Alum**	**$FeCl_3$**
Model	5	11396.35	13657.59	2279.72	2731.52	18.62	21.96	0.0006 (significant)	0.0004 (significant)
X_1	1	1950.37	3495.54	1950.37	3495.54	15.93	28.10	0.0052	0.0011
X_2	1	2172.18	1835.17	2172.18	1835.17	17.74	14.75	0.0040	0.0064
X_1X_2	1	225.00	156.25	225.00	156.25	1.84	1.26	0.2173	0.2994
X_1^2	1	5405.33	5665.31	5405.33	5665.31	44.15	45.55	0.0003	0.0003
X_2^2	1	2478.37	3533.49	2478.37	3533.49	20.24	28.41	0.0028	0.0011
Residual	7	856.96	870.72	122.42	124.39	-	-	-	-
Lack of Fit	3	856.98	867.92	285.32	289.31	1141.28	413.29	<0.0001 (significant)	< 0.0001 (significant)
Pure Error	4	1.00	2.80	0.25	0.70	-	-	-	-

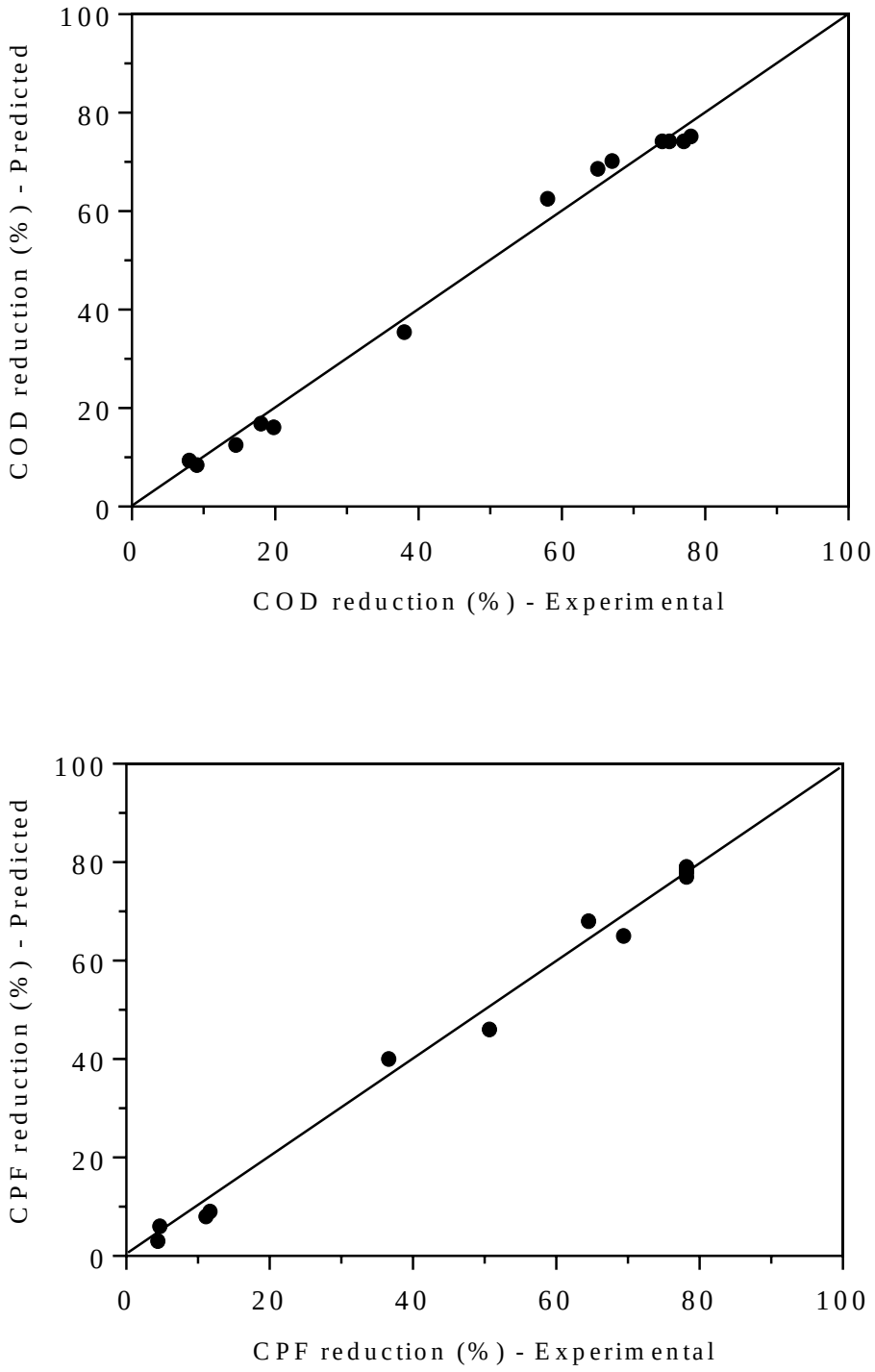

Figure 6.1: Comparison of experimental (actual) and predicted values of the responses using $FeCl_3$ for COD and CPF reduction.

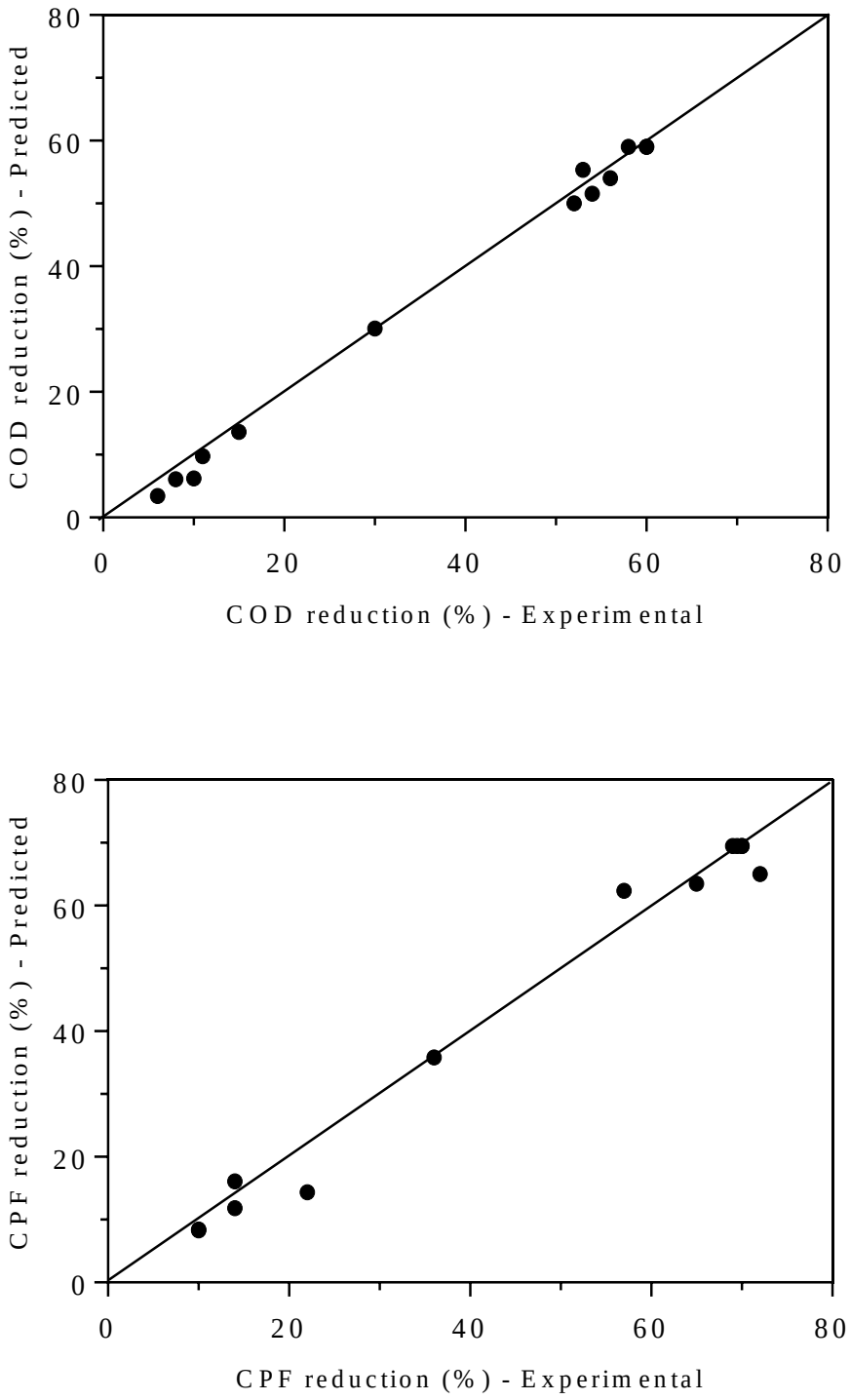

Figure 6.2: Comparison of experimental (actual) and predicted values of the responses using alum for COD and CPF reduction.

6.1.4 Response surface and contour plots

In order to figure out the impact of pH and coagulant dose on the two responses, three dimensional (3D) response surface and the corresponding contour plots are used. Figure 6.3(a) indicates a maximum (67%) COD removed. Likewise, Figure 6.3(b) demonstrates that the optimum reduction of 76% of CPF from wastewater occurred at around pH 3.2 using $FeCl_3$. The COD reduction response surfaces indicate reduction efficiencies of 65% for COD (Figure 6.4 (a)) and 72% for CPF concentration (Figure 6.4 (b)) in simulated wastewater using alum. From these figures it can be concluded that both pH and coagulant dose have positive effect on the reduction efficiency. The process efficiency for the two responses is in the order: pesticide reduction > COD reduction. The three dimensional response surface plots are moderately symmetrical in shape with nearly circular contours. All response surface plots show clear peaks. The peaks in plots indicate that the optimum conditions for maximum values of the responses are attributed in the design range of pH and coagulant dosage. Standard deviation and mean of responses in CPF wastewater were found to be 11.06 and 40.73, respectively using alum and 11.15 and 46.77, respectively using $FeCl_3$.

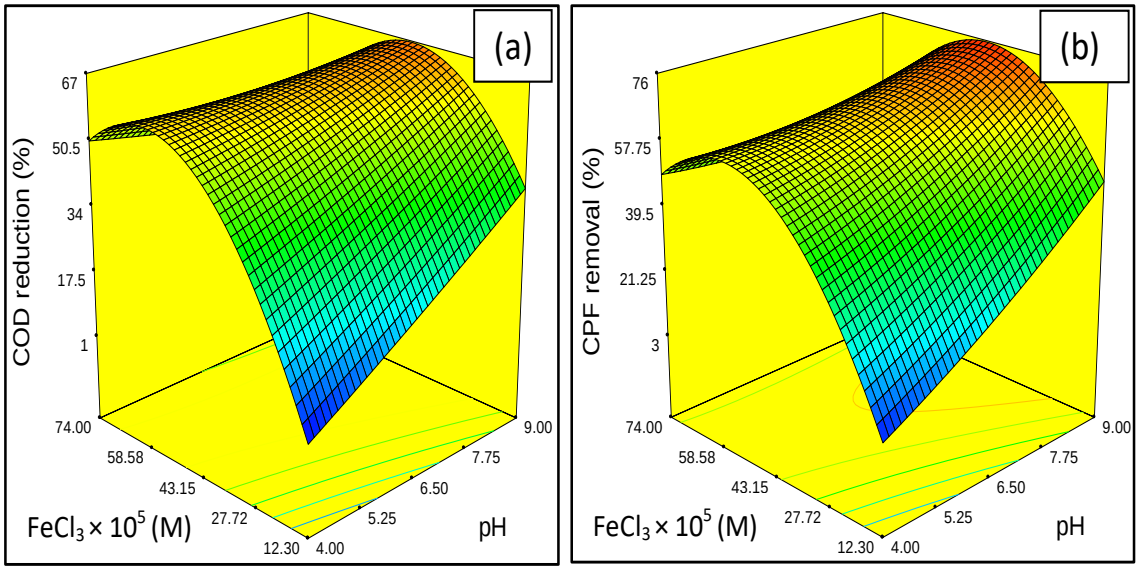

Figure 6.3: Design-expert plot: response surface plot for optimization of (a) COD, (b) CPF removal using $FeCl_3$.

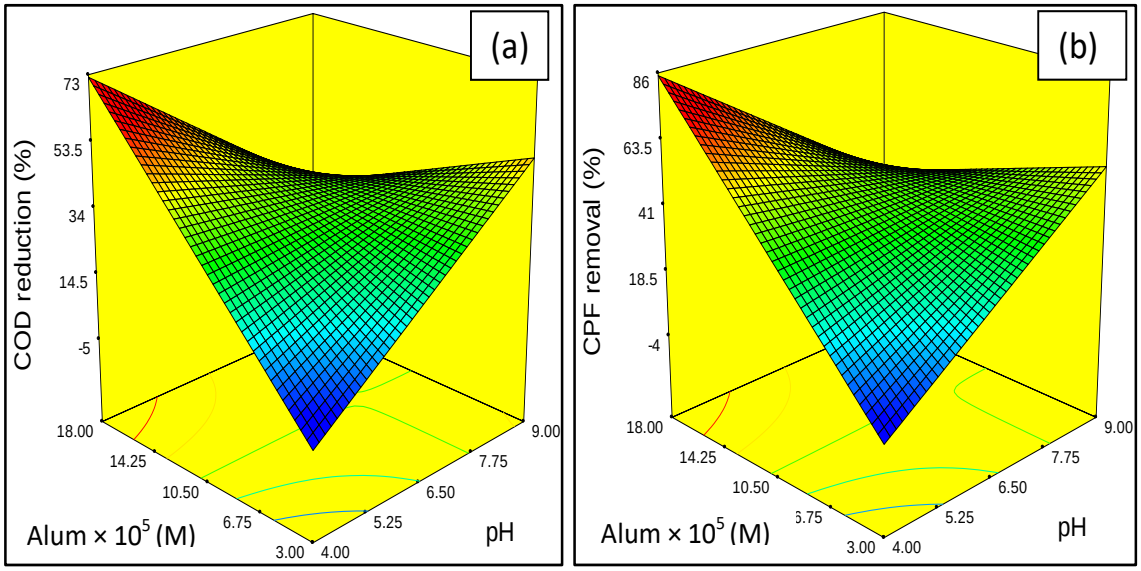

Figure 6.4: Design-expert plot: response surface plot for optimization of (a) COD and (b) CPF removal using alum.

6.1.5 Effect of pH on treatment of MP, CPF and CF

Among several parameters affecting the performance of coagulation, the pH plays a predominant role when coagulants like aluminium salts (alum) and ferric and ferrous salts are added to wastewater. The efficiency of coagulation/flocculation process gets reduced under highly acidic and alkaline pH (Montgomery, 1985). In this study, the

reduction efficiencies were observed to be optimum at pH 5 for $FeCl_3$ whereas it was at pH 6 for alum. The constant concentration of $FeCl_3$ 37.0×10^{-5} M (60 mg/L) and alum 9×10^{-5} M (60 mg/L) were used in the runs. The final pH of the solution was measured after completion of the process and it was observed that the final pH of the solution decreased with $FeCl_3$ and increased with alum concentration.

The initial pH of the MP bearing wastewater was 6.5. At optimum pH, the COD reduction for MP bearing wastewater was 57.81 and 66.23% with alum and $FeCl_3$, respectively and the reduction in MP concentration was 70.03 and 75.82%, respectively. The initial pH of the CPF bearing wastewater was 6.7. At the optimum pH, the CPF reduction was 73.44 and 77.69% with alum and $FeCl_3$, respectively, and COD reduction was 59.19 and 69.1%, respectively. The results are shown in Figures 6.5 and 6.6, respectively. Results show that when the pH of the solution was increased, the reduction efficiency increased up to a maximum value and then decreased further with increase in pH. Fe salts have better removal performance because of higher charge density.

At optimum pH, the CF reduction was 73.13 and 67.19% with $FeCl_3$ and alum, respectively. The corresponding COD reduction was 64.13 and 55.68%, respectively. With $FeCl_3$ and alum dosing, the maximum concentration and COD reductions resulted in the pH range of 5–6. Results also show that percentage reduction decreased with increasing pH (>6) with minimum reduction occurring at pH 8 for both the coagulants tested, as can be seen in Figure 6.7 for CF. Experimental data are presented in Appendix-B (Table B-1 to B-3).

The positively charged hydroxide flocs and negatively charged pesticide molecules get removed because of charge neutralization by the monomeric charges Fe species result in formation of insoluble precipitates in the pH range of 7-9. The surface charge of $Fe(OH)_3$ shifts in a positive direction at pH less than 8.5 (known to be zero point charge

(ZPC) for iron hydroxide) and here the positively charged Fe species will remain in the solution. Rapid amorphous precipitation occurs at pH above 4 (Stumm and Melia, 1968). When solution pH increases to 7 the positive charge of hydrolyzed substances of metal salts decreases, reducing the coagulants capability to neutralize the negative charge of dissolved organic matter, and consequently leading to less removal (Hussain et al., 2014).

Hydrolyzed aluminium and iron species are important for the efficient alum and iron coagulation–flocculation process, because contaminants present in solution are frequently removed via interactions with different hydrolyzed aluminium and iron species (Liu et al., 2009). Once $FeCl_3$ and alum are added into the water, a series of hydrolysis processes take place forming different kinds of hydrolyzed products based on solution pH (Wang et al., 2013). Generally, in weakly acidic conditions aluminium and iron species have less solubility; hence aluminium (Al) and iron (Fe) hydroxide flocs readily form in this region (Duan and Gregory, 2003). The hydroxide flocs may favour MP, CPF and CF removal through coprecipitation into hydroxides forms and adsorption on preformed hydroxide flocs. Consequently, hydrous Al oxide was found to be more soluble in water than hydrous Fe oxide, which produced less flocs during the coagulation-flocculation process (Hu et al., 2015). Such factors might be responsible for better performance of $FeCl_3$ in comparison to alum.

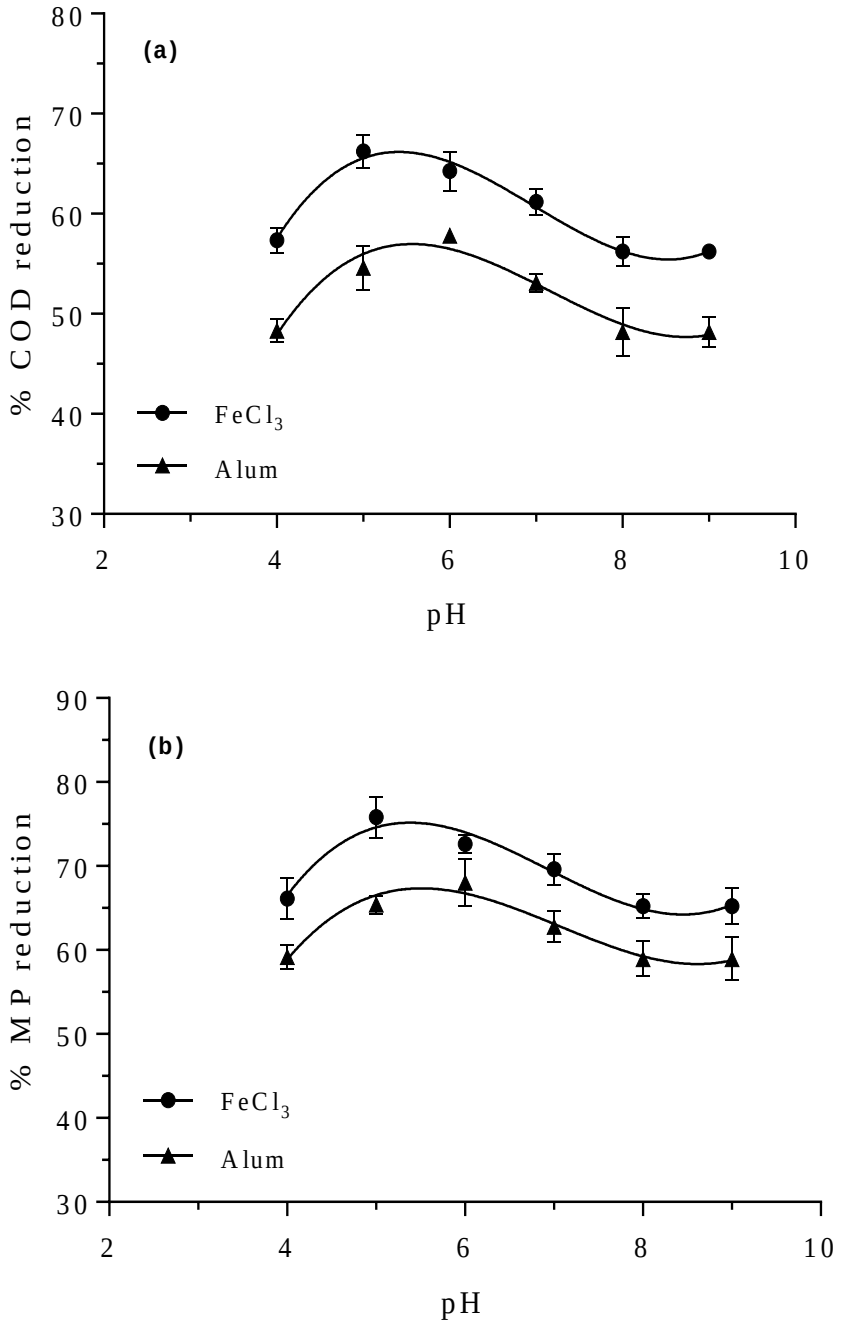

Figure 6.5: Methyl parathion: Effect of pH on reduction efficiency of (a) COD and (b) MP. (MP_0 = 11.4 × 10^{-5} M, COD_0 = 440 mg/L, Temperature = 25 ºC, $FeCl_3$ dose = 37.0 × 10^{-5} M, alum dose = 9 × 10^{-5} M).

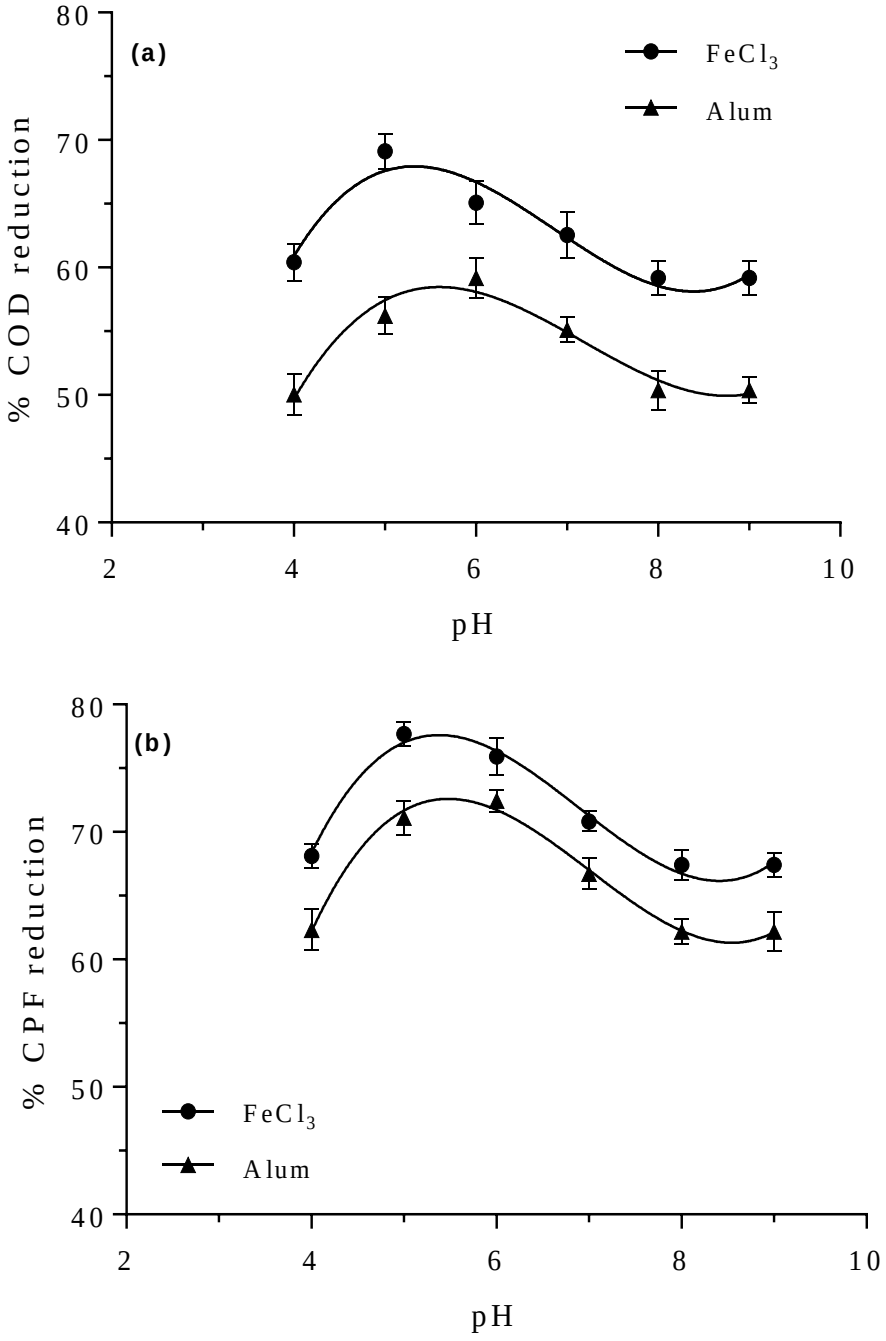

Figure 6.6: Chlorpyrifos: Effect of pH on reduction efficiency of (a) COD and (b) CPF. (CPF_0 = 8.65 ×10^{-5} M, COD_0 = 385 mg/L, Temperature = 25 ºC, $FeCl_3$ dose = 37.0 × 10^{-5} M, alum dose = 9 × 10^{-5} M).

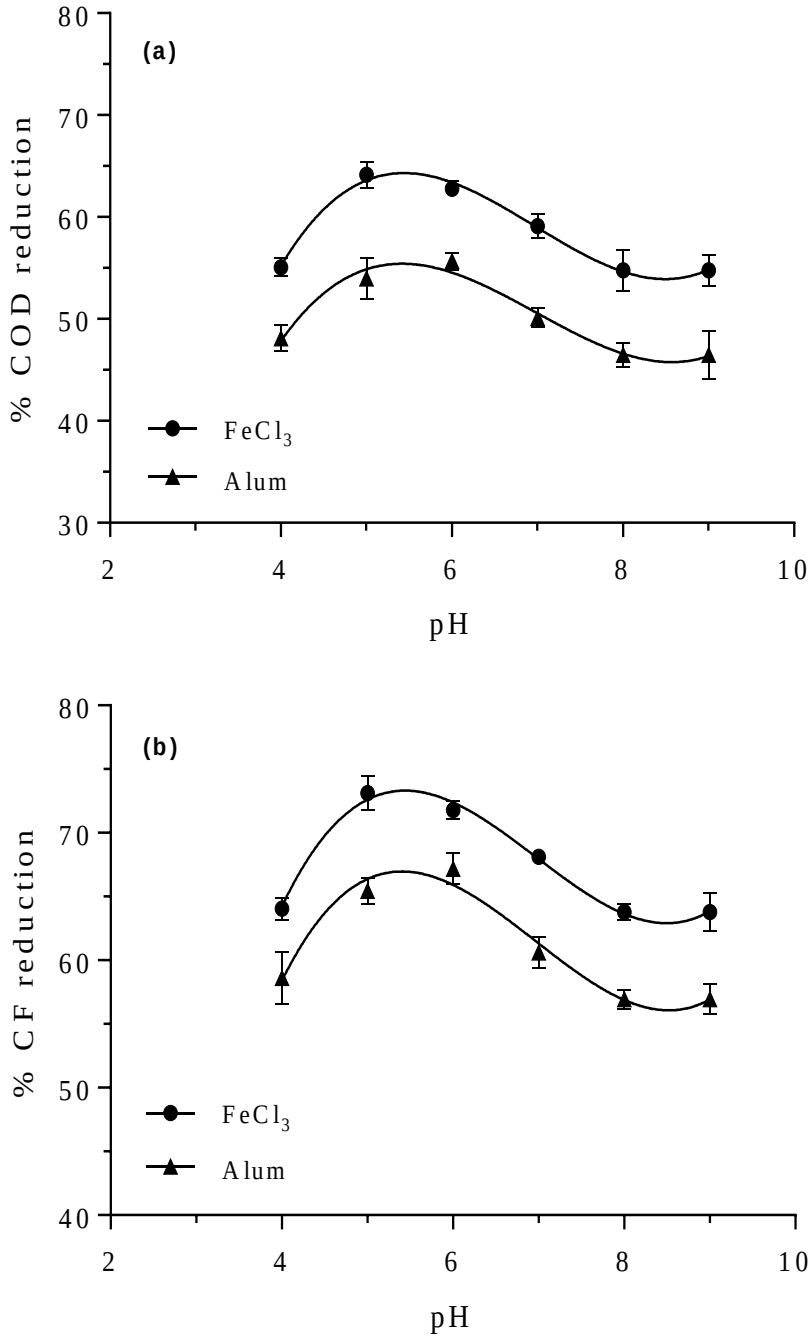

Figure 6.7: Carbofuran: Effect of pH on reduction efficiency of (a) COD and (b) CF. (CF_0 = 13.5 ×10^{-5} M, COD_0 = 510 mg/L, Temperature = 25 ºC, $FeCl_3$ dose = 37.0 × 10^{-5} M, alum dose = 9 × 10^{-5} M).

6.1.6 Effect of coagulant dose on treatment of MP, CPF and CF

The effect of coagulants dose was examined in the range of 12.3×10^{-5} to 74.0×10^{-5} M (20-120 mg/L) for $FeCl_3$ and 3×10^{-5} to 18×10^{-5} M (20-120 mg/L) for alum. The pH was kept constant at 5 for $FeCl_3$ and at 6 for alum (optimum pH values). $FeCl_3$ was found to be the best at 49.3×10^{-5} M dose, whereas the dose of 12×10^{-5} M was best for alum. On increasing the dose of $FeCl_3$ and alum, reduction efficiency increased up to certain point and then declined to a lower value and/or became constant.

The maximum MP reduction was 77.5% with alum and 79% with $FeCl_3$ whereas CPF reduction was 79% with alum and 82% with $FeCl_3$. Corresponding COD reductions were 68.5 and 59%, respectively for MP and 79 and 64%, respectively for CPF. The CF reduction was observed as 75.13% with $FeCl_3$ and 71.86% with alum, respectively. The corresponding COD reductions were observed as 65.98% with $FeCl_3$ and 59.95% with alum. The plots of variation in reduction efficiency with coagulant doses are shown in Figures 6.8, 6.9 and 6.10 for MP, CPF and CF, respectively and corresponding results are listed in Appendix-B (Tables B-4 through B-6).

When alum is added to water, the reaction between alum and water causes hydrolysis of the sulfate with subsequent generation of insoluble Al species and the aluminium hydroxide precipitates out. Following reaction occurs in the aqueous solution:

$$Al_2(SO_4)_3.18H_2O + 6H_2O \Leftrightarrow 2Al(OH)_3 \downarrow + 6H^+ + 3SO_4^{2-} + 18H_2O \qquad (6.5)$$

The reaction mechanism is influenced not only by the wastewater characteristics, but also depends on the Al species and precipitated aluminum hydroxide, which take place quickly after the addition of coagulant (Trinh and Kang, 2011). If the wastewater is not buffered, the resulting H^+ formation causes increase in pH. Similarly, on addition of ferric chloride to water, the reaction between ferric chloride and water causes the

hydrolysis of the ferric chloride with the subsequent generation of insoluble ferric hydroxide, according to the following reaction:

$$FeCl_3 + 3H_2O \Leftrightarrow Fe(OH)_3 \downarrow + 3H^+ + 3Cl^- \quad (6.6)$$

The insoluble aluminium and ferric hydroxide species help to aggregate various particles into larger flocs of precipitate responsible for colloids removal. The behaviour of $FeCl_3$ can be attributed to the presence of hydrolysed species of ferric iron. Amor et al. (2015) used four types of coagulants including $FeCl_3$ for the treatment of landfill leachate and found $FeCl_3$ to be the most efficient. Hu et al. (2015) reported that for removal of monomethylarsenate (MMA) and dimethylarsenate (DMA) from drinking water the coagulant $FeCl_3$ was more efficient than $AlCl_3$ and polyaluminum chloride (PACl). Amorphous solid hydroxide of Fe is less soluble than the amorphous hydrous Al oxide (Hering et al., 1997), which is responsible for greater flocs formation and thus giving higher removal of pesticide. The reported data on solubility product constants of aluminum hydroxide and ferric hydroxide are about 10^{-33} and 10^{-38}, respectively (Duan and Gregory, 2003). Therefore, formation of Fe hydroxide during coagulation results in flocs having large available surface area for absorbing pesticides than Al hydroxide (Kang et al., 2003), thus leading to higher removal of MP, CPF and CF.

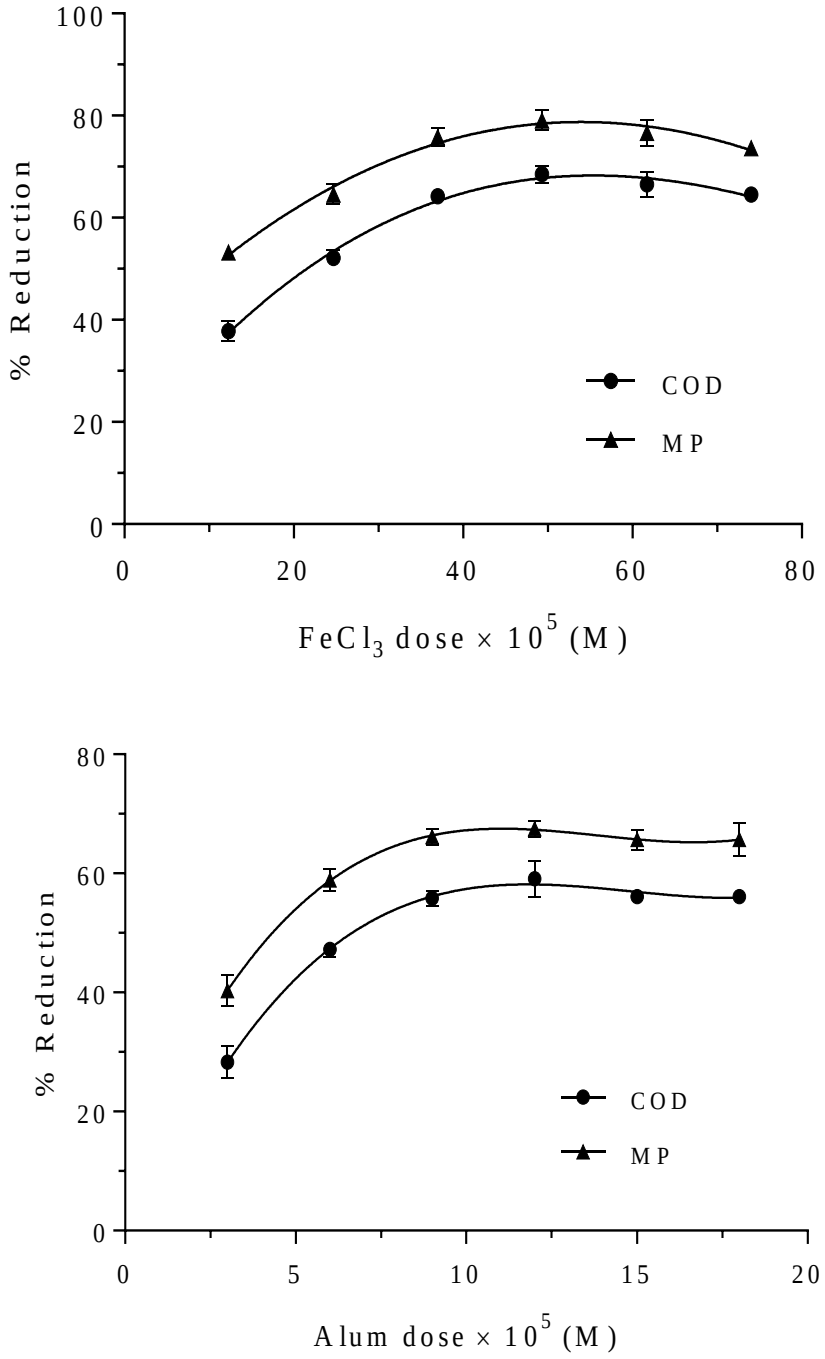

Figure 6.8: Methyl parathion: Effect of coagulant dose on reduction efficiency of COD and MP. ($MP_0 = 11.4 \times 10^{-5}$ M, COD_0 = 440 mg/L, pH = 5 for $FeCl_3$, pH = 6 for alum, Temperature = 25 ºC).

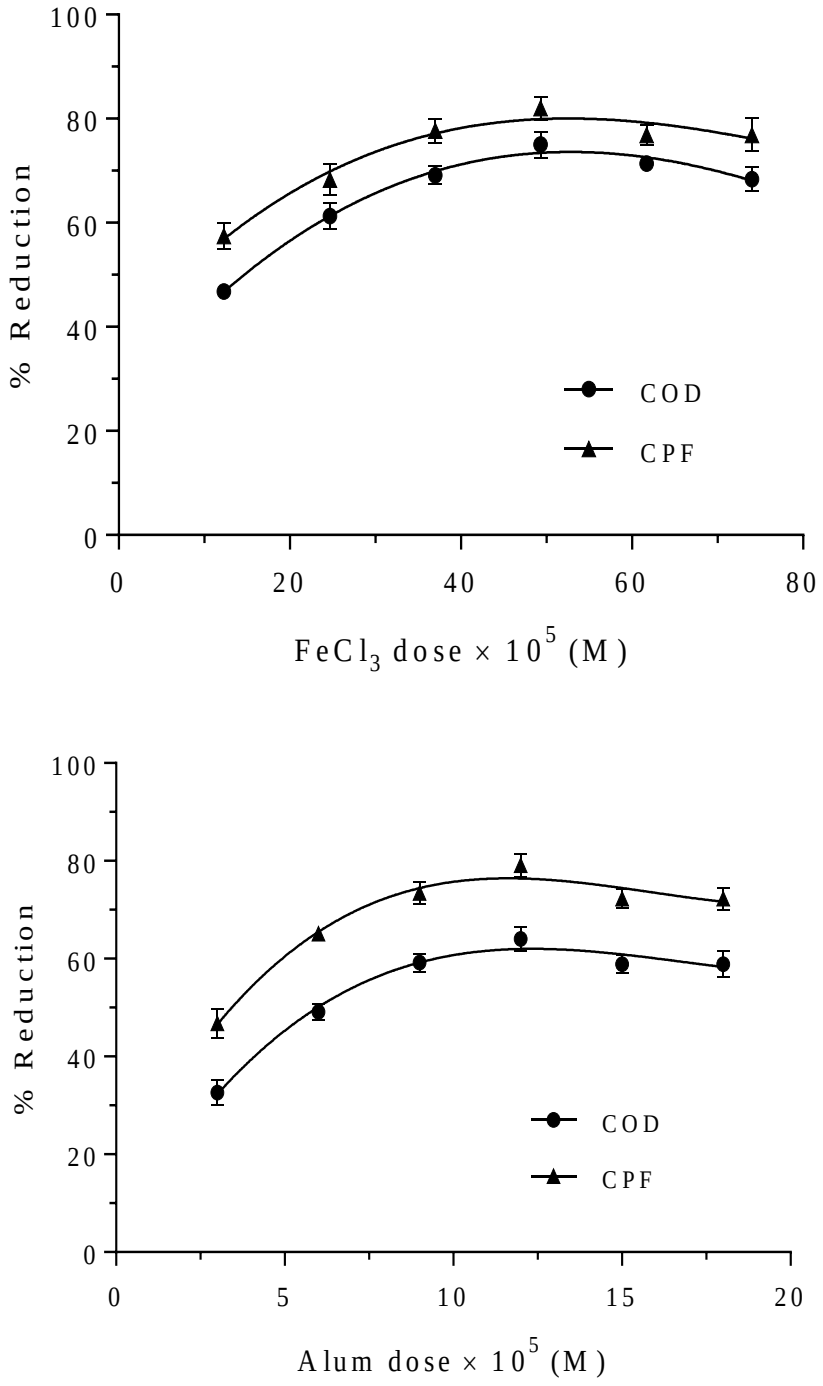

Figure 6.9: Chlorpyrifos: Effect of coagulant dose on reduction efficiency of COD and CPF. (CPF_0 = 8.65 ×10^{-5} M, COD_0 = 385 mg/L, pH = 5 for $FeCl_3$, pH = 6 for alum, Temperature = 25 ºC).

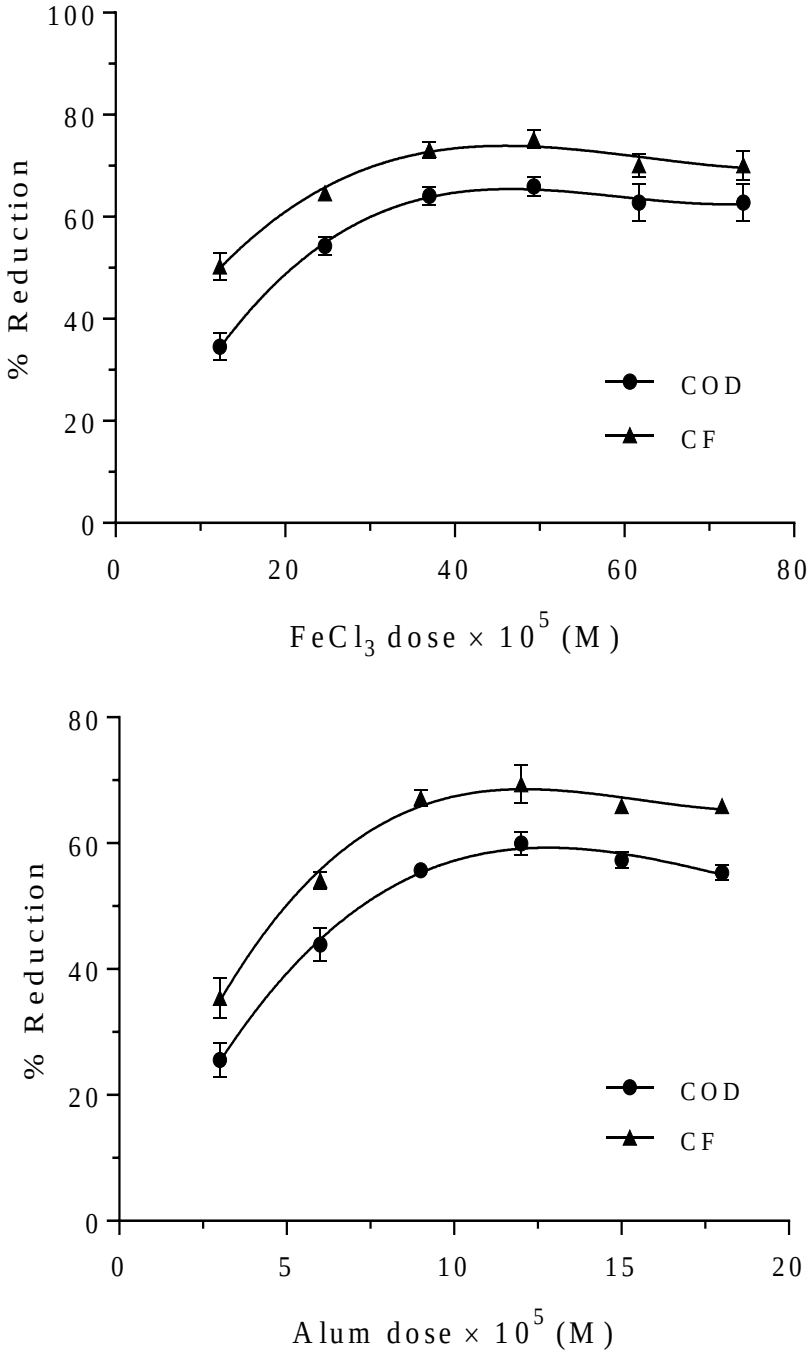

Figure 6.10: Carbofuran: Effect of coagulant dose on reduction efficiency of COD and CF. (CF_0 = 13.5 ×10^{-5} M, COD_0 = 510 mg/L, pH = 5 for $FeCl_3$, pH = 6 for alum, Temperature = 25 ºC).

6.1.7 Effect of operating time and initial pesticide concentration (equilibrium studies)

Equilibrium studies were conducted by adding a fixed dose of alum (12×10^{-5} M) and $FeCl_3$ (49.3×10^{-5} M) into 1000 mL beakers containing 200 mL of MP (3.8×10^{-5} to 19×10^{-5} M) / CPF (2.85×10^{-5} to 14.3×10^{-5} M) / CF (4.52×10^{-5} to 22.6×10^{-5} M) solutions. The pH was kept constant at 5 for $FeCl_3$ whereas 6 for alum. Figures 6.11 through 6.13 show the effect of initial concentration of pesticides. Experimental data showing variation of concentration with time are given in Tables B-7 and B-8 for MP, Tables B-9 and B-10 for CPF and Tables B-11 and B-12 for CF. It can be seen from these figures, that the equilibrium concentration is achieved in 30 min at lower concentration, while it takes 90 min at higher concentration. The experiment, however, was performed up to 120 min to ensure that full equilibrium is attained. Experimental data also show that an increase in initial pesticide concentration leads to decrease in the percentage removal. This indicates that the initial pesticide concentration plays an important role in the coagulation-flocculation. The physical characteristics of samples before and after each run under the most efficient experimental conditions are presented in Table 6.5.

Table 6.5: Characteristics of samples before and after treatment under the optimum experimental conditions.

Parameter	MP			CPF			CF		
	Raw	**Alum**	**$FeCl_3$**	**Raw**	**Alum**	**$FeCl_3$**	**Raw**	**Alum**	**$FeCl_3$**
$pH_{initial}$	6.5	6.0	5.0	6.7	6.5	6.0	6.2	5.8	5.4
pH_{final}	-	7.5	4.9	-	7.7	5.3	-	7.1	5.3
Concentration (M)	11.4×10^{-5}	3.71×10^{-5}	2.38×10^{-5}	8.65×10^{-5}	1.79×10^{-5}	1.54×10^{-5}	13.5×10^{-5}	4.14×10^{-5}	3.34×10^{-5}
COD (mg/L)	440	180	139	385	139	81	510	204	173

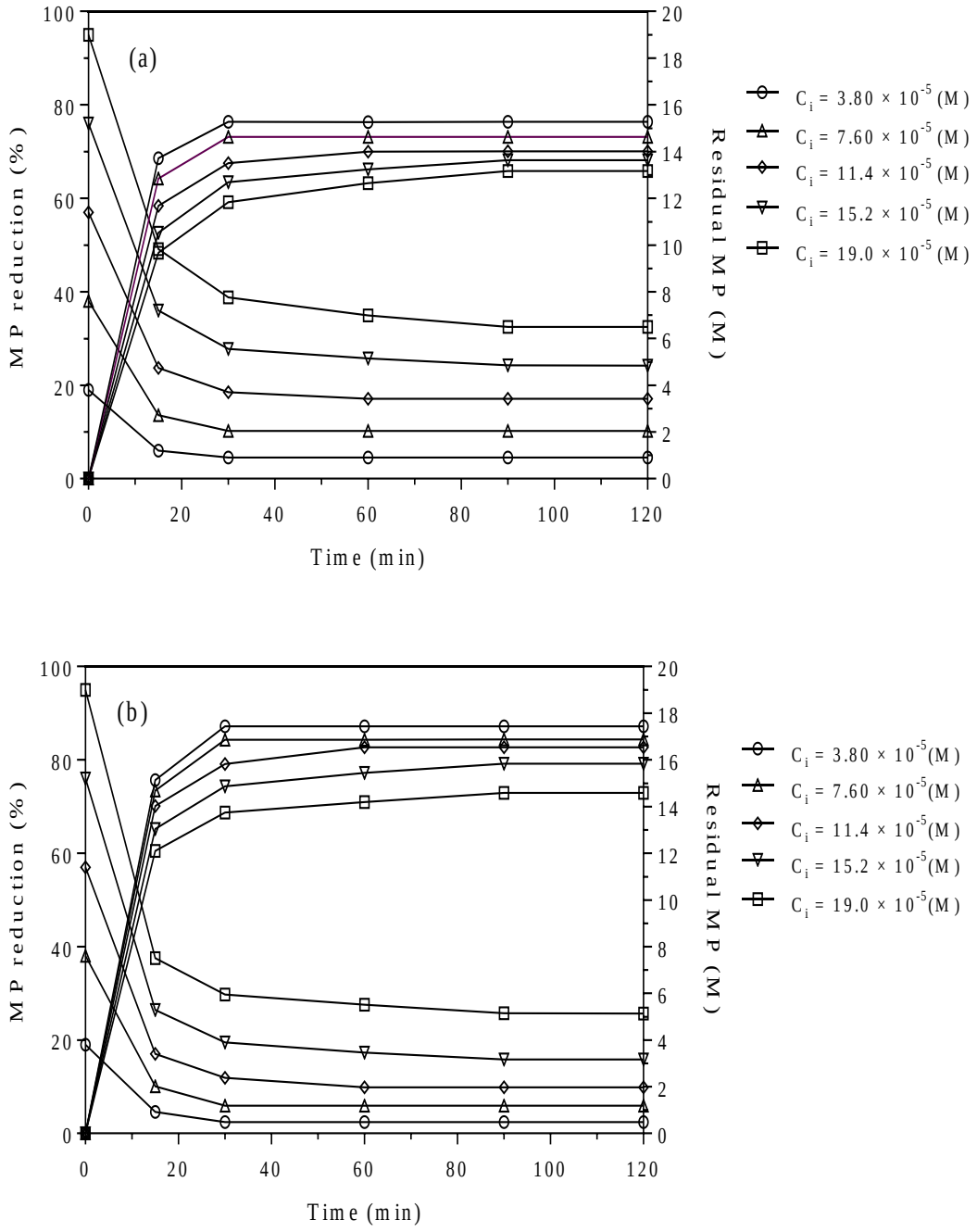

Figure 6.11: Effect of operating time on MP reduction using (a) alum and (b) $FeCl_3$ as coagulant at different initial MP concentrations under optimum conditions.

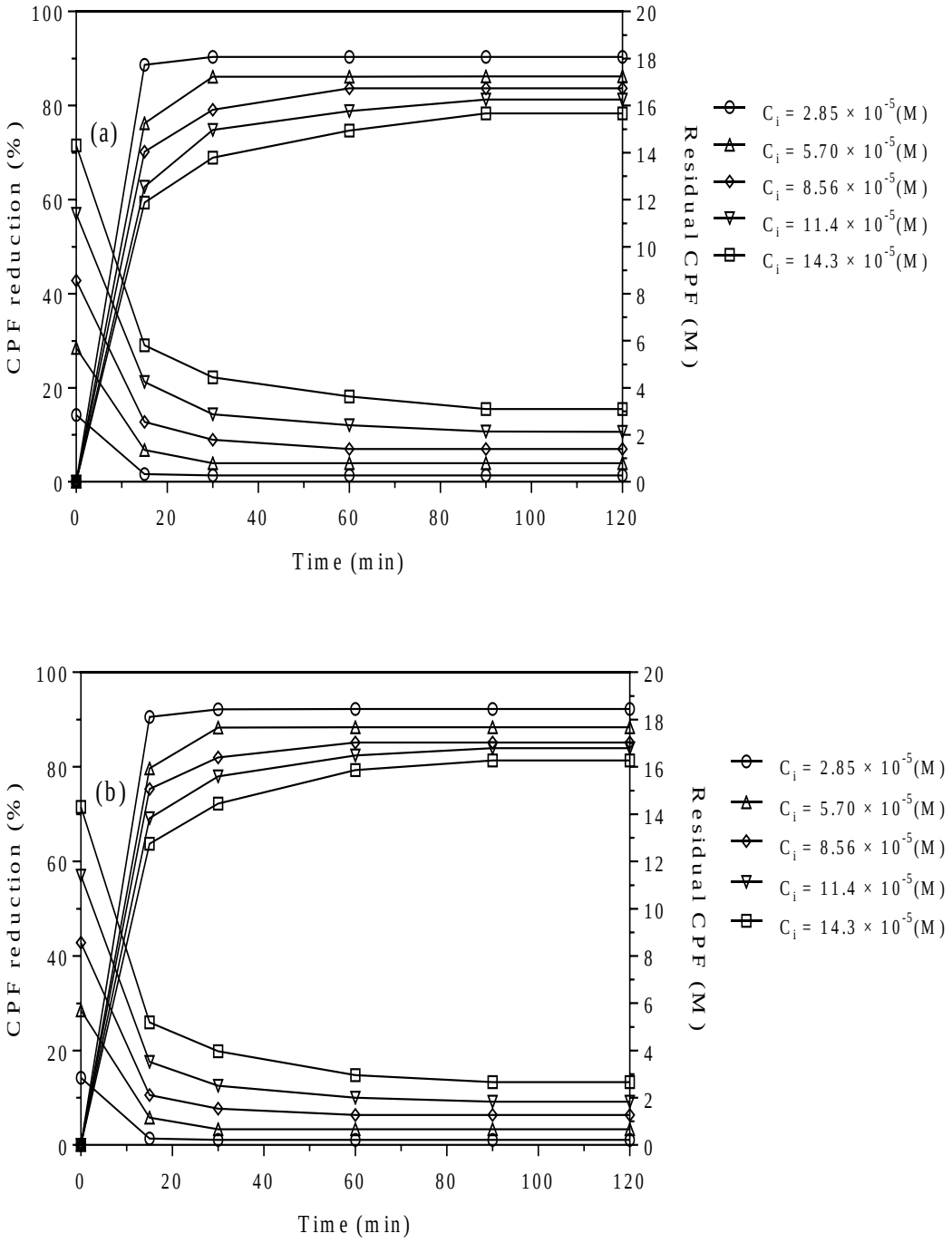

Figure 6.12: Effect of operating time on CPF reduction using (a) alum and (b) $FeCl_3$ as coagulant at different initial CPF concentrations under optimum conditions.

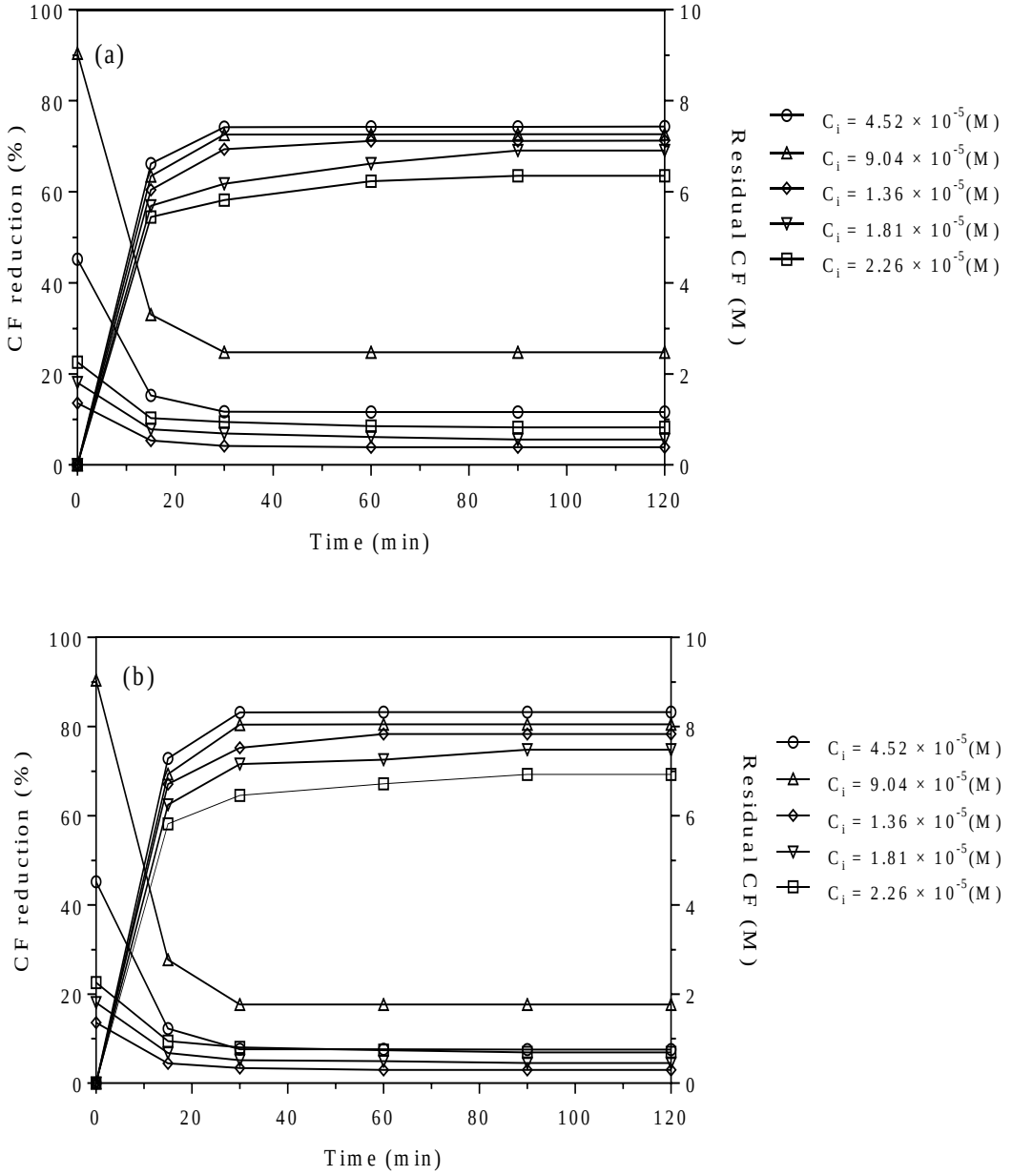

Figure 6.13: Effect of operating time on CF reduction using (a) alum and (b) $FeCl_3$ as coagulant at different initial CF concentrations under optimum conditions.

6.1.8 Adsorption isotherm

During coagulation-flocculation, the metal coagulants (such as alum and ferric chloride) undergo charge neutralization. According to Duan and Gregory (2003) charge neutralization mechanism involves adsorption of monomeric hydrated metal ions and

various hydrolysed species on the surface of colloids. It is generally recognized that hydrolysed cationic species can be adsorbed more strongly on negative charge surfaces than the free hydrated metal ions (Matijevic, 1973).

Adsorption of organic matter onto the flocs generated during coagulation is mostly similar to conventional adsorption process. The adsorption isotherms are useful to evaluate adsorption capacities of adsorbents and its thermodynamic parameters. Two isotherm models were tested to describe the adsorption mechanism using coagulants, namely the Langmuir and the Freundlich isotherms. The Langmuir model (Hussain et al., 2013) is based on the assumption that maximum adsorption corresponds to a saturated monolayer of solute molecules on the adsorbent surface, with no lateral interaction between the sorbed molecules. A basic assumption of Langmuir theory is that sorption takes place at specific homogeneous sites within the adsorbent. It is then assumed that once an adsorbate molecule occupies a site, no further adsorption can take place at that site. Theoretically, therefore a saturation level is reached beyond which no further sorption can take place.

Langmuir isotherm model is given by the Equation (6.7) (Hussain et al., 2013):

$$q_e = \frac{q_{max} K_L C_e}{(1+K_L C_e)} \tag{6.7}$$

The linearized form of Langmuir isotherm Equation (6.7) is expressed as:

$$\frac{C_e}{q_e} = \frac{1}{q_{max} \times K_L} + \frac{C_e}{q_{max}} \tag{6.8}$$

The Freundlich isotherm (multilayer adsorption) is derived by assuming a heterogeneous surface with a non-uniform distribution of heat of adsorption over the surface. The mathematical expression of Freundlich isotherms can be expressed as:

$$q_e = K_F \times C_e^{(\frac{1}{n})} \quad (6.9)$$

The linearized form of Equation (6.9) is represented by the following equation:

$$ln\ q_e = \ln K_F + \frac{1}{n} \ln C_e \quad (6.10)$$

where, C_e is the equilibrium liquid phase concentration (mol/L), q_e (mol/mol) is the amount of pesticide adsorbed per unit of hydroxides of Al (III) and Fe(III) formed, K_L (L/mol) is a Langmuir constant, K_F ((mol/mol)/((mol/L)$^{1/n}$)) is Freundlich constant related to adsorption capacity and n is a dimensionless Freundlich constant.

Both isotherms are plotted in Figures 6.14 and 6.15. Adsorption of pesticides on *in-situ* formed hydroxides of Al(III) and Fe(III) is better fitted with Langmuir isotherm. Maximum adsorption capacities (q_{max}) of MP was 0.644 mole/mole Al and 0.716 mole/mole Fe and in case of CPF it was 0.774 mole/mole Al and 0.806 mole/mole Fe, also for CF it was 0.622 mole/mole Al and 0.679 mole/mole Fe. The Freundlich and Langmuir isotherm data are presented in Table 6.6.

Table 6.6: Adsorption isotherm parameters of flocs formed during coagulation-flocculation.

Coagulant	Pesticides	Langmuir isotherm model			Freundlich isotherm model		
		q_{max} (mole/mole)	K_L (L/mole)	R^2	K_F ((mole/mol)/((mole/L)$^{1/n}$))	n	R^2
Alum	MP	0.644	-4.665	0.9991	1.220	13.53	0.9788
	CPF	0.774	-13.57	0.9991	1.098	17.05	0.9790
	CF	0.622	-2.84	0.9961	1.231	13.89	0.8103
$FeCl_3$	MP	0.716	-5.39	0.9972	1.105	14.14	0.8722
	CPF	0.806	-19.61	0.9994	1.070	16.45	0.9922
	CF	0.679	-3.63	0.9970	1.131	12.82	0.8870

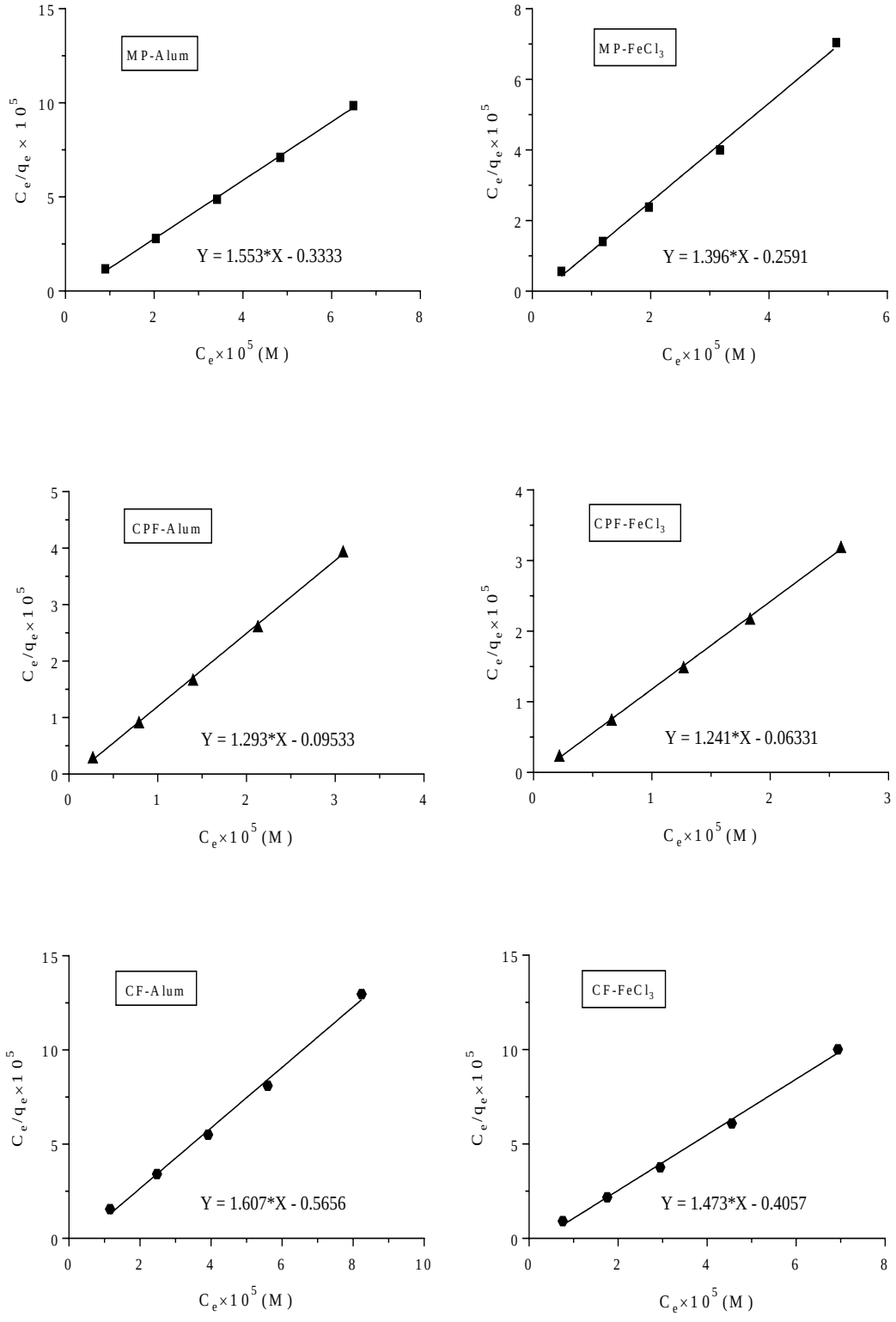

Figure 6.14: Langmuir isotherm plot for adsorption of pesticides onto the surface of flocs generated during coagulation – flocculation using alum and $FeCl_3$ coagulants.

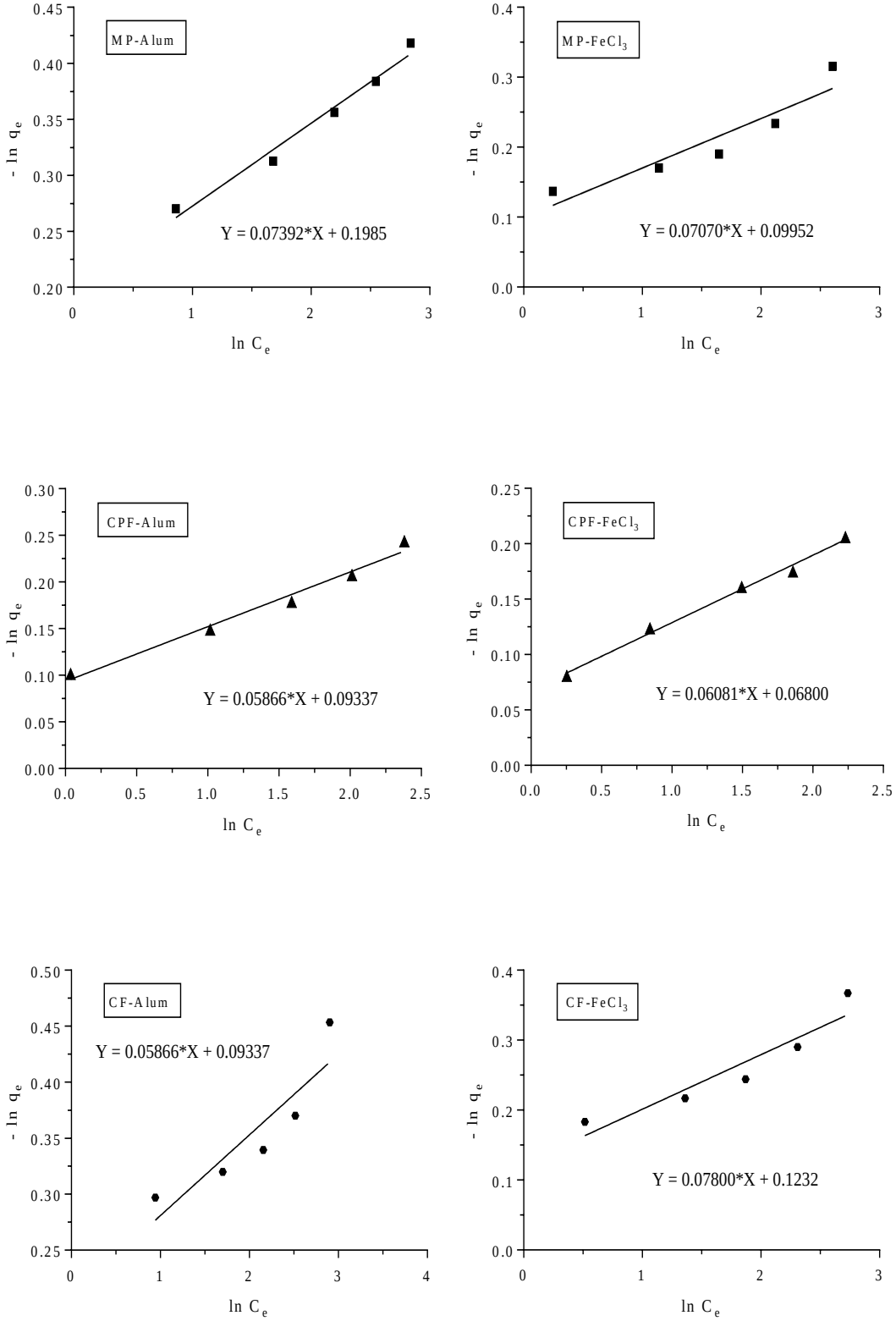

Figure 6.15: Freundlich isotherm plot for adsorption of pesticides onto the surface of flocs generated during coagulation – flocculation using alum and $FeCl_3$ coagulants.

6.1.9 Settling characteristic of the flocs

During conventional coagulation–flocculation treatment, the settling speed of the flocs influences the efficiency and overall cost of the process. In order to estimate this factor, the settling behaviour of the flocs at different time in jar-tests was evaluated. The coagulant addition significantly affects the settling time. At the initial stage, a fast and steady reduction in the height of the flocs-supernatant interface with time was seen for both $FeCl_3$ and alum coagulants. This phenomenon is called the regime of zone settling. Thereafter, the height of the flocs-supernatant interface reduced slowly with time approaching a steady state (transition settling), finally a position called start of the compression settling of slurry is seen. The increase in flocs size the flocs settling speed and hence diminishes the settling time of the flocs generated. The difference in the trends shown by different coagulants might be due to the charge neutralization, sweep flocculation and patch aggregation (Wei et al., 2015).

Various methods have been proposed for calculating the compression zone height in continuous thickeners from batch sedimentation data (Font et al., 1999; Larue and Vorobiev, 2003). The method proposed by Richardson et al. (2003) to design a continuous thickener based on single batch sedimentation test seems to be the most appropriate. The effect of coagulants ($FeCl_3$ and alum) under optimum conditions on the settling characteristics of flocs obtained after treatment by coagulation was conducted using a 250 mL measuring cylinder. Figures 6.16 through 6.18 show the behaviour of treated effluent during sedimentation.

The calculation of sedimentation velocity (u_c), concentration C, and the sedimentation flux were done using the Kynch theory (Richardson et al., 2003). The sedimentation velocity (u_c) was found as the slope of the tangent at a given solids concentration, C. The concentration of sludge at a time t was determined using following relationship:

$$C = C_0 \frac{\text{Total height}}{\text{Height of suspension after time t}} \quad (6.11)$$

The concentration of solids required in the underflow, C_u, for the effluents are presented in Table 6.7 to 6.12.

The maximum value of $[\{(1/C)-(1/C_u)\}/U_c]$ thus determined were used to calculate the area of the sedimentation tank by the following relation:

$$A = v_f C_0 \frac{\left[\left(\frac{1}{C}\right)-\left(\frac{1}{C_u}\right)\right]}{u_c} \quad (6.12)$$

where, v_f is the volumetric flow rate of the effluent (m^3/s) and C_0 is the initial solids concentration (kg/m^3).

From Table 6.7, it can be seen that for C_u = 0.62 kg/m^3 (for MP treatment using $FeCl_3$).

Maximum value $\frac{\frac{1}{C}-\frac{1}{C_u}}{u_c} = 522.581 \times 10^2$,

So, for a feed rate of Q_0 = 10 m^3/min, the area of the tank (A) can be computed by the following formula:

$$A = Q_0 C_0 \left[\frac{\frac{1}{C}-\frac{1}{C_u}}{u_c}\right]_{max} = 696.77 \text{ m}^2 \quad (6.13)$$

Similarly, the maximum value of $\frac{\frac{1}{C}-\frac{1}{C_u}}{u_c}$, and area $A = Q_0 C_0 \left[\frac{\frac{1}{C}-\frac{1}{C_u}}{u_c}\right]_{max}$ can be calculated for different wastewater at different operating conditions.

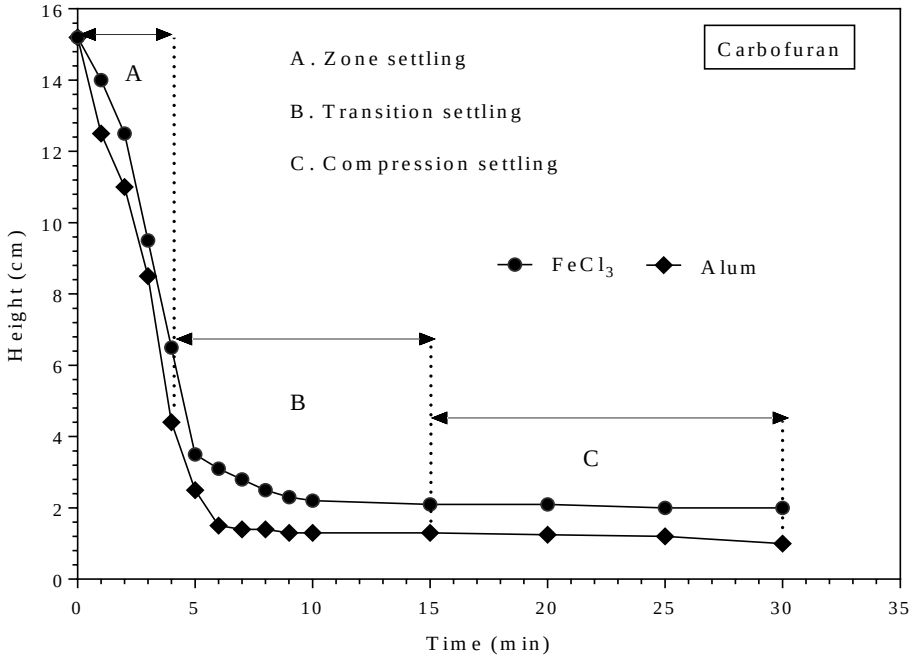

Figure 6.16: Settling curve of flocs formed during coagulation-flocculation process of carbofuran using various coagulants ($FeCl_3$ and alum) under optimum conditions.

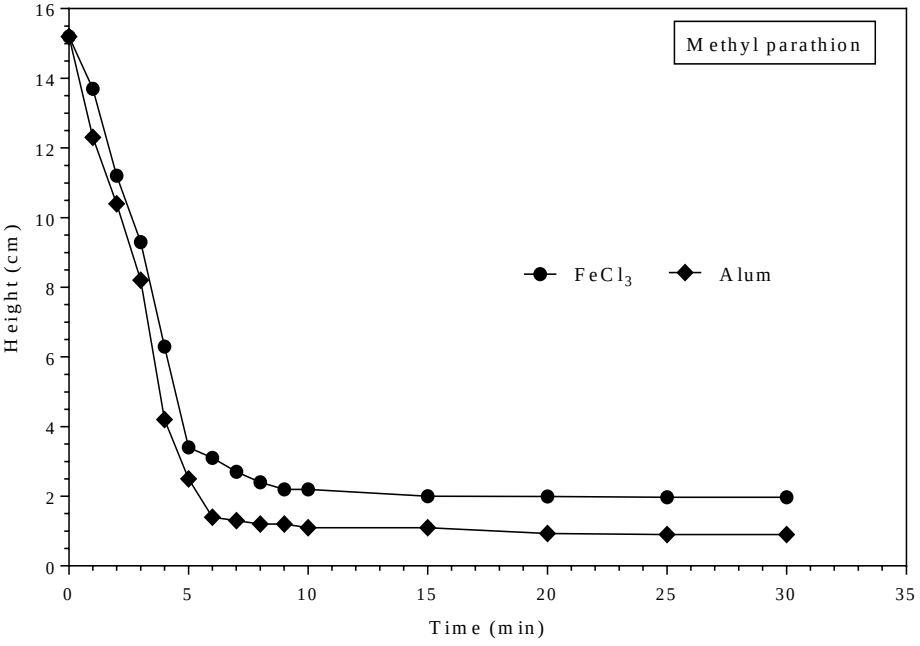

Figure 6.17: Settling curve of flocs formed during coagulation-flocculation process of methyl parathion using various coagulants ($FeCl_3$ and alum) under optimum conditions.

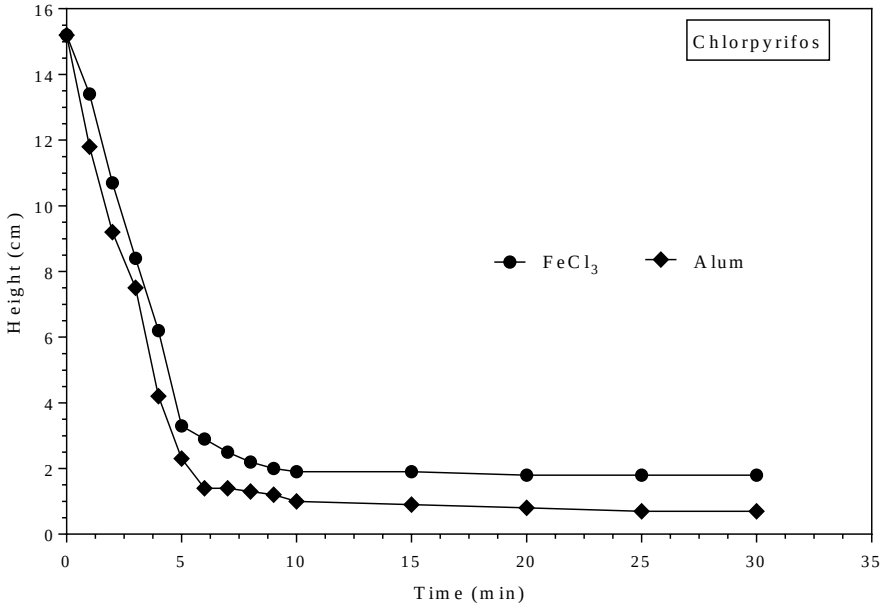

Figure 6.18: Settling curve of flocs formed during coagulation-flocculation process of chlorpyrifos using various coagulants ($FeCl_3$ and alum) under optimum conditions.

Table 6.7: Settling characteristics of MP simulated wastewater after coagulation under optimum conditions using $FeCl_3$. (C_0 = 0.08 kg/m^3, C_u = 0.62 kg/m^3)

S. No.	Time (min)	Height (cm)	u_c (m/s) $\times 10^4$	C (kg/m^3)	Sedimentation flux (kg/m^{2}s) $\times 10^6$	1000 (1/C-1/C_u) (m^3/kg)	u_c/(1/C-1/C_u) $\times 10^6$	(1/C-1/C_u)/u_c $\times 10^{-2}$
1	0	15.2	2.083	0.080	16.67	10887.09	19.14	522.58
2	1	13.7	2.083	0.089	18.49	9653.544	21.58	463.37
3	2	11.2	2.083	0.109	22.62	7597.62	27.42	364.69
4	3	9.3	2.083	0.131	27.24	6035.12	34.52	289.68
5	4	6.3	2.083	0.193	40.21	3568.01	58.390	171.26
6	5	3.4	1.235	0.358	44.17	1183.14	104.38	95.80
7	6	3.1	1.235	0.392	48.44	936.43	131.88	75.82
8	7	2.7	1.235	0.450	55.62	607.49	203.29	49.19
9	8	2.4	1.235	0.507	62.57	360.78	342.31	29.21
10	9	2.2	1.235	0.553	68.26	196.30	629.12	15.89
11	10	2.2	1.235	0.553	68.26	196.30	629.12	15.89
12	15	2	0.212	0.608	12.87	31.83	664.92	15.04
13	20	1.99	0.212	0.611	12.93	23.61	896.515	11.15
14	25	1.97	0.212	0.617	13.07	7.16	2955.18	3.38
15	30	1.97	0.212	0.617	13.07	7.16	2955.18	3.38

Table 6.8: Settling characteristics of MP simulated wastewater after coagulation under optimum conditions using alum. (C_0 = 0.08 kg/m^3, C_u = 1.35 kg/m^3)

S. No.	Time (min)	Height (cm)	u_c (m/s) $\times 10^4$	C (kg/m^3)	Sedimentation flux (kg/m^{2}s) $\times 10^6$	1000 (1/C-1/C_u) (m^3/kg)	u_c/(1/C-1/C_u) $\times 10^6$	(1/C-1/C_u)/u_c $\times 10^{-2}$
1	0	15.2	2.783	0.080	22.27	11759.25	23.67	422.48
2	1	12.3	2.783	0.099	27.52	9374.39	29.69	336.80
3	2	10.4	2.783	0.117	32.54	7811.89	35.63	280.66
4	3	8.2	2.783	0.148	41.27	6002.68	46.37	215.66
5	4	4.2	2.217	0.290	64.18	2713.20	81.70	122.40
6	5	2.5	2.217	0.486	107.82	1315.18	168.54	59.33
7	6	1.4	0.122	0.869	10.57	410.57	29.63	337.45
8	7	1.3	0.122	0.935	11.38	328.33	37.06	269.86
9	8	1.2	0.122	1.013	12.33	246.10	49.44	202.27
10	9	1.2	0.122	1.013	12.33	246.10	49.44	202.27
11	10	1.1	0.122	1.105	13.45	163.86	74.25	134.68
12	15	1.1	0.122	1.105	13.45	163.86	74.25	134.68
13	20	0.93	0.122	1.308	15.91	24.06	050564	19.77
14	25	0.9	0.122	1.351	16.44	-	-	-
15	30	0.9	0.122	1.351	16.44	-	-	-

Table 6.9: Settling characteristics of CPF simulated wastewater after coagulation under optimum conditions using $FeCl_3$. (C_0 = 0.08 kg/m^3, C_u = 0.68 kg/m^3)

S. No.	Time (min)	Height (cm)	u_c (m/s) $\times 10^4$	C (kg/m^3)	Sedimentation flux (kg/m^{2}s) $\times 10^6$	1000 (1/C-1/C_u) (m^3/kg)	u_c/(1/C-1/C_u) $\times 10^6$	(1/C-1/C_u)/u_c $\times 10^{-2}$
1	0	15.2	2.017	0.080	16.13	11029.41	18.28	546.92
2	1	13.4	2.017	0.091	18.30	9549.14	21.12	473.51
3	2	10.7	2.017	0.114	22.92	7328.75	27.52	363.40
4	3	8.4	2.017	0.145	29.19	5437.30	37.08	269.61
5	4	6.2	2.017	0.196	39.55	3628.09	55.58	179.90
6	5	3.3	1.383	0.368	50.97	1243.22	111.27	89.87
7	6	2.9	1.383	0.419	58.00	914.28	151.30	66.09
8	7	2.5	1.383	0.486	67.29	585.33	236.33	42.31
9	8	2.2	1.383	0.553	76.46	338.62	408.52	24.47
10	9	2	1.383	0.608	84.11	174.14	794.34	12.58
11	10	1.9	1.383	0.640	88.53	91.91	1505.06	6.64
12	15	1.9	0.22	0.640	14.08	91.91	239.36	4.177
13	20	1.8	0.22	0.676	14.86	9.67	2273.92	4.39
14	25	1.8	0.22	0.676	14.86	9.67	2273.92	4.39
15	30	1.8	0.22	0.676	14.86	9.67	2273.92	4.39

Table 6.10: Settling characteristics of CPF simulated wastewater after coagulation under optimum conditions using alum. (C_0 = 0.08 kg/m^3, C_u = 1.75 kg/m^3)

S. No.	Time (min)	Height (cm)	u_c (m/s) $\times 10^4$	C (kg/m^3)	Sedimentation flux (kg/m^{2}s) $\times 10^6$	1000 (1/C-1/C_u) (m^3/kg)	u_c/(1/C-1/C_u) $\times 10^6$	(1/C-1/C_u)/u_c $\times 10^{-2}$
1	0	15.2	2.85	0.080	22.80	11928.57	23.89	418.54
2	1	11.8	2.85	0.103	29.37	9132.51	31.21	320.43
3	2	9.2	2.85	0.132	37.67	6994.36	40.75	245.41
4	3	7.5	2.85	0.162	46.21	5596.33	50.93	196.36
5	4	4.2	2.267	0.290	65.63	2882.51	78.63	127.16
6	5	2.3	2.267	0.529	119.84	1320.01	171.71	58.23
7	6	1.4	0.115	0.869	9.99	579.88	19.83	504.24
8	7	1.4	0.115	0.869	9.99	579.88	19.83	504.24
9	8	1.3	0.115	0.935	10.76	497.65	23.11	432.73
10	9	1.2	0.115	1.013	11.65	415.41	27.68	361.22
11	10	1	0.115	1.216	13.98	250.93	45.83	218.20
12	15	0.9	0.115	1.351	15.54	168.70	68.17	146.69
13	20	0.8	0.115	1.520	17.48	86.46	133.00	75.18
14	25	0.7	0.115	1.737	19.98	4.22	2719.11	3.67
15	30	0.7	0.115	1.737	19.98	4.22	2719.11	3.67

Table 6.11: Settling characteristics of CF simulated wastewater after coagulation under optimum conditions using $FeCl_3$. (C_0 = 0.08 kg/m^3, C_u = 0.60 kg/m^3)

S. No.	Time (min)	Height (cm)	u_c (m/s) $\times 10^4$	C (kg/m^3)	Sedimentation flux (kg/m^{2}s) $\times 10^6$	1000 (1/C-1/C_u) (m^3/kg)	u_c/(1/C-1/C_u) $\times 10^6$	(1/C-1/C_u)/u_c $\times 10^{-2}$
1	0	15.2	1.90	0.080	15.20	10833.33	17.53	570.17
2	1	14	1.90	0.087	16.50	9846.49	19.29	518.23
3	2	12.5	1.90	0.097	18.48	8612.93	22.05	453.31
4	3	9.5	1.90	0.128	24.32	6145.83	30.91	323.46
5	4	6.5	1.90	0.187	35.54	3678.72	51.64	193.61
6	5	3.5	1.90	0.347	66.01	1211.62	156.81	63.76
7	6	3.1	1.083	0.392	42.49	882.67	122.73	81.47
8	7	2.8	1.083	0.434	47.05	635.96	170.35	58.70
9	8	2.5	1.083	0.486	52.69	389.25	278.31	35.93
10	9	2.3	1.083	0.529	57.28	224.78	481.95	20.74
11	10	2.2	1.083	0.553	59.88	142.54	760.00	13.15
12	15	2.1	1.083	0.579	6273	60.30	1796.36	5.56
13	20	2.1	1.083	0.579	62.73	60.30	1796.36	5.56
14	25	2	1.083	0.608	65.87	-	-	-
15	30	2	1.083	0.608	65.87	-	-	-

Table 6.12: Settling characteristics of CF simulated wastewater after coagulation under optimum conditions using alum. (C_0 = 0.08 kg/m^3, C_u = 1.22 kg/m^3)

S. No.	Time (min)	Height (cm)	u_c (m/s) $\times 10^4$	C (kg/m^3)	Sedimentation flux (kg/m^{2}s) $\times 10^6$	1000 (1/C-1/C_u) (m^3/kg)	u_c/(1/C-1/C_u) $\times 10^6$	(1/C-1/C_u)/u_c $\times 10^{-2}$
1	0	15.2	1.85	0.080	14.80	11680.32	15.84	631.36
2	1	12.5	1.85	0.097	18.00	9459.93	19.56	511.34
3	2	11	1.85	0.111	20.45	8226.38	22.49	444.66
4	3	8.5	1.85	0.143	26.47	6170.45	29.98	333.53
5	4	4.4	1.85	0.276	51.13	2798.74	66.10	151.28
6	5	2.5	1.85	0.486	89.98	1236.24	149.65	66.82
7	6	1.5	0.6	0.811	51.34	413.88	153.02	65.34
8	7	1.4	0.6	0.869	55.01	331.64	190.97	52.36
9	8	1.4	0.6	0.869	55.01	331.64	190.97	52.36
10	9	1.3	0.6	0.935	59.24	249.40	253.94	39.38
11	10	1.3	0.6	0.935	59.24	249.40	25394	39.38
12	15	1.3	0.6	0.935	59.24	249.40	253.94	39.38
13	20	1.25	0.6	0.973	6161	208.28	304.07	32.88
14	25	1.2	0.6	1.013	64.18	167.16	378.86	26.39
15	30	1	0.6	1.216	77.01	2.69	2349.07	0.42

6.1.10 FTIR spectroscopic analysis of sludge

FTIR analysis of $FeCl_3$ and alum sludge was carried out after coagulation process. Figures 6.19 through 6.24 show the plots between absorbance and wavenumbers (cm^{-1}). The overall inspection of the infrared spectra confirms the adsorption of MP, CPF and CF in the sludge formed after coagulation.

FTIR spectra of $FeCl_3$ sludge obtained after treatment of MP bearing wastewater is shown in Figure 6.19. Peaks at 3648.7 and 3600.6 cm^{-1} are due to −OH group of water. This is further supported by the presence of a band in the region 3508.7 to 3209.4 cm^{-1} due to −OH group of polymer. Band in the range 3148.3 to 1679.5 cm^{-1} suggests the presence of −C−H group. The sharp peaks at 1559.2 and 899.9 cm^{-1} corresponding to

strong and medium intensity, respectively, confirm the presence of NO_2 functional group. Adsorption of MP on sludge is confirmed due to the presence of P═O functional group at 1049.3 and 899.9 cm^{-1}. Peak in the region 800.8 − 674.3 cm^{-1} indicates the presence of aromatic ring (Silverstein et al., 2005).

The FTIR spectra of alum sludge after treatment of MP solution are depicted in Figure 6.20. Peak in the region 3406.0 to 3442.6 cm^{-1} shows −OH stretching in the sample. O−H bands start to appear at lower frequencies, 3550 − 3200 cm^{-1}. NO_2 group caused symmetrical absorption in the 1661 − 1499 cm^{-1} region. Peak at 1568.7 and 1523.3 cm^{-1}, represents strong NO_2 group in the sample. Phosphorus compounds have absorbed in the 870 − 1299 cm^{-1} region. Peak at 900.6 and 1056.9 cm^{-1} shows the presence of phosphorus compound in the sample. Formation of P ═ O in sludge at peak 1145.7 cm^{-1} confirms the adsorption of MP. Band at the region 781.1 to 709.9 cm^{-1} confirms the presence of aromatic ring.

Figure 6.21 shows FTIR spectra of $FeCl_3$ sludge obtained after treatment of CPF wastewater. Peak in the region 3675 and 3636.0 cm^{-1} suggests the presence of water or −OH group. Strong band at 1897.4 cm^{-1} depicts carbonyl stretching (−C═O). Band at 3497.1 and 3439.9 cm^{-1} shows the characteristics of −C═C in aromatic ring. A band at 3497.1 and 3439.9 cm^{-1} is ascribed to the vibrations of −NH. Sharp peak at 1197.2 cm^{-1} exists due to the P═O functional group and proof the adsorption of CPF on $FeCl_3$ sludge. The absorption band at around 748.6 and 711.8 cm^{-1} confirms the presence of aromatic ring. Band in the region 657.4 and 578.1cm^{-1} represents the −C−Cl group.

Figure 6.22 shows FTIR spectra of alum sludge obtained after treatment of CPF wastewater. Strong vibration peaks in the region 3603.9 − 3286.2 cm^{-1} are attributed to the vibrations of −OH or –NH functional groups. The 3126.6 and 2976.1 cm^{-1} and shows the presence of C−H asymmetric stretching vibration. The peaks at 1679.4 and

1253.4 cm^{-1} are due to the presence of −C═O and C−N− stretching, respectively. Band in the region 859.6 to 717.6 cm^{-1} reveals the aromatic ring. The peak occuring in the region of 643.5 − 517.7 cm^{-1} indicates the presence of −C−Cl or $-CH_2Cl$ functional group.

Figure 6.23 shows FTIR spectra of $FeCl_3$ sludge obtained after treatment of CF wastewater. A band between 3679.8 and 3745.2 cm^{-1} indicates the presence of water or −OH group. The peak in the region 3522.6 to 3437.1 cm^{-1} reveals the presence of –NH stretching. The weak band at 3003.0 cm^{-1} assigned to the −C−H stretching mode, represents the alphabetic nature of the sludge. A sharp peak at 2738.0 cm^{-1} confirms the presence of −CHO functional group. The band in the region 1962.9 to 1682.9 cm^{-1} reveals the −C═O stretching in carboxylic group. Sharp peak at 1473.7 cm^{-1} shows the −N═O stretching vibration and adsorption of CF on $FeCl_3$ sludge Presence of aromatic ring is indicated by the peaks in the region 886.2 − 714.9 cm^{-1}.

Figure 6.24 shows FTIR spectra of alum sludge obtained after treatment of CF bearing wastewater. The O−H bending vibration occurs in the region 3761.7 to 3300 cm^{-1}. Band in the region 3102.4 − 2821.4 cm^{-1} reveals the C−H stretching vibration. Nitroaromatic compounds show a −N═O stretching vibration at 1464.1 and 1299.1 cm^{-1}. All these confirm the adsorption of CF on alum sludge.

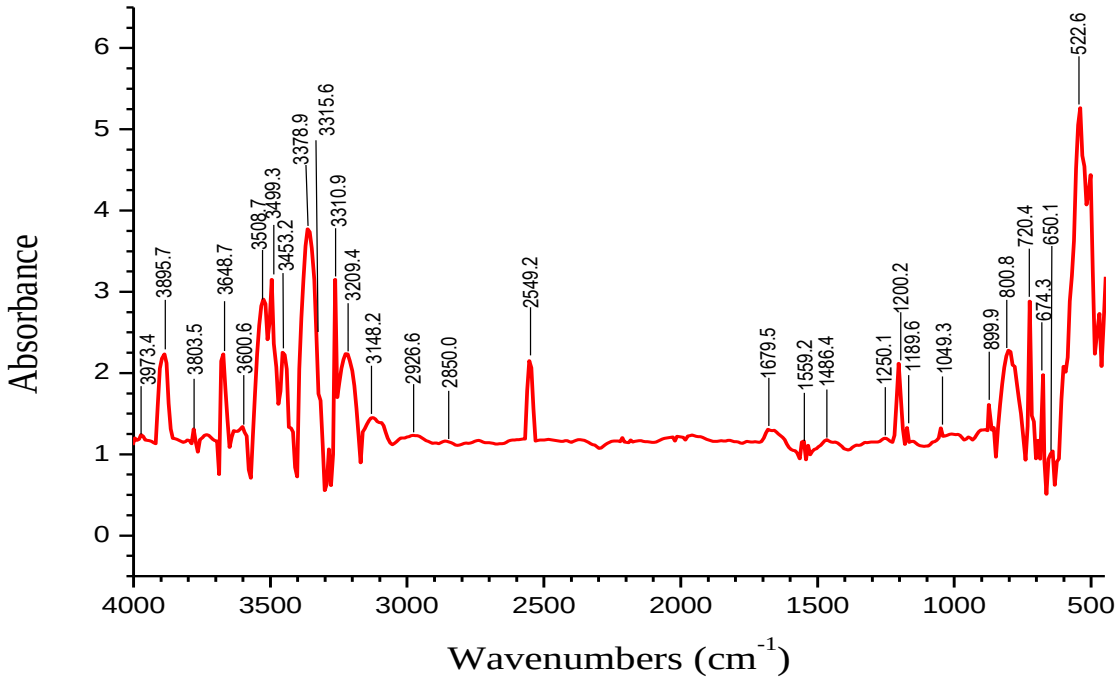

Figure 6.19: FTIR spectra of sludge formed by coagulation process after treatment of MP solution using $FeCl_3$ coagulant.

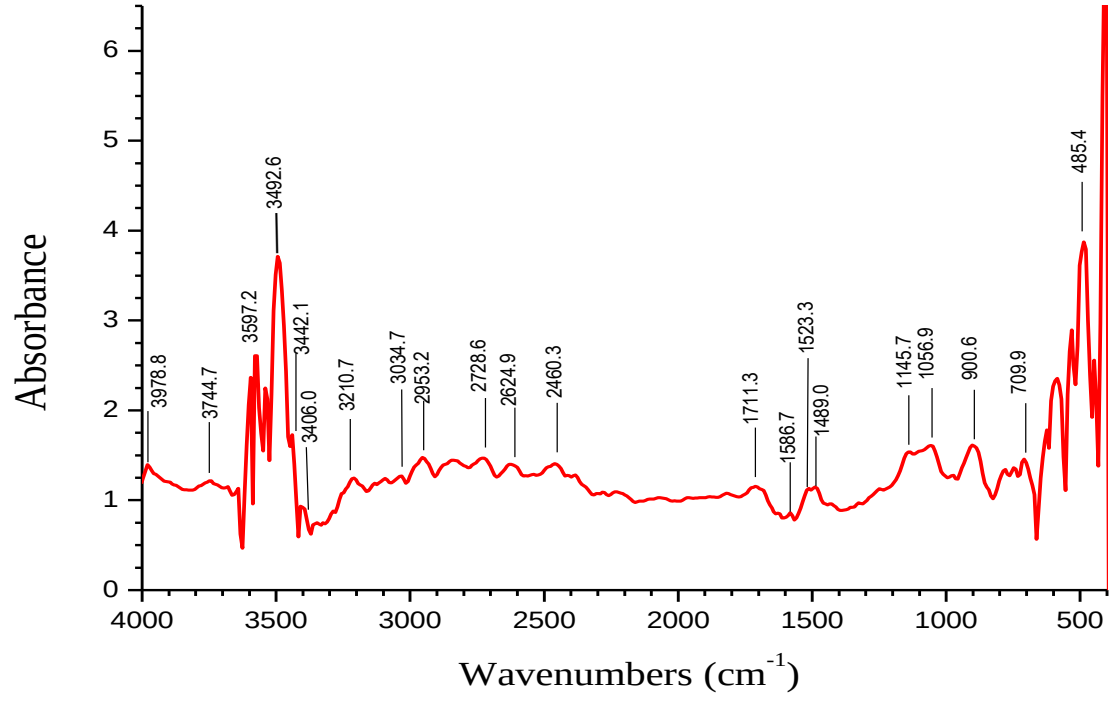

Figure 6.20: FTIR spectra of sludge formed by coagulation process after treatment of MP solution using alum coagulant.

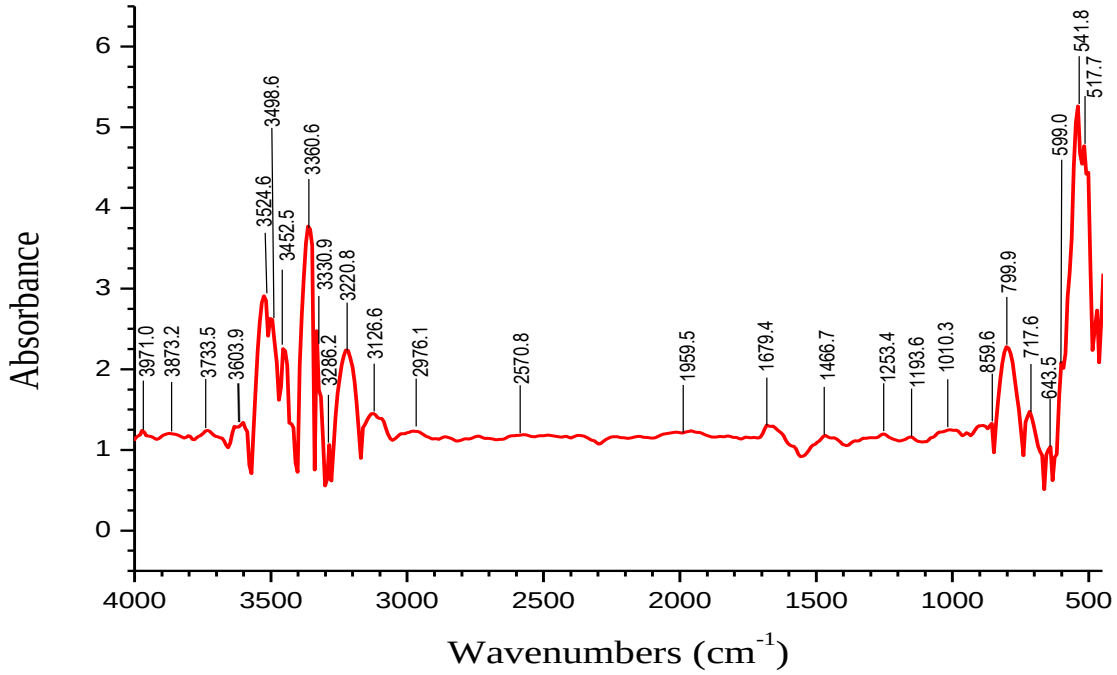

Figure 6.21: FTIR spectra of sludge formed by coagulation process after treatment of CPF solution using $FeCl_3$ coagulant.

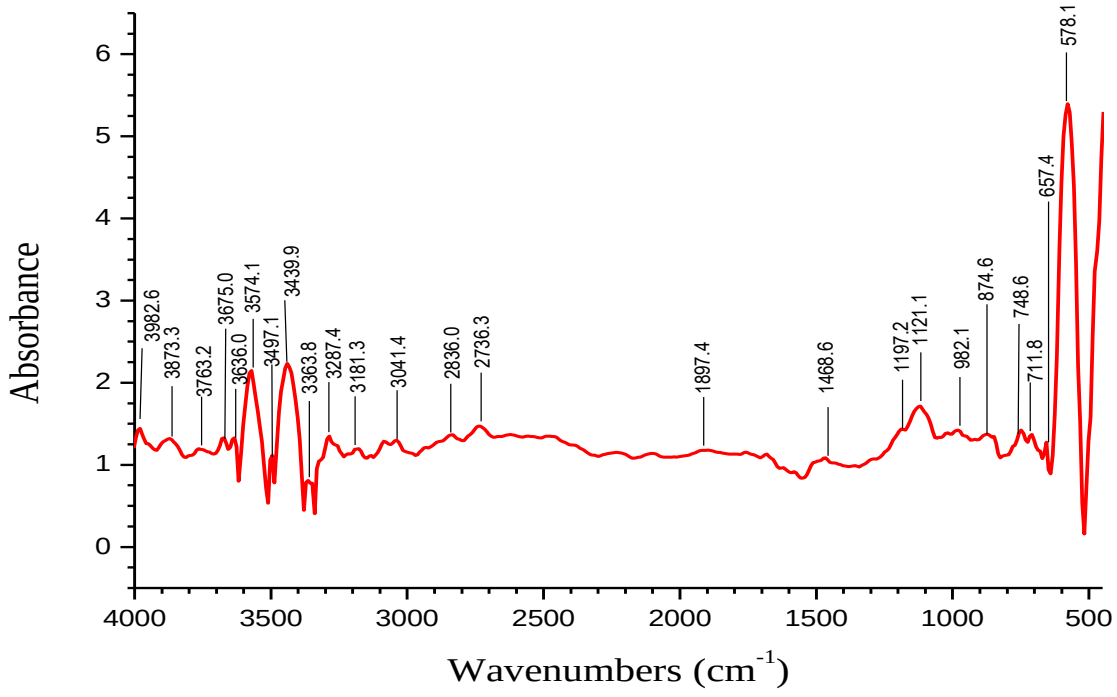

Figure 6.22: FTIR spectra of sludge formed by coagulation process after treatment of CPF solution using alum coagulant.

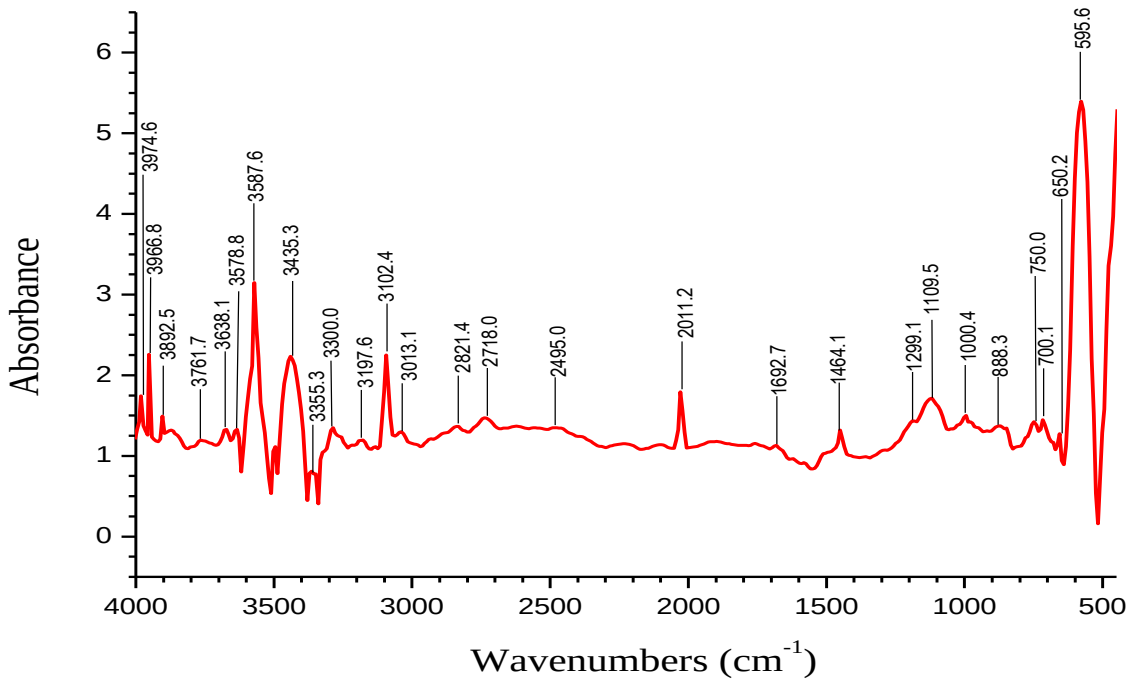

Figure 6.23: FTIR spectra of sludge formed by coagulation process after treatment of CF solution using $FeCl_3$ coagulant.

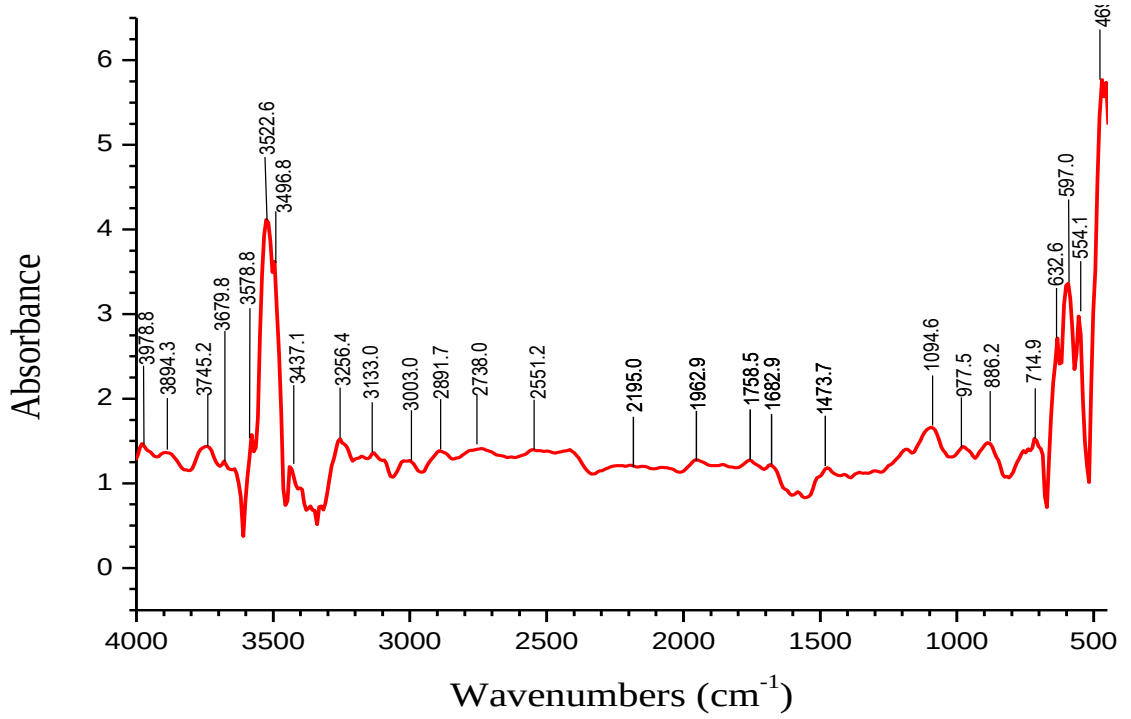

Figure 6.24: FTIR spectra of sludge formed by coagulation process after treatment of CF solution using alum coagulant.

6.1.11 Microstructural and EDX analysis

Figures 6.25 to 6.30 show the surface morphology and EDX spectra of flocs after coagulation/flocculation process. The EDX analysis shows the adsorption of MP, CPF and CF on $FeCl_3$ and alum flocs. The major elements of $FeCl_3$ flocs are N, Fe, O, Cl, P, S and of alum are N, Al, O, K, P, S. The weight % of element N, P and S defined the adsorption of MP, CPF and CF on $FeCl_3$ and alum. The floc of $FeCl_3$ contains, higher weight % of N as compared to alum, as can be seen in Table 6.13. The pesticides and $FeCl_3$ did not contain any potassium compound (K), thereby K values were not detected when $FeCl_3$, was used.

Table 6.13: Chemical composition of the flocs formed by coagulation.

Pesticides	Coagulant	% Element in the flocs								
		N	Al	C	Fe	O	K	Cl	S	P
MP	$FeCl_3$	10.79	-	3.54	17.71	20.69	-	24.38	14.25	9.64
	Alum	7.6	6.32	4.44	-	53.78	7.89	-	11.24	8.73
CPF	$FeCl_3$	11.78	-	3.51	10.78	22.48	-	26.65	15.63	9.17
	Alum	7.12	6.45	5.53	-	52.27	5.82	-	13.39	9.42
CF	$FeCl_3$	12.23	0.87	5.68	32.54	22.71	-	25.97	-	-
	Alum	9.15	6.49	5.12	-	54.53	7.99	-	16.16	-

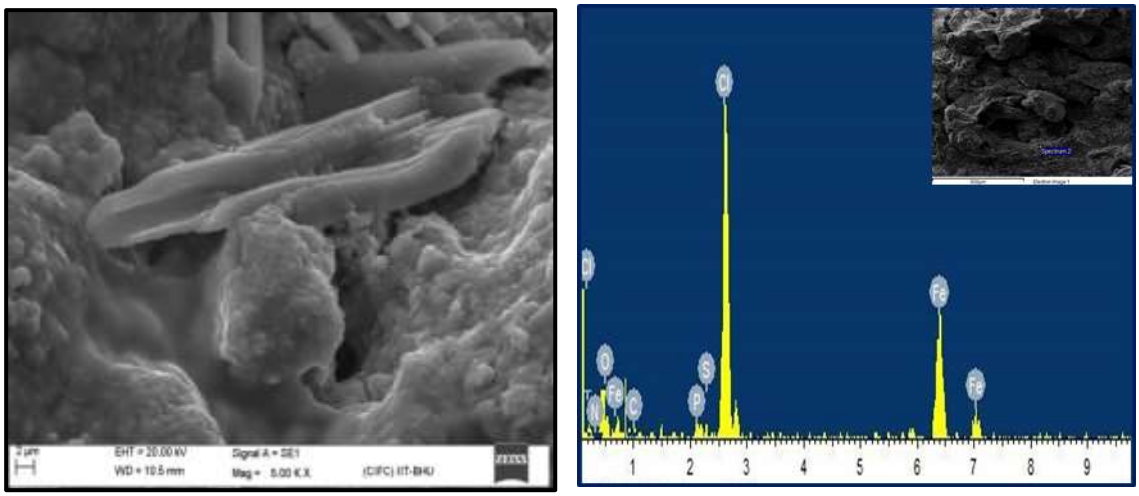

Figure 6.25: Methyl parathion: SEM micrographs and EDX analysis of flocs formed after $FeCl_3$ treatment.

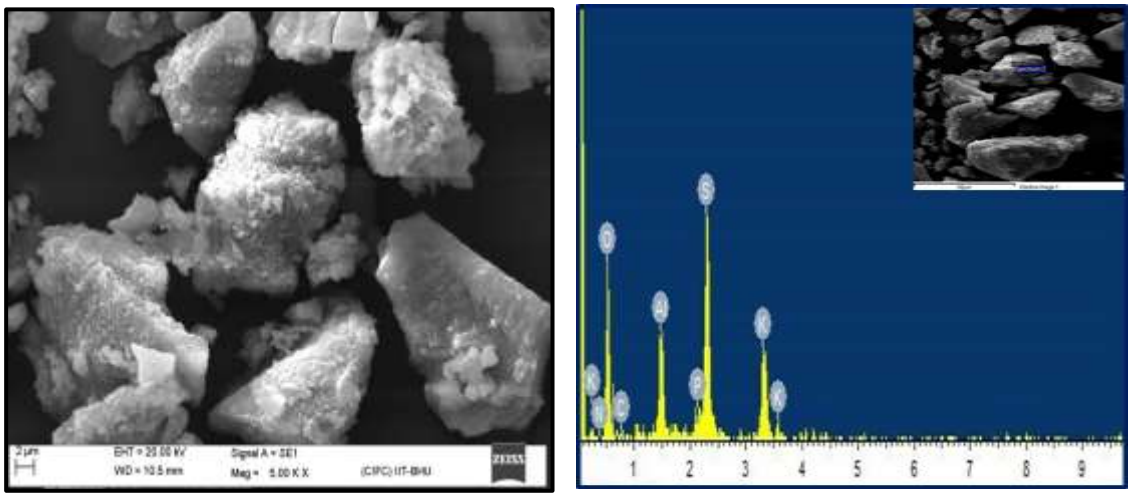

Figure 6.26: Methyl parathion: SEM micrographs and EDX analysis of flocs formed after alum treatment.

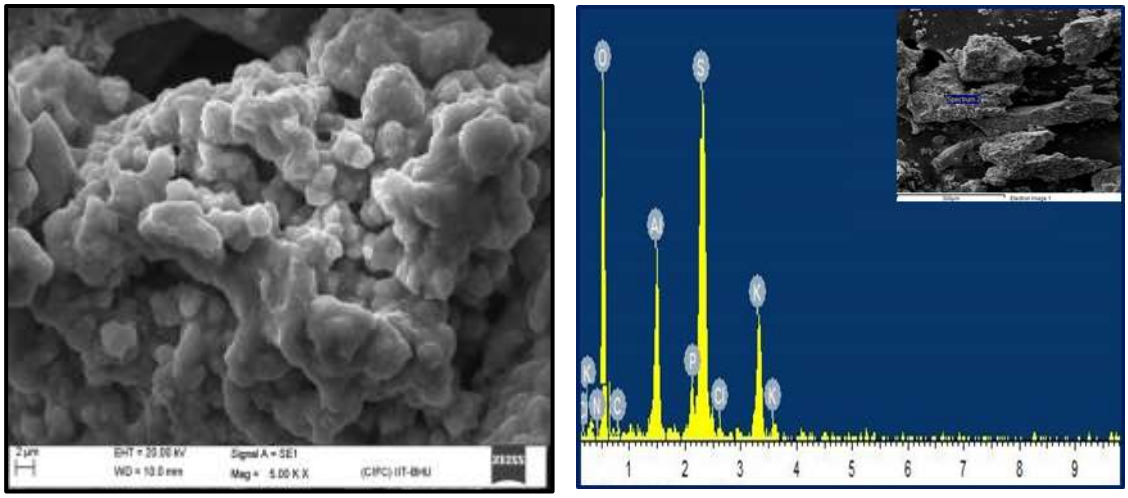

Figure 6.27: Chlorpyrifos: SEM micrographs and EDX analysis of flocs formed after $FeCl_3$ treatment.

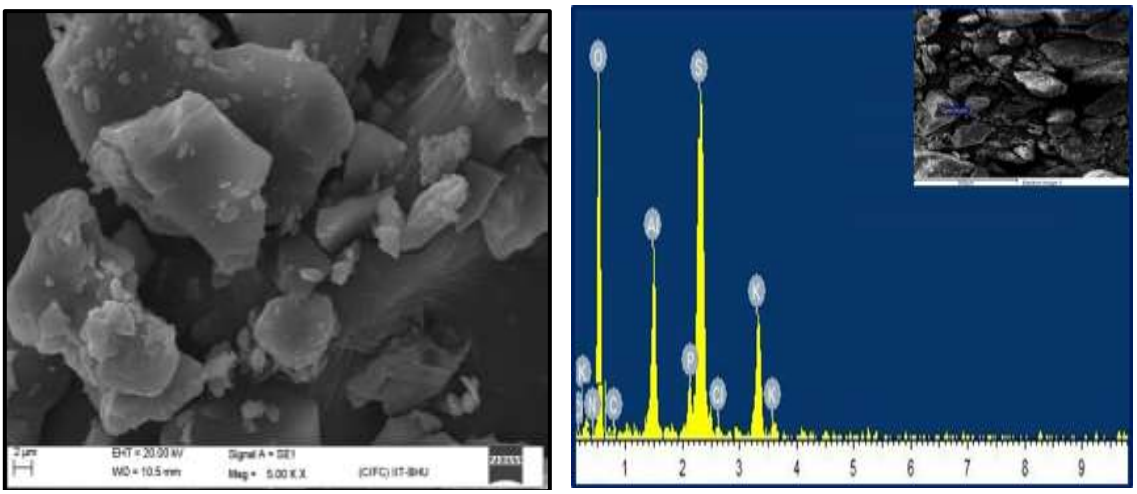

Figure 6.28: Chlorpyrifos: SEM micrographs and EDX analysis of flocs formed after alum treatment.

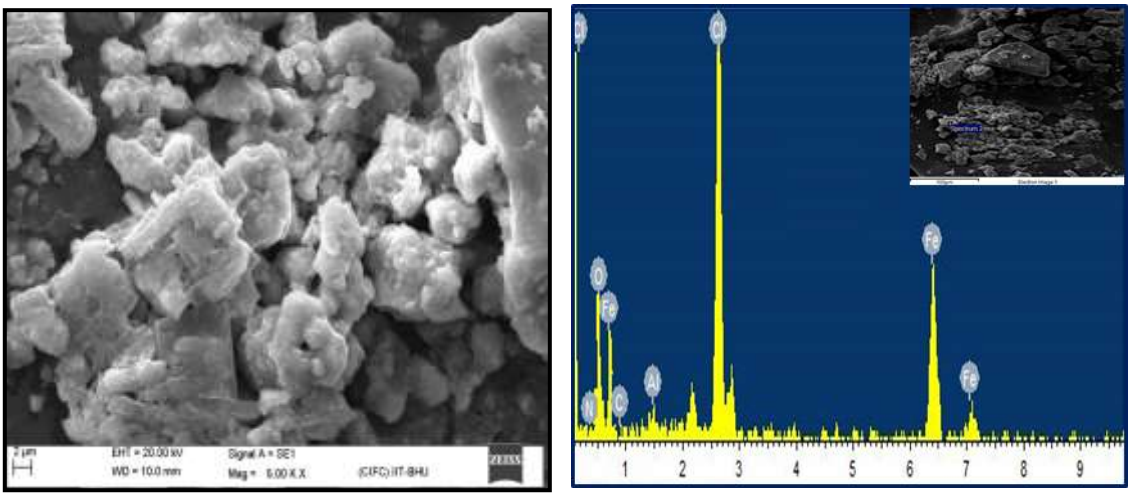

Figure 6.29: Carbofuran: SEM micrographs and EDX analysis of flocs formed after $FeCl_3$ treatment.

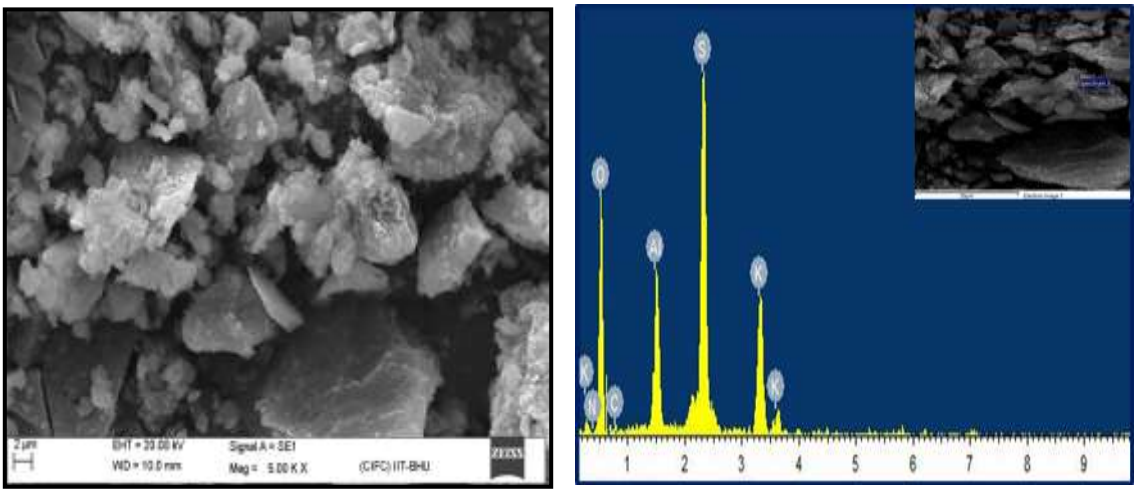

Figure 6.30: Carbofuran: SEM micrographs and EDX analysis of flocs formed after alum treatment.

6.1.11 Thermal analysis of residue (TGA-DTA)

The thermo gravimetric studies were conducted for the precipitated sludge of MP, CPF and CF simulated wastewater in order to understand the combustion characteristics and the prospect of being used as a solid fuel. The information on the temperature of dehydration and volatilization, their rates and heat evolved/consumed during the process were obtained.

It is of prime importance for further use and disposal of sludge, where it is dried and thermally degraded. The bottom ash obtained after its combustion can be blended with the cementitious mixtures. In this analysis, the weight of samples for $FeCl_3$ and alum sludge was taken as 76.112 mg and 63.484 mg, respectively, air flashing rate was maintained at 60 mL/min and heating rate was 10 ºC/min. The TGA and DTA curves were obtained for $FeCl_3$ and alum are presented in Figure 6.31. The TGA trace of the $FeCl_3$ sludge in the oxidizing atmosphere shows the loss of moisture and the evolution of some light weight water molecules including water at low temperature. Higher temperature drying occurs due to loss of the surface bound water.

In case of MP-$FeCl_3$ sludge (Figure 6.31) 34.17% weight loss occurred up to 300 ºC. Another weight loss was observed in the range of 300 to 550 ºC (5.21% weight loss). In the last temperature range between 350 to 1000 ºC, there is 0.09% weight loss. The strong exothermic peak occurring at 160.4 ºC is due to the oxidative degradation of the sludge. This region, as observed from the first derivative weight loss curve, may be due to the combustion of carbon species. At about 362 ºC, the organic component of the insecticide got oxidized, leaving the ash fraction in sludge. It was noted that the ash content is high in the sludge (residual mass = 27.06%). The nature of the TG curve shows the temperature span as an exothermic.

The TG/DT analysis behaviour of MP-alum sludge is shown in Figure 6.31. TGA analysis shows that sludge loses moisture up to temperature 100 ºC. A sharp decrease in weight loss of 22.63% occurs between 110 to 230 ºC. The rate of weight loss from 230 ºC onwards up to 760 ºC was extremely slow with cumulative weight loss being only 7.55%. Beyond 760 ºC maximum weight loss of about 27.57% was observed between 760 to 820 ºC. This might be due to the molecular level rearrangement. The residual mass of 37.32% remains as ash at temperature 997.8 ºC.

The TGA profile for CPF-$FeCl_3$ sludge (Figure 6.31) shows the exothermic weight loss of 38.83% in the temperature range 100 to 200 ºC. This is due to dehydration of sample along with the removal of organics. A weight loss of 4.20% occurs exothermically in the temperature range of 250 to 500 ºC. The strong exothermic peak occurring at 158.8 ºC. The exothermic weight loss with heat requirement suggests the involvement of energy in the oxidation of C and H containing organic substance followed by their removal. In the last temperature range between 500 to 998.3 ºC, there is 0.06% weight loss.

The TGA/DTA results of CPF-alum sludge is shown in Figure 6.31. A percent weight loss of the order of 36.55 % occurs up to 200 ºC. This is maximum weight loss during the entire process. The TGA curve shows a steady weight loss of 8.17% between 240 ºC to 730 ºC and 24.87 % decrease in weight between 750 to 810 ºC. From 810 to 1000 ºC, there is a very little weight loss and residual weight loss of 30.40% is observed at 999.87 ºC.

In case of CF-$FeCl_3$ sludge (Figure 6.31) the highest weight loss of 28.12% occurs exothermically up to 200 ºC. A sharp weight loss of 6.89% in a very narrow temperature range of 200 to 450 ºC occurs exothermically. Between 450 to 800 ºC the variation in weight is only 0.08%. The weight remains constant on thee further

increment of temperature up to 1000 ºC. The residue obtained at temperature 1000 ºC is 42.40%.

The TG/DT analysis of CF-alum sludge are shown in Figure 6.31. The weight loss in earlier temperature zone represents the removal of organic volatiles. During the entire operation of heating up to 1000 ºC, there has been weight loss at three locations (i) up to 225 ºC, (ii) between 150 to 350 ºC and (iii) between 350 ºC to 850 ºC losing 19.36, 7.55 and 27.57% of weight, respectively. These zones correspond to evaporation of higher hydrocarbons.

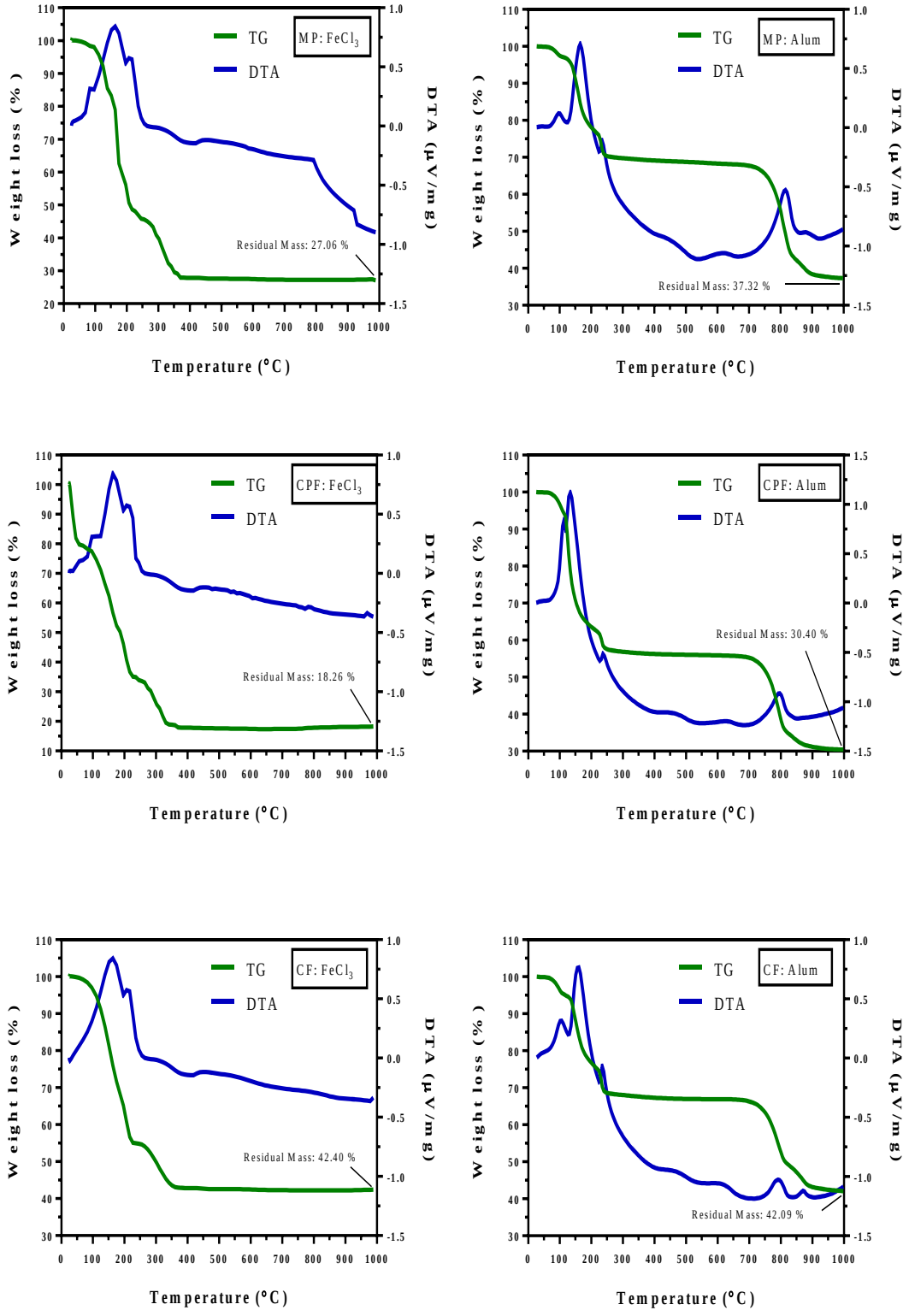

Figure 6.31: TGA/DTA of $FeCl_3$ and alum sludge obtained by coagulation. Conditions: atmosphere = air, sample weight = 76.112 mg ($FeCl_3$) and 63.484 mg (alum), air flow rate = 60 mL/min and heating rate = 10 ºC/min.

6.2 Fenton Oxidation

Fenton oxidation, an AOP, has been considered as an attractive method for the treatment of pesticides bearing wastewater. In the present study, the treatment of MP, CPF and CF present in simulated wastewater has been carried out by Fenton oxidation using Fe^{2+} as catalyst and the results obtained are discussed below.

6.2.1 Analysis of results of experiments

The experiments were designed by CCD of RSM and ANFIS for CPF reduction from simulated wastewater. The ANFIS computing technique was used to support the RSM results. Finally optimization was performed to find out the optimum values for the experiments using both techniques.

6.2.2 Data analysis and experimental design

Fenton oxidation for COD and CPF reduction were optimized and the effects of the variables: initial pH (*A*), hydrogen peroxide dose (*B*) and ferrous iron dose (*C*) were evaluated using RSM combined with the CCD. The applied ranges of process parameters were: [pH] = 2 − 7, $[H_2O_2]$ = 0.336 − 0.816 M and $[Fe^{2+}] = 3.60 \times 10^{-3} - 14.4 \times 10^{-3}$ M. The levels defined in this method as low, central and high represent -1, 0 and +1, respectively, as shown in Table 6.14. The required number of experiments (N) is given by the expression: 2^k (2^3 = 8; fact points) + 2 k (2*3 = 6; axial points) + 6 (center points; 6 replications). Twenty experimental runs with 3 factors and 2 levels were performed, including four central points in order to provide statistical consistency to the mathematical model (Table 6.15). Two responses, the CPF concentration ($Y_{Conc.}$) and the COD (Y_{COD}) were chosen to evaluate the efficiency of Fenton process.

Table 6.14: Experimental range and levels of the factor in the CCD design.

Input factors	Symbol	Factor range and levels		
		-1	**0**	**+1**
Initial pH	*A*	2	4.5	7
H_2O_2 dose (mol/L)	*B*	0.34	0.571	0.82
Fe^{2+} dose × 10^{-3} (M)	*C*	3.6	9	14.4

Table 6.15: Experimental design matrix and response variables of CPF.

Run	Experimental design			Response variables (%)	
	pH (*A*)	**H_2O_2 (*B*) (M)**	**Fe^{2+} (*C*) (M)**	**CPF concentration**	**COD**
1	0.0	0.0	0.0	88.84	74.35
2	-1.0	-1.0	-1.0	69.14	58.65
3	1.0	1.0	1.0	40.33	23.78
4	-1.0	1.0	-1.0	74.02	65.12
5	0.0	0.0	0.0	88.91	74.12
6	0.0	0.0	0.0	89.10	74.44
7	0.0	-1.682	0.0	75.56	66.57
8	0.0	0.0	-1.682	68.70	55.18
9	-1.0	-1.0	1.0	70.06	62.03
10	0.0	0.0	1.682	88.00	73.70
11	1.0	-1.0	-1.0	39.12	26.11
12	1.0	1.0	-1.0	30.22	21.89
13	0.0	0.0	0.0	94.00	83.51
14	1.0	-1.0	1.0	38.41	29.23
15	1.682	0.0	0.0	55.89	43.74
16	0.0	0.0	0.0	93.16	82.33
17	0.0	1.682	0.0	65.22	59.11
18	-1.0	1.0	1.0	76.21	69.34
19	0.0	0.0	0.0	88.92	73.00
20	-1.682	0.0	0.0	57.89	50.11

6.2.3 ANOVA regression analysis

The fitting of a polynomial model with three factors (initial pH, H_2O_2 & Fe^{2+} dose) and two responses (CPF concentration and COD) were implemented in the experimental design and the results obtained from Fenton experiments were analysed by the ANOVA, to check the "Goodness of Fit" of the model (Table 6.16). The p-values ("Prob > F" less that 0.05) indicate that the models are statistically significant for prediction of response values (Lim et al., 2009). Comparison of experimental (actual) and predicted values of the responses is shown in Figure 6.32. The final quadratic models in terms of coded factors for both responses are given in Equations (6.14) and (6.15). The plus and minus signs in the models have predictions which indicate synergistic or antagonistic effects, respectively (Pouran et al., 2015).

$$Y_{Conc.(CPF)}\ (\%) = 90.89 - 10.60\,A - 0.98\,B + 3.29\,C - 14.52\,A^2 - 9.75\,B^2 - 6.93\,C^2 - 2.25\,AB + 0.79\,AC + 1.51\,BC \quad (6.14)$$

$$Y_{COD(CPF)}\ (\%) = 77.36 - 12.07\,A - 0.62\,B + 3.20\,C - 13.24\,A^2 - 7.61\,B^2 - 7.04\,C^2 - 2.93\,AB - 0.32\,AC - 0.049\,BC \quad (6.15)$$

The ANOVA regression analysis demonstrated the legitimacy of the quadratic model ($p < 0.01$, F-test). The values of the coefficient of determination (R^2) are 0.974 and 0.968 for responses $Y_{conc.}$ and Y_{COD}, respectively. The change in R_{adj}^2 and R_{pred}^2 values is close to each other. "Adeq Precision" represents the signal/noise ratio. A signal to noise ratio >4 is desirable. In this case the ratios 6.569 and 6.306 for concentration and COD, respectively indicate an adequate signal. The corresponding Fisher variation ratios (F-value) 4.24 and 3.78 imply that the model is noteworthy for responses $Y_{conc.}$ and Y_{COD}, respectively. The lack of fit exemplifies the disparity of data all over the place to the fitted model. The standard deviations for the responses $Y_{conc.}$ and Y_{COD} are 12.68 and 12.95, respectively and the corresponding means for the responses $Y_{conc.}$ and Y_{COD} are 69.59 and 58.32.

Table 6.16: ANOVA regression analysis of response surface quadratic model for CPF.

Source	Degree of freedom	Sum of squares		Mean square		F value		p-value (Prob>F)	
		CPF Concentration	COD	CPF Concentration	COD	CPF Concentration	COD	CPF Concentration	COD
Model	9	6131.57	5696.94	681.29	632.99	4.24	3.78	0.0171 (significant)	0.0251 (significant)
A	1	1533.44	1989.71	1533.44	1989.71	9.54	11.87	0.0115	0.0063
B	1	1898.75	1279.59	1898.75	1279.59	4.51	6.27	0.0371	0.0407
C	1	1937.83	2531.67	1937.83	2531.67	9.50	13.39	0.0178	0.0033
AB	1	2406.68	2019.87	2406.68	2019.87	6.26	12.55	0.0409	0.0081
AC	1	1467.73	1989.95	1467.73	1989.95	4.89	7.68	0.0089	0.0075
BC	1	2698.16	2217.90	2698.16	2217.90	15.45	13.23	0.0351	0.0128
A^2	1	3038.98	2524.69	3038.98	2524.69	18.90	15.06	0.0014	0.0031
B^2	1	1369.57	834.38	1369.57	834.38	8.52	4.98	0.0153	0.0211
C^2	1	2633.52	2273.07	2633.52	2273.07	59.72	51.26	0.0009	0.0072
Residual	10	1607.60	1567.88	160.76	313.58	-	-	-	-
Lack of Fit	5	1578.54	1567.88	315.71	313.58	54.31	14.43	0.00002 (significant)	0.0054 (significant)

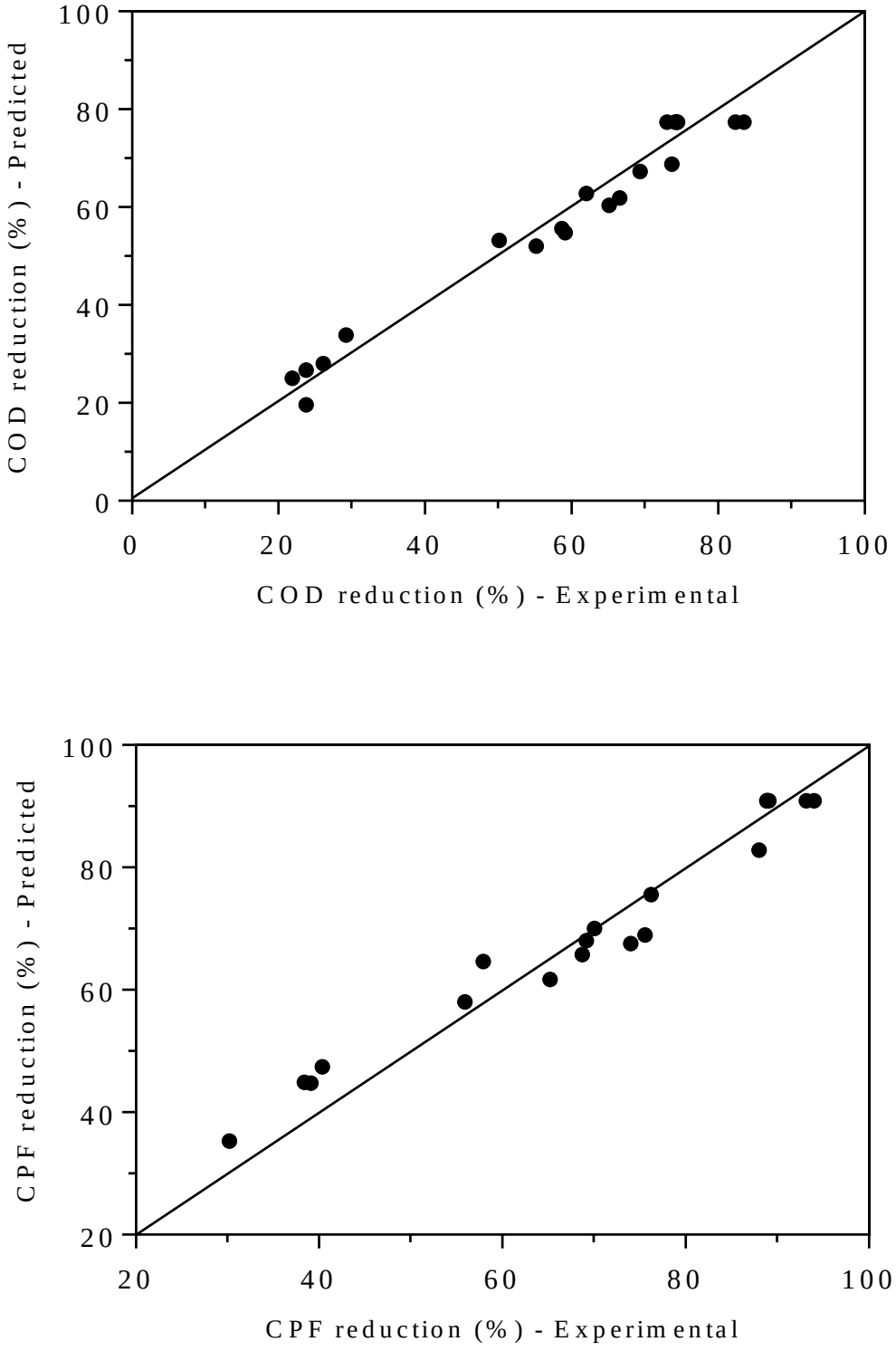

Figure 6.32: Comparison of experimental (actual) and predicted values of the responses using Fenton oxidation for COD and CPF reduction.

6.2.4 Response surface and contour plots

The polynomial regression model is presented as graphical three-dimensional surface plots. The plots for CPF concentration and COD reduction are shown in Figure 6.33 in terms of *AB*, *AC* and *BC* factors. The plots show the affiliation between the response and factors. Each response surface plot exhibits a clear peak and the bottom point (Guo et al., 2012). Twenty experiments were performed to determine the optimum condition with three factors, initial pH and concentrations of H_2O_2 and Fe^{2+}. The optimum conditions for CPF concentration and COD reduction are obtained as pH 3.25, H_2O_2 concentration 0.58 M and Fe^{2+} concentration 1.08×10^{-2} g/L. Under these conditions the measured values of CPF concentration and COD reduction are 94.23 and 84.19% and the corresponding predicted values are 92.5 and 80.11%, respectively.

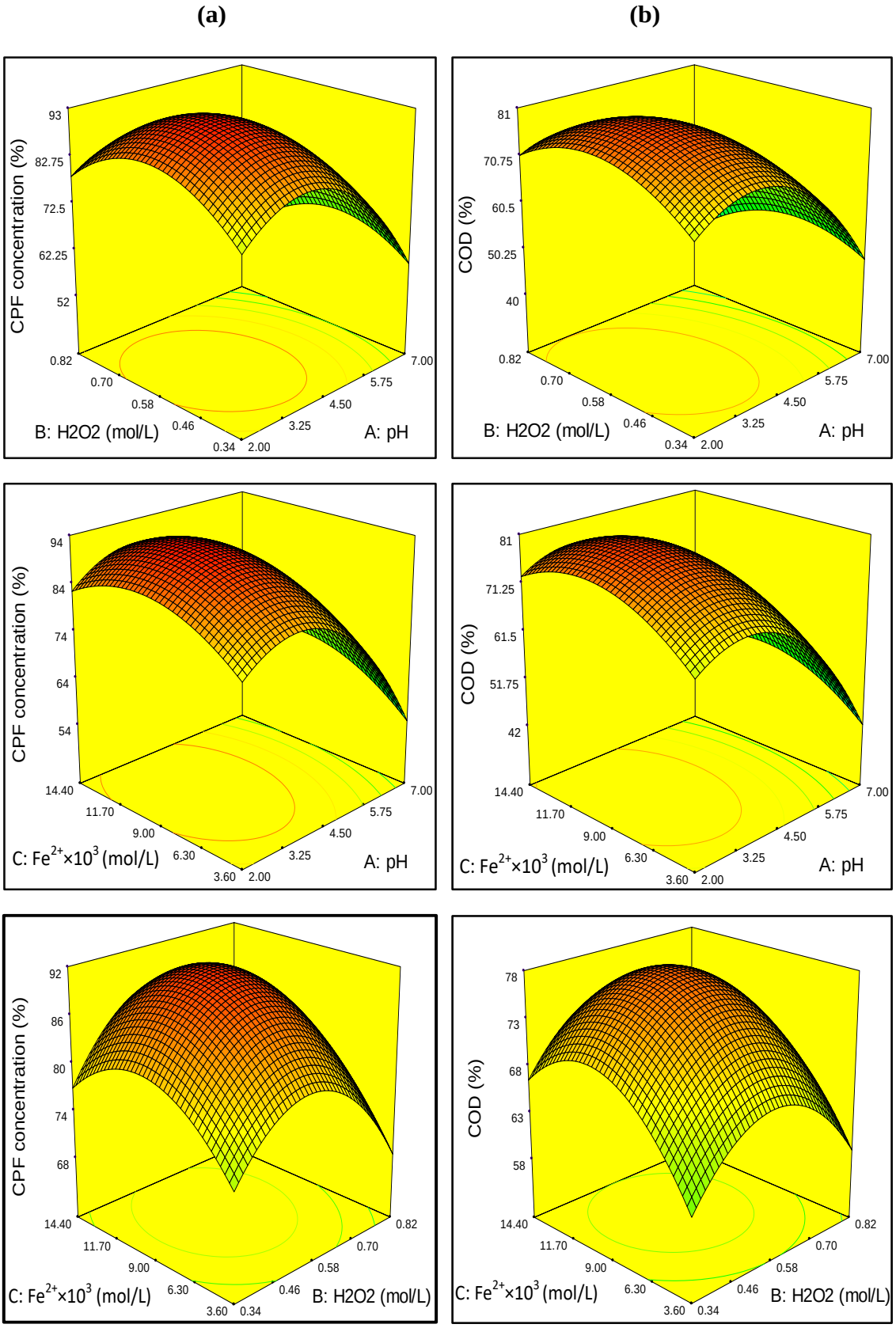

Figure 6.33: The response surface plot for optimization of (a) CPF concentration and (b) COD reduction at optimum condition.

6.2.5 Test of ANFIS model

Gaussian type three bell-shaped membership functions were planned for ANFIS input. Figure 6.34 illustrates the fuzzy rule structure of each ANFIS model with 3 inputs and 2 outputs. The functioning of ANFIS was influenced by the size of training and test data. Rule editor of Matlab-Fuzzy Logic Tool Box and ANFIS modelling system with 27 rules are given in Figure 6.35 and 6.36, respectively.

Testing of ANFIS output with training data as shown in Figure 6.37. This predicts that FIS output has good agreement with the training data. The lower values of MSE and RMSE indicate better performance of the model (Kavitha and Palanivelu, 2005). The decision surfaces plot is shown in Figure 6.38 for estimation of reduction efficiencies of CPF concentration and COD for three input combinations. The concentration reduction correlation coefficient (R^2) is 0.972 and MSE is 0.543 whereas for COD reduction these are 0.966 and 0.689, respectively.

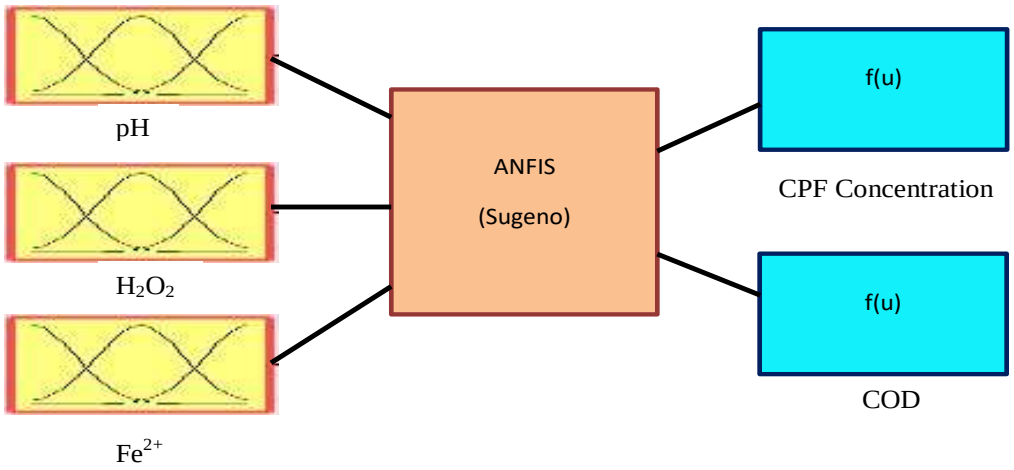

Figure 6.34: Fuzzy rule architecture of each ANFIS model. System ANFIS: 3 inputs and 2 outputs.

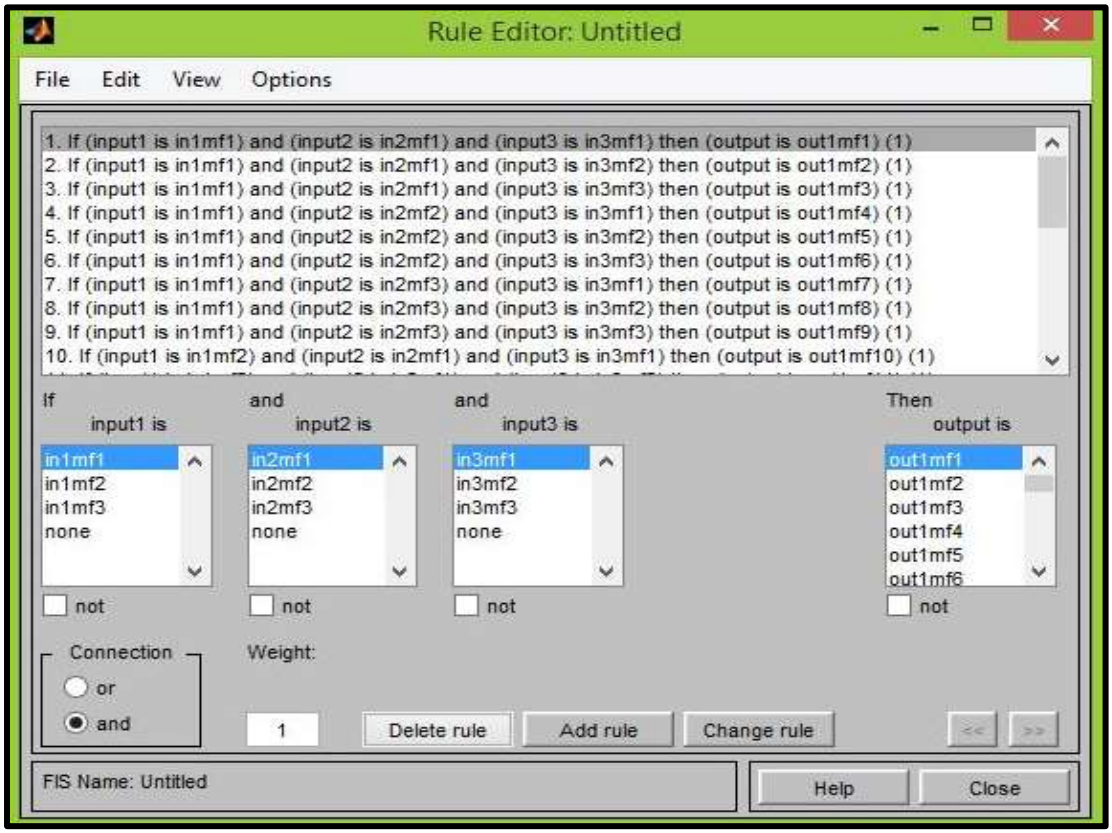

Figure 6.35: Rule editor of Matlab-Fuzzy Logic Tool Box.

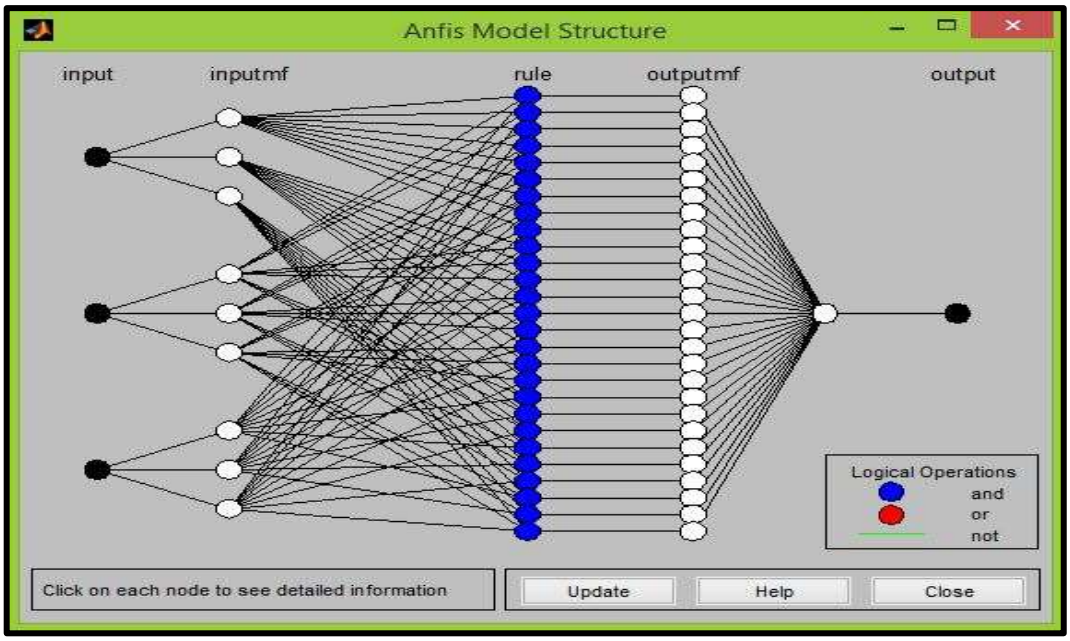

Figure 6.36: The ANFIS modelling system for Fenton oxidation with 27 rules.

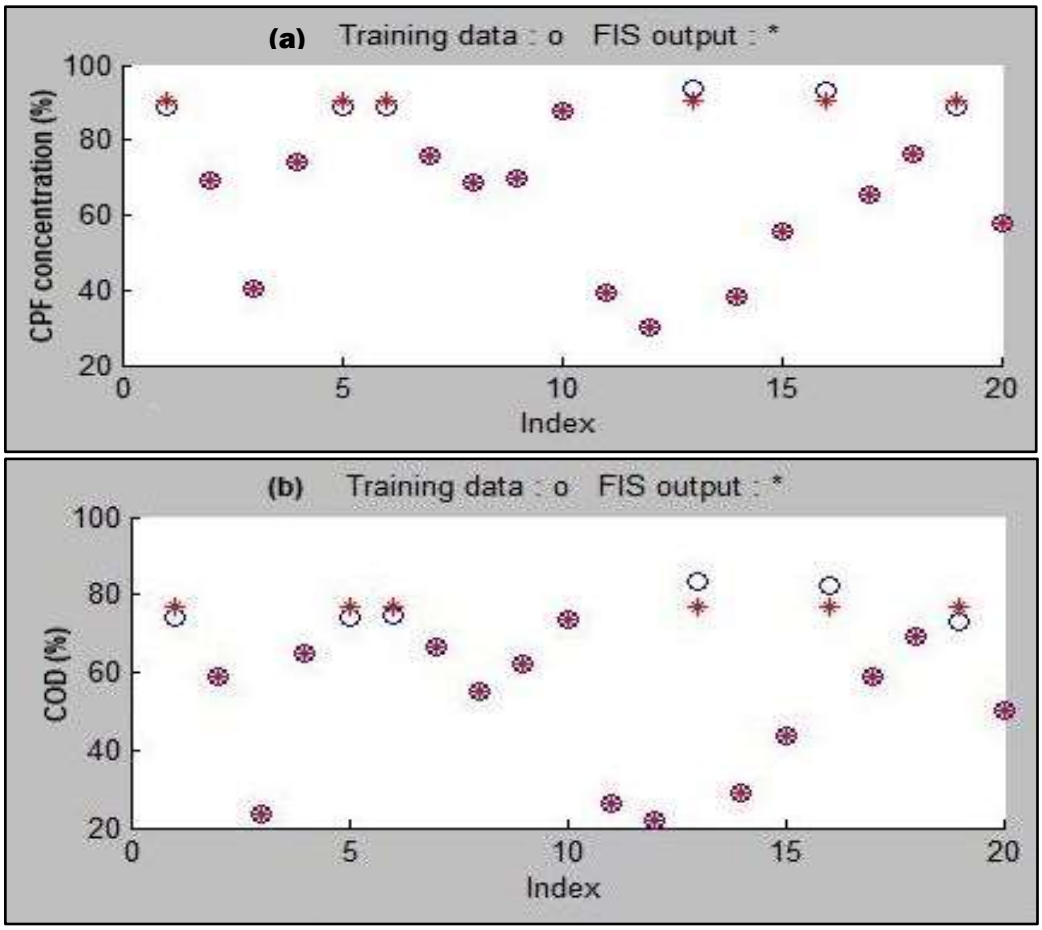

Figure 6.37: Testing the FIS output with training data set: (a) CPF concentration and (b) COD.

(a) **(b)**

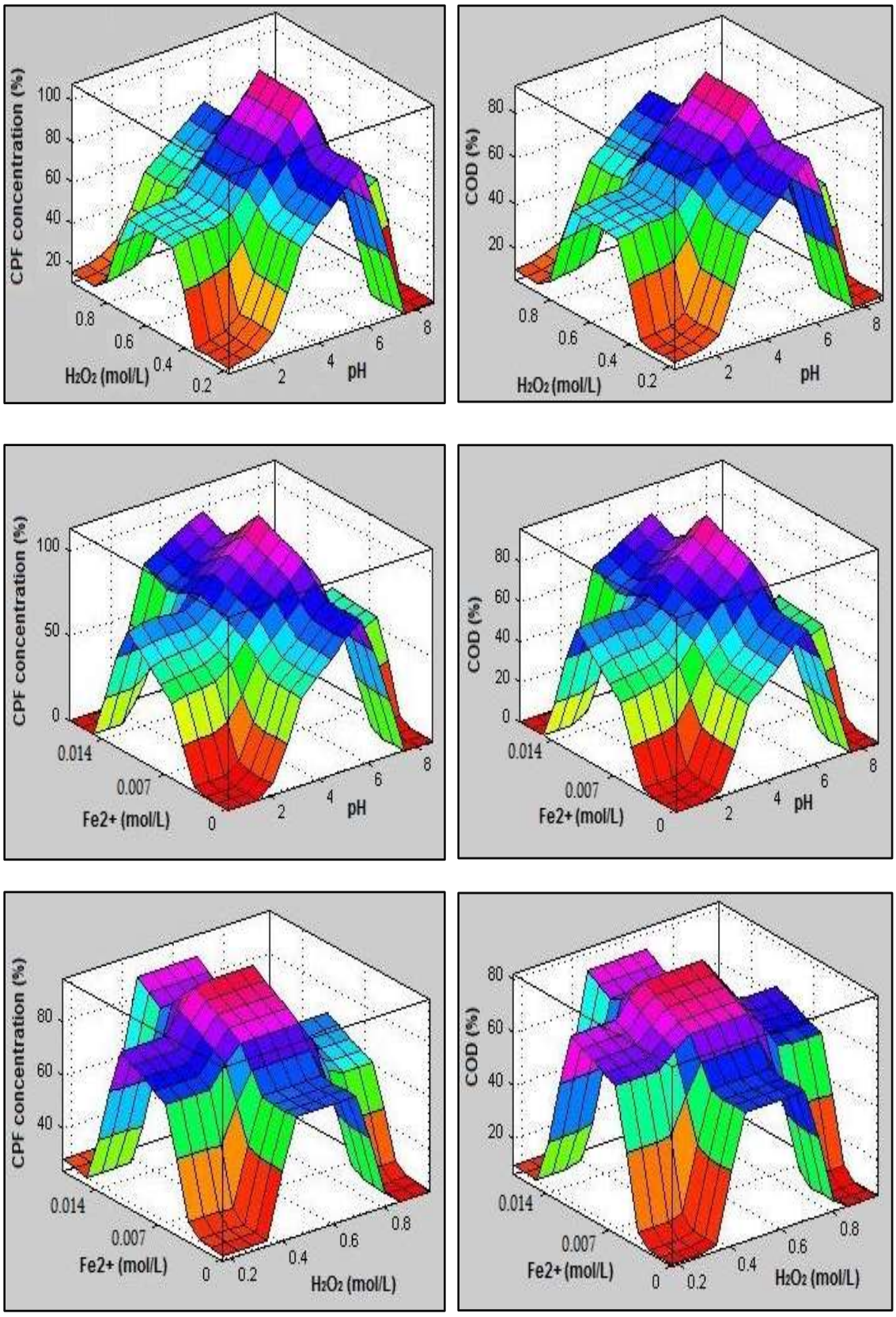

Figure 6.38: ANFIS surface plots for estimation of percentage reduction (a) CPF concentration and (b) COD.

6.2.6 Effect of initial pH on treatment of MP, CPF and CF

An essential characteristic of the Fenton oxidation is that it is feasible only in acidic range of pH. The pH affects the formation of hydroxyl radicals in Fenton oxidation and hence the oxidation efficiency. In order to test the effect of pH on reduction efficiency 7.19×10^{-4} M of $FeSO_4 \cdot 7H_2O$ and 6.53×10^{-2} M H_2O_2 solutions were added to 100 mL of 11.4×10^{-5} M MP, 8.65×10^{-5} M CPF and 13.5×10^{-5} M CF pesticides solution separately for Fenton oxidation. The pH of the solution was varied in the range of 2 to 7 and temperature was kept constant at 25 ºC.

Analysis revealed that maximum reduction efficiency of 74% was obtained for the MP solution at a pH 3. Figure 6.39 (a) shows that maximum COD reduction is achieved at pH 3 and after that it decreases with increasing pH. The effect of pH on the reduction efficiency of MP also shows that the degradation pattern is same as for COD. The degradation efficiency for MP was observed to increase from 66 to 74% when pH of the solution was increased from 2 to 3 and after that the degradation efficiency decreased from 68 to 38% when the pH of the solution increased from 4 to 7. Similarly, COD reduction increased from 55 to 64% when the pH of the solution increased from 2 to 3 and after that COD reduction decreased from 60 to 21% when the pH from increased 4 to 7.

The decrease in CPF concentration and COD with increase in pH is similar. Control experiments showed that reduction of CPF increased from 69.14 to 78.6% when the pH of the CPF increased from 2 to 3, thereafter it decreased from 71.11 to 40.33% with increase in pH from 4 to 7. The corresponding COD reduction increased from 58.25 to 68.94% with increase in pH from 2 to 3 and it decreased from 62.55 to 23.67% with increase in pH from 4 to 7 as shown in Figure 6.39 (b). Similar behaviour was also observed for CF (Figure 6.39 (c)). Maximum decrease in CF concentration and COD

were 63.78% and 54.71%, respectively. Results showing effect of pH on the reduction of three pesticides are summarized in Table B-13.

The analysis of experimental results showed that pH influenced the removal of pesticide and COD. Under pH > 4 iron precipitates as hydroxide ($Fe(OH)_3$), decreasing the concentration of dissolved Fe^{3+} and consequently that of Fe^{2+} species as well as the oxidation rate (Kwon et al., 1999; Joseph et al. 2000; Kavitha and Palanivelu, 2005). Ferric hydroxide precipitates and settles at the bottom, thus the availability of ferrous ions in the solution gets reduced (Shen et al., 2013). Additionally, hydrogen peroxide is stable at low pH because the reaction of H_2O_2 with Fe^{2+} is extremely pretentious. This causes degeneration in hydroxyl radical production, owing to the high concentration of H^+ to form stable oxonium ion ($H_3O_2^+$). Hydrogen peroxide undergoes a significant removal in its reactivity with ferrous ion and stability at high pH. Although, at high pH the oxidation potential of the hydroxyl radical is known to decrease, which reduces the process efficiency (Kwon et al., 1999; Elmolla et al., 2010). Alternatively, at pH less than 3 the reduction efficiency also decreases since the regeneration of Fe^{2+} (through reaction between Fe^{3+} and $H_2O_2^{\cdot-}$) is partly inhibited (Rodrigues et al., 2009). At lower pH, Fenton reaction is inhibitated due to the unwarranted H^+ reacting with $^{\bullet}OH$, decreasing the oxidation potential as shown below (Fan et al., 2011).

$$^{\bullet}OH + H^+ + e^- \rightarrow H_2O \qquad (6.16)$$

Hence, further experiments, except for the evaluation of effect of pH, were carried out at pH of 3.

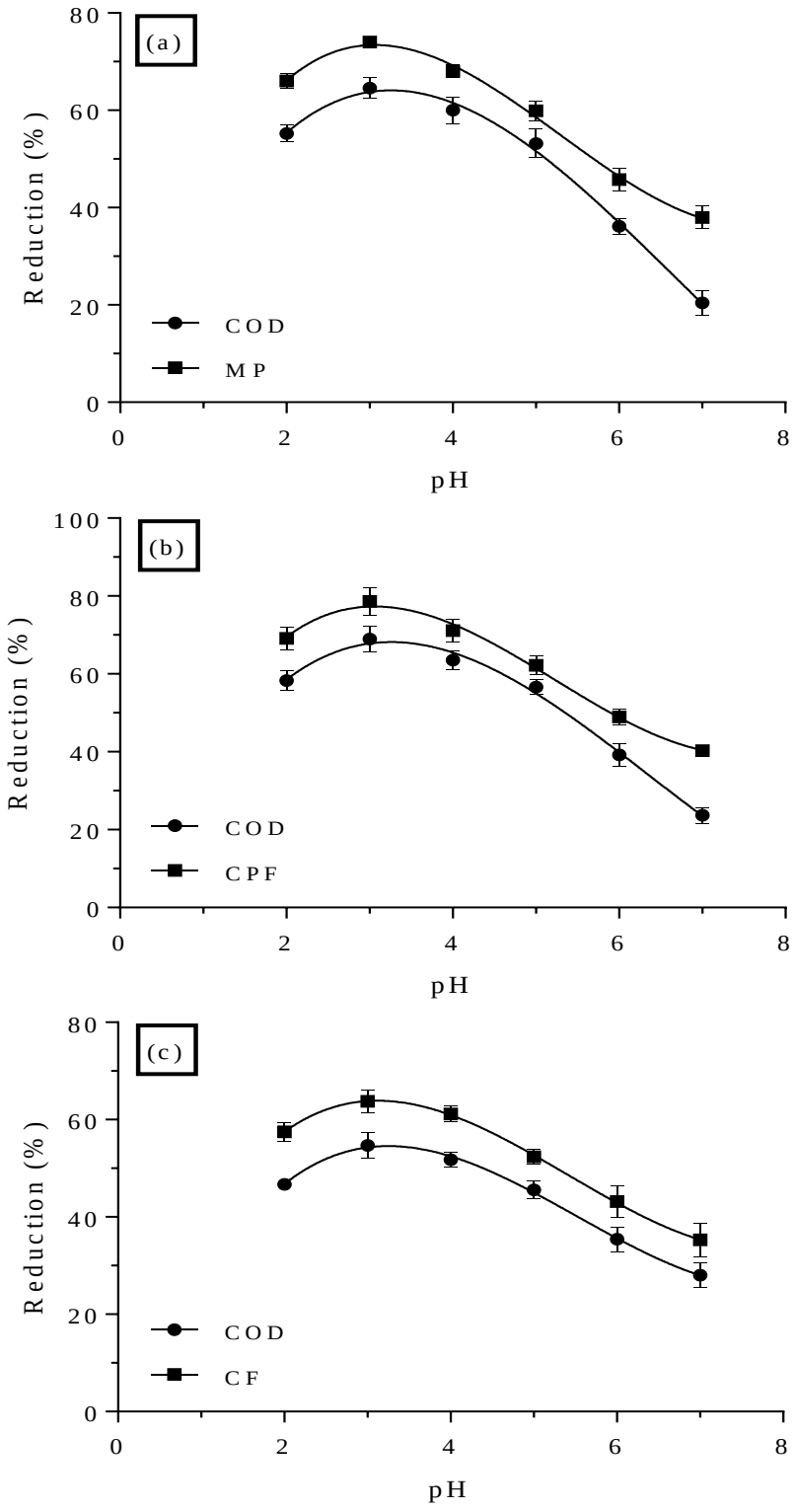

Figure 6.39: Influence of pH on reduction efficiency. Experimental conditions: Fe^{2+} = 7.19 ×10^{-4} M, H_2O_2 = 6.53 × 10^{-2} M, time = 60 min, temperature = 25 ºC. Initial concentration (a) MP = 11.4 × 10^{-5} M, (b) CPF = 8.56 × 10^{-5} M and (c) CF = 13.5 × 10^{-5} M.

6.2.7 Effect of hydrogen peroxide dosage on treatment of MP, CPF and CF

In Fenton oxidation, concentration of hydrogen peroxide has vital role in deciding the overall efficiency of the process and is one of the most imperative factors for the reaction and should be considered as the limiting reagent. In order to explore the effect of H_2O_2 dose and to identify the optimum dosage, studies were conducted at 25 °C and optimum pH 3 with Fe^{2+} dosage of 8.99×10^{-3} M by varying the H_2O_2 concentration from 3.36×10^{-1} to 8.16×10^{-1} M. It has been observed that when dosage of hydrogen peroxide increases the degradation efficiency of the pollutant increases (Lin and Lo, 1997; Kang and Hwang, 2000). In Fenton oxidation, reduction in amount of Fenton's reagent is highly essential to determine the operating cost as well as efficiency.

The COD reduction and MP reduction at various concentrations of H_2O_2 are shown in Figure 6.40 (a). It has been seen that the COD reduction and MP degradation increases from 59 to 79% and 70 to 92%, respectively, with increase in H_2O_2 dose from 3.36×10^{-1} to 6.53×10^{-1} M with further increase in H_2O_2 dose from 7.34×10^{-1} to 8.16×10^{-1} M both COD reduction and MP degradation decreased from 69 to 36% and 83 to 46%, respectively. Analysis showed that reduction efficiency of MP increased when dosage of H_2O_2 was increased, which is caused by the formation of more $^{\bullet}OH$. The maximum COD reductions of 79.2% and MP degradation of 92% were obtained at the optimum H_2O_2 dose of 6.53×10^{-1} M.

The CPF concentration reduction after 60 min were 73.65, 80.34, 86.77, 94.0, 91.56, 84.19 and 78.12% at Fe^{2+}: H_2O_2 ratio of 1:4.4, 1:5.6, 1:6.7, 1:7.8, 1:8.9, 1:10 and 1:11, respectively. The corresponding COD reduction are 64.58, 69.33, 76.23, 83.51, 80.25, 74.33 and 67.9%, respectively. The effect of H_2O_2 concentration on the reduction of CPF concentration and COD is shown Figure 6.40 (b). The optimum dose of H_2O_2 for maximum reduction in CPF concentration (94%) and COD (83.51%) were observed at

5.71×10^{-1} M. The reduction of COD is lower than the reduction of CPF concentration. Experimental results confirm that in the range investigated the CPF concentration and COD reduction increase when the H_2O_2 dosage is raised from 3.36×10^{-1} to 5.71×10^{-1} M. It is worth recognizing that when the dose of H_2O_2 is less the reduction efficiency increases and when it is high ($> 5.71 \times 10^{-1}$ M), the reduction efficiency decreases. However, no enhancement in the percentage reduction was observed when the H_2O_2 was overdosed, i.e. beyond 5.71×10^{-1} M.

The COD reduction and CF degradation increased from 53.73 to 76.28% and 67.91 to 89.34%, respectively with the increase in H_2O_2 dose from 3.36×10^{-1} to 6.53×10^{-1} M. On further increase in H_2O_2 dose from 7.34×10^{-1} to 8.16×10^{-1} M both COD reduction and CF degradation decreased from 66.86 to 32.16% and 79.18 to 41.22%, respectively. The maximum COD reductions of 76.28% and CF degradation of 89.34% were obtained at the optimum H_2O_2 dose of 6.53×10^{-1} M. The effect of H_2O_2 concentration on the reduction of CF concentration and COD can be seen in Figure 6.40 (c). The experimental data are given in Table B-14. The decrease in degradation efficiency after the optimum dose may be due to auto-decomposition of H_2O_2 to oxygen and water, and further H_2O_2 again reacts with $^{\bullet}OH$ radicals as shown in reactions 6.17 and 6.18 (Lin and Lo, 1997; Affam et al., 2012).

$$2H_2O_2 \rightarrow 2H_2O + O_2 \quad (6.17)$$

$$^{\bullet}OH + H_2O_2 \rightarrow H_2O + {}^{\bullet}O_2H \quad (6.18)$$

Accordingly, as the reaction proceeds the productivity of hydroxyl radicals ($HO^{\bullet}$) decreases and an unconventional radical having smaller oxidation potential than hydroxyl radical is generated ($HO_2^{\bullet}$), which affects the oxidation efficiency (Rodrigues et al., 2009).

Hydrogen peroxide in Fenton oxidation acts as a radical generator, however, it has a negative effect when large quantities of hydrogen peroxide are present causing scavenging of generated hydroxyl radicals (reaction 6.11). The unused amount of H_2O_2 during the Fenton oxidation contributes to COD and hence surplus amount of H_2O_2 is not recommended (Zhao and Lou, 2016).

6.2.8 Hydrogen peroxide consumption

The effect of instantaneous addition of H_2O_2 (addition of the entire amount at the begining of the experiment) on the performance of the Fenton reaction was studied. The instantaneous addition of H_2O_2 produced a higher quantity of hydroxyl radicals at the beginning of the experiment. The residual H_2O_2 concentration was analysed after the reaction time of 60 min. Figure 6.41 depicts the conversion of H_2O_2 upon Fenton oxidation at different H_2O_2 concentrations (initial) on treatment of MP, CPF and CF bearing simulated wastewater.

During the treatment of MP bearing wastewater the conversion increased from 96 to 98% when the initial concentration of H_2O_2 was increased from 0.336 to 0.653 mol/L (Figure 6.41(a)) and on further increase in H_2O_2 concentration its conversion decreased from 98 to 91%. In Figure 6.41 (b) a considerable increase in the H_2O_2 conversion from 98 to 100% is observed when the initial concentration of H_2O_2 is increased from 0.336 to 0.571 mol/L. However, when H_2O_2 was overdosed beyond 0.571 mol/L, H_2O_2 conversion decreased from 100 to 93% (in CPF bearing wastewater). Figure 6.41 (c) shows the conversion of 95% at 0.653 mol/L H_2O_2 for the treatment of CF bearing wastewater.

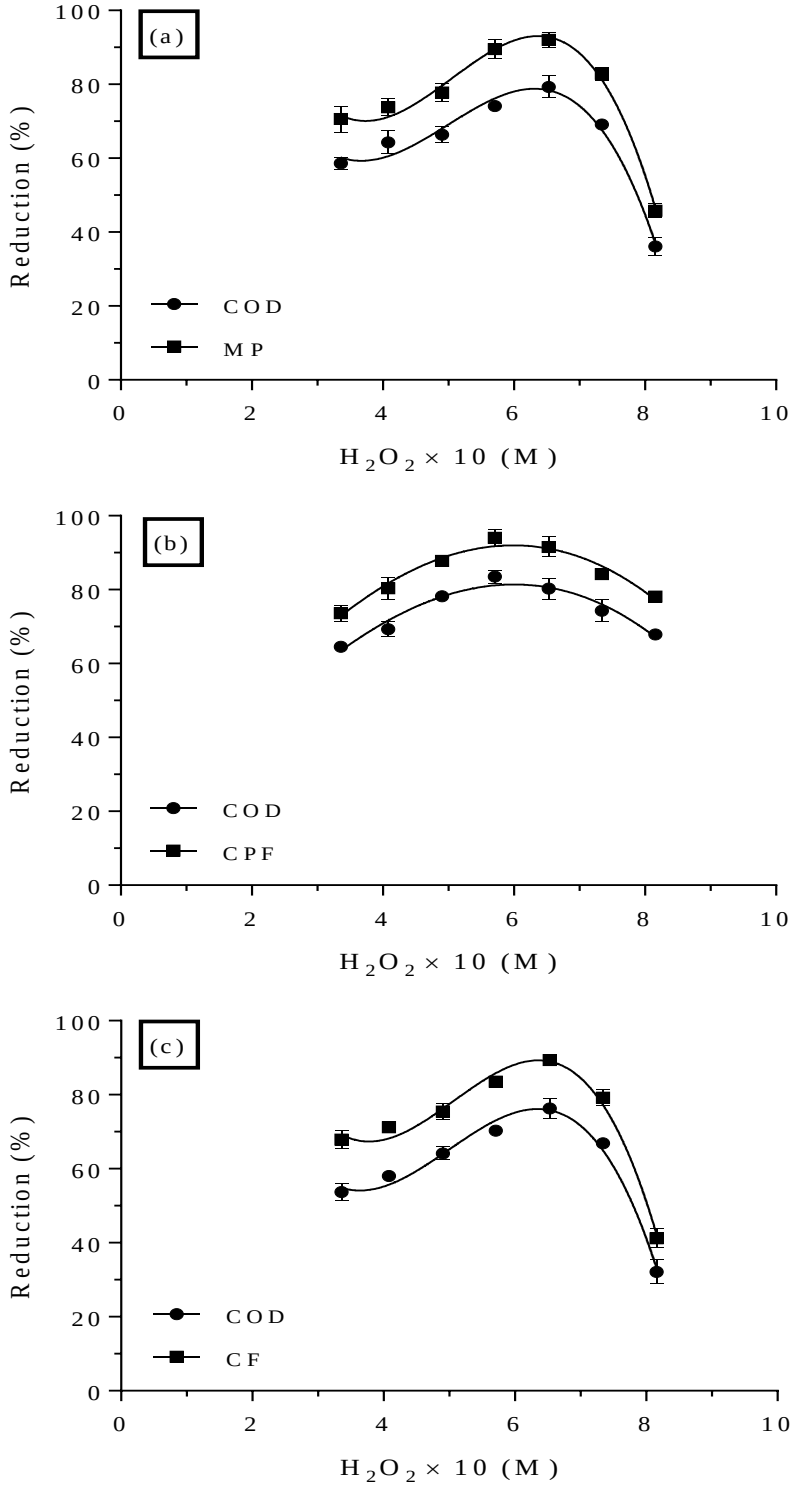

Figure 6.40: Influence of H_2O_2 dosage on reduction efficiency. Experimental conditions: $Fe^{2+} = 8.99 \times 10^{-3}$ M, $H_2O_2 = 3.36 – 8.16 \times 10^{-1}$ M, pH = 3, time = 60 min, temperature = 25 ºC. Initial concentration (a) MP = 11.4×10^{-5} M, (b) CPF = 8.56×10^{-5} M and (c) CF = 13.5×10^{-5} M.

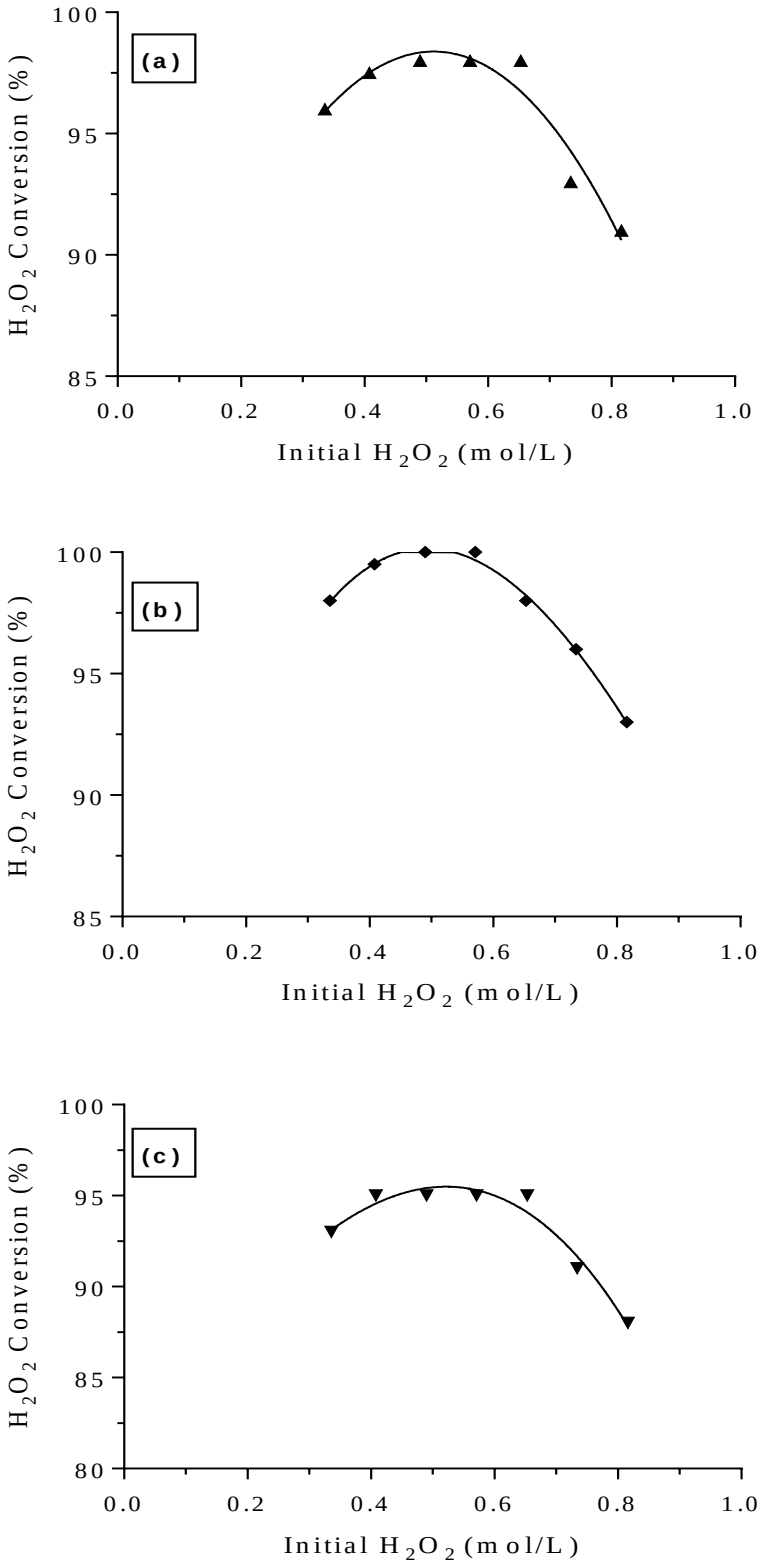

Figure 6.41: H_2O_2 conversion (%) as a function of initial H_2O_2 concentration (a) MP, (b) CPF and (c) CF.

6.2.9 Effect of ferrous iron dosage on treatment of MP, CPF and CF

Dosage of Fenton reagent plays a crucial role in deciding the overall cost of the process for oxidation of organics (Deng and Englehardt, 2006). Generally the rate of degradation increases as the dosage of Fe^{2+} increases, but a massive increase in Fe^{2+} ions lead to increase in the total amount of dissolved iron ions resulting in sludge formation in the solution. Therefore, care should be taken to avoid excessive formation of the sludge. While investigating the effect of amount of $FeSO_4.7H_2O$ dose on Fenton oxidation, the concentration of Fe^{2+} was varied in the range of 3.60×10^{-3} to 14.4×10^{-3} M at constant pH of 3.

The dose of H_2O_2 was kept constant at 6.53×10^{-1} M while studying the oxidation of MP solutions. The COD reduction and MP degradation, increased from 48 to 71% and 59 to 87%, respectively, when Fe^{2+} dose varied from 3.60×10^{-3} to 8.99×10^{-3} M, then both decreased from 71 to 62% and 87 to 75%, respectively on increasing the Fe^{2+} dose from 10.8×10^{-3} to 14.4×10^{-3} M. Percentage COD and MP reductions under various concentrations of Fe^{2+} are shown in Figure 6.42 (a). The, COD reduction efficiency is lower than the reduction efficiency of MP under the similar operating conditions. It has been also observed that the COD reduction increased with increase in Fe^{2+} dosage, attains maximum at 8.99×10^{-3} M of Fe^{2+}, and finally tends to decrease.

In order to evaluate the optimum Fe^{2+} concentration for CPF, experiments were carried out with H_2O_2 dose of 5.71×10^{-1} M. The percentage reduction under various Fe^{2+} dosages is shown in Figure 6.42 (b). Based on these findings, the maximum reduction of CPF concentration and COD were observed as 89.34 and 74.44%, respectively at 10.8×10^{-3} M of Fe^{2+} dose.

In case of CF oxidation the H_2O_2 was kept constant at 6.53×10^{-1} M to observe the effect of Fe^{2+} dose. The percentage reductions under various Fe^{2+} dosages are shown in

Figure 6.42 (c). Maximum reduction in CF concentration and COD are 89.34 and 76.28%, respectively at 8.99×10^{-3} M of Fe^{2+}. Values of percentage reduction with Fe^{2+} concentrations are given in Table B-15.

The experiments indicated that percentage reduction increased with increase in Fe^{2+} dose upto a certain level and thereafter further increase in the dose of Fe^{2+} did not increase the reduction efficiency. This phenomenon can be attributed to the influence of Fe^{2+} on decomposition of H_2O_2. This decrease may be due to the detrimental effect of unnecessary catalyst dosages which decrease the quantity of hydroxyl radicals ($HO^{\bullet}$), as per the reactions 6.19 and 6.20:

$$Fe^{2+} + HO^{\bullet} \rightarrow Fe^{3+} + OH^{-} \quad (6.19)$$

$$Fe^{2+} + HO_2^{\bullet} \rightarrow Fe^{3+} + HO_2^{-} \quad (6.20)$$

Based on environmental concerns and economics, a higher dose of Fe^{2+} ions will form a higher quantity of Fe^{3+} sludge. To avoid the formation of sludge the dose of Fe^{2+} ions should be as minimal as possible (Rodrigues et al., 2009).

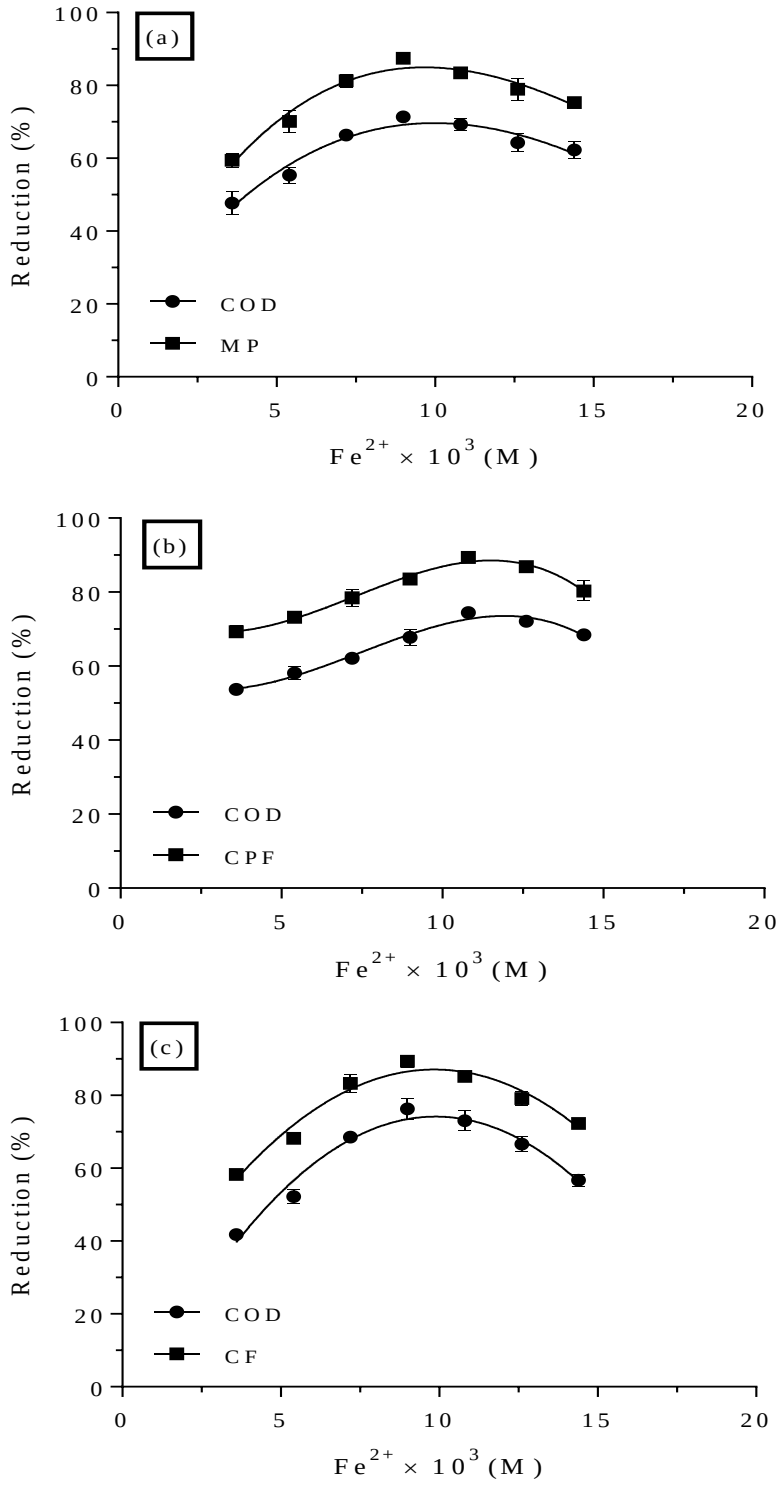

Figure 6.42: Influence of Fe^{2+} dosage on reduction efficiency. Experimental conditions: $Fe^{2+} = 3.60 \times 10^{-3}$ - 14.4×10^{-3} M, pH = 3, time = 60 min, temperature = 25 ºC. Initial concentration (a) MP = 11.4×10^{-5} M, $H_2O_2 = 6.53 \times 10^{-1}$ M, (b) CPF = 8.56×10^{-5} M, $H_2O_2 = 5.71 \times 10^{-1}$ M and (c) CF = 13.5×10^{-5} M, $H_2O_2 = 6.53 \times 10^{-1}$ M.

6.2.10 Effect of initial concentration on treatment of MP, CPF and CF

The effect of initial concentration of pesticides on percentage reduction was observed at pH 3, H_2O_2 concentration of 6.53×10^{-1} M and Fe^{2+} concentration of 8.99×10^{-3} M. Figure 6.43 (a) displays the percentage reduction of COD and degradation of MP as function of initial concentration. As seen from the figure, the initial concentration of MP has a significant effect on the degradation. As the MP concentration was increased from 3.80×10^{-5} to 15.2×10^{-5} M, the COD reduction and MP degradation decreased from 80.5 to 69.3% and 96.5 to 84%, respectively. Similarly the CPF and CF reduction also decreased from 97.67 to 89.18% and 94.13 to 82.26%, respectively on increasing the concentration (Figure 6.43 (b) and Figure 6.43 (c)). Related data are presented in Table B-16.

The increase in the pesticide concentration leads to increase in the number of organic molecules in the solution, on the other hand it does not enhance the amount of $^{\bullet}OH$ radicals. Therefore, the degradation of MP, CPF and CF exhibits with increasing MP, CPF and CF concentration (Tunc and Gurkana, 2012).

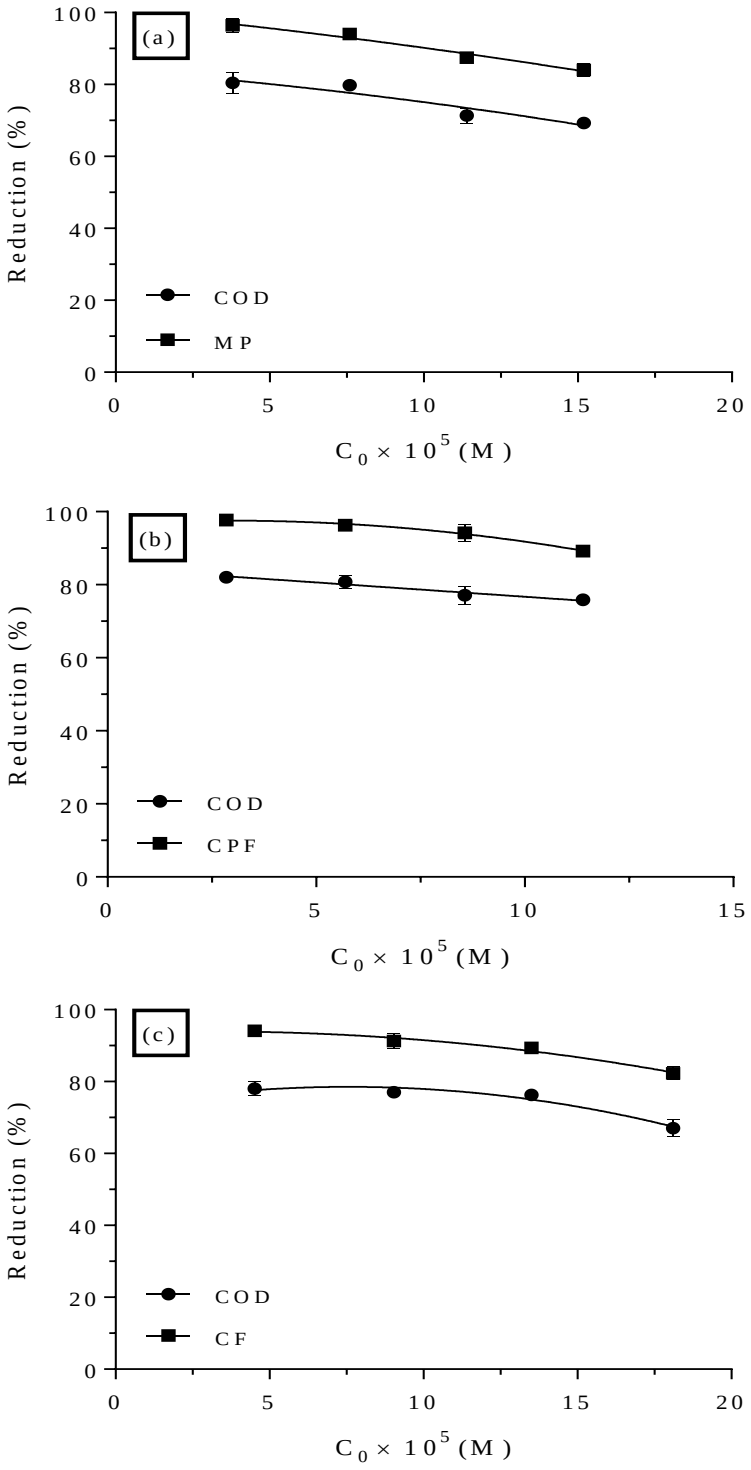

Figure 6.43: Influence of initial pesticide concentrations on reduction efficiency. Experimental conditions: pH = 3, time = 60 min, temperature = 25 ºC. Initial concentration (a) MP = 3.80×10^{-5} - 15.2×10^{-5} M, $H_2O_2 = 6.53 \times 10^{-1}$ M, $Fe^{2+} = 8.99 \times 10^{-3}$ M, (b) CPF = 2.85×10^{-5} - 11.4×10^{-5} M, $H_2O_2 = 5.71 \times 10^{-1}$ M, $Fe^{2+} = 10.8 \times 10^{-3}$ M and (c) CF = 4.52×10^{-5} - 18.1×10^{-5} M, $H_2O_2 = 6.53 \times 10^{-1}$ M, $Fe^{2+} = 8.99 \times 10^{-3}$ M.

6.2.11 Effect of temperature on treatment of MP, CPF and CF

Limited studies are available on the effect of temperature on pesticide removal. Therefore, experiments were performed by varying the temperature in the range of 25 to 45 ºC at pH 3, H_2O_2 concentration 6.53×10^{-1} M and Fe^{2+} concentration 8.99×10^{-3} M. After a reaction time of 60 min, the degradation of MP, CPF and CF increased from 60.13 to 94%, 79.18 to 96.34% and 57.35 to 92.32%, respectively, by changing the temperature 15 to 45 ºC, respectively.

It is observed from Figure 6.44 that the degradation efficiency increased with increasing reaction temperature. This is due to: (1) availability of more energy at higher temperatures for the reactant species to overcome the activation energy for reaction; resulting in faster degradation, and (2) enhanced rate of $^{\bullet}OH$ formation (Xu et al., 2014; Monsalvo et al., 2015). Data are given in Table B-17.

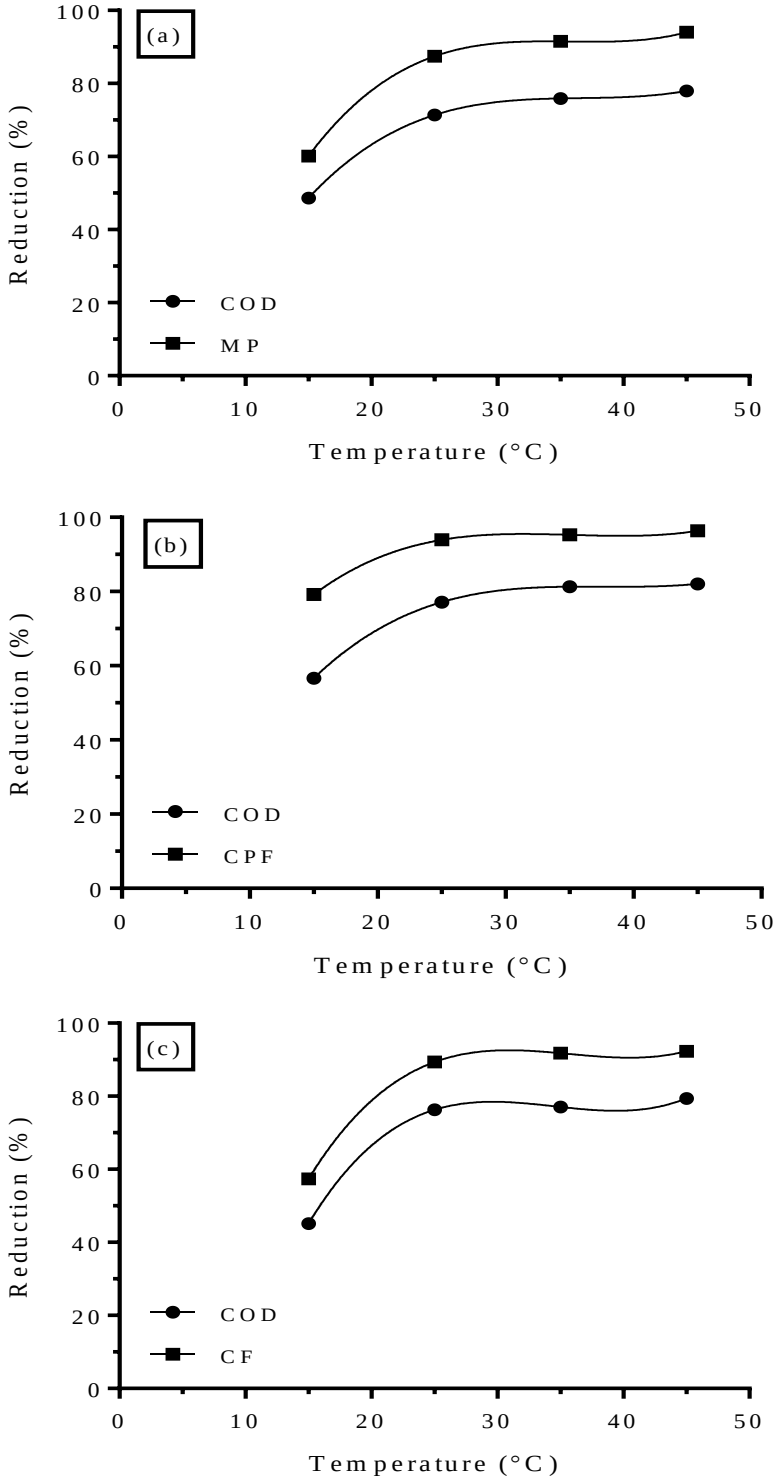

Figure 6.44: Influence of temperature on reduction efficiency. Experimental conditions: pH = 3, time = 60 min, temperature = 25 – 45 ºC. Initial concentration (a) MP = 11.4×10^{-5} M, $H_2O_2 = 6.53 \times 10^{-1}$ M, $Fe^{2+} = 8.99 \times 10^{-3}$ M, (b) CPF = 8.56×10^{-5} M, $H_2O_2 = 5.71 \times 10^{-1}$ M, $Fe^{2+} = 10.8 \times 10^{-3}$ M and (c) CF = 13.5×10^{-5} M, $H_2O_2 = 6.53 \times 10^{-1}$ M, $Fe^{2+} = 8.99 \times 10^{-3}$ M.

6.2.12 Degradation kinetics of MP, CPF and CF

The kinetic parameters of different models and their correlation coefficients (R^2) for the degradation of MP, CPF and CF at different operating conditions were estimated by applying of linear regression analysis using first-order, second-order and Behnajady-Modirshahla-Ghanbery rate model. Plots are shown in Figures 6.45 through 6.47. The calculated reaction parameters are given in Tables B-18 to B-20. It has been observed that the second-order kinetic model gives a better fit compared to the first-order model.

The Behnajady–Modirshahla–Ghanbery model has a higher correlation coefficient compared to the first and second-order models. The correlation coefficients as reported in the tables indicate that the MP, CPF and CF decay kinetics is well described by the Behnajady–Modirshahla–Ghanbery model at different operating conditions using Fenton oxidation. The values of constants 1/m and 1/b indicate the initial degradation rate of MP, CPF and CF and the theoretical maximum degradation fraction (Tunc and Gurkana 2012). These constants can be correlated with various operating parameters such as pH, H_2O_2 concentration, Fe^{2+} concentration, MP, CPF and CF concentration and temperature. The high 1/m value shows the faster decay rate of MP, CPF and CF (Behnajady et al., 2007).

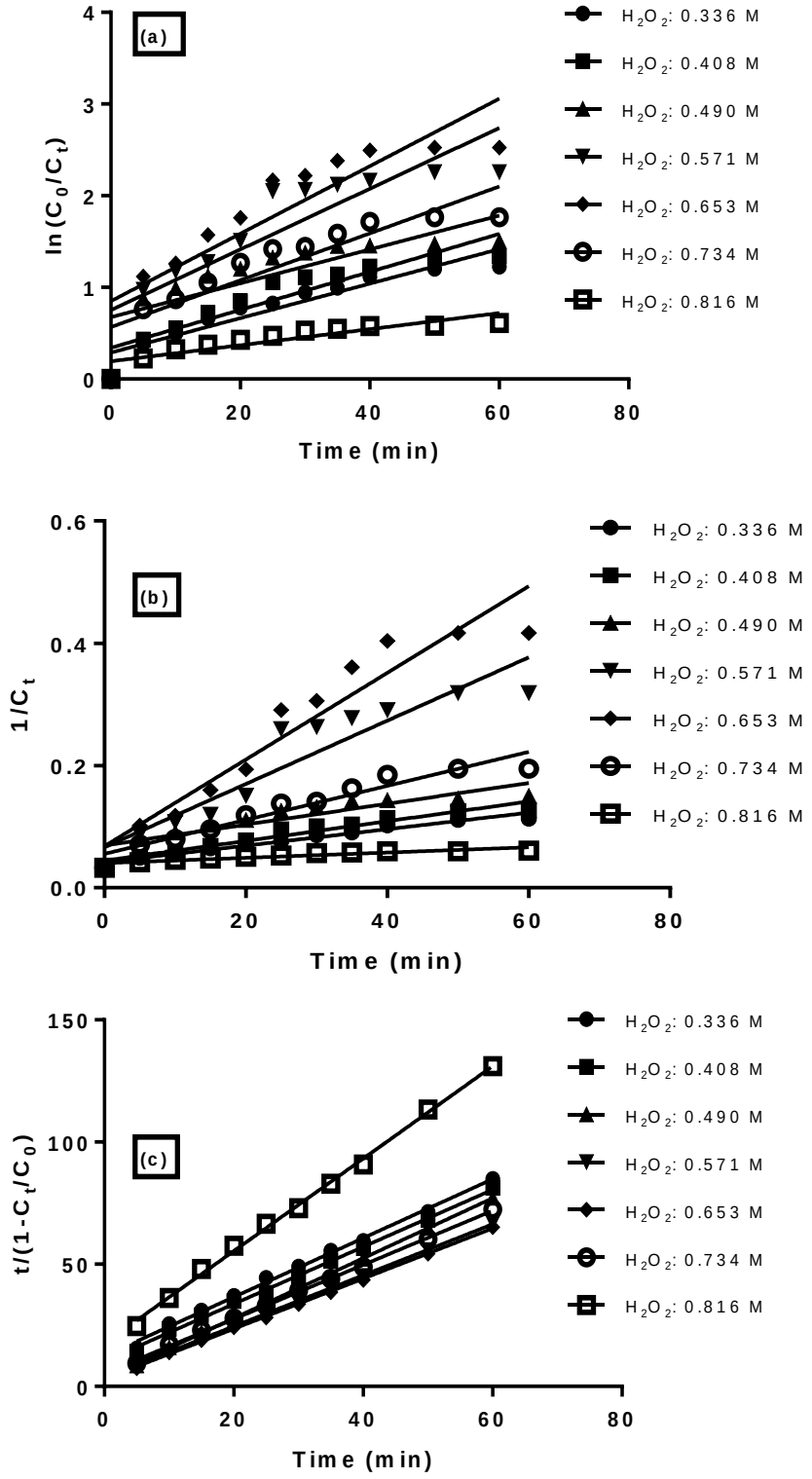

Figure 6.45: (a) First order kinetics, (b) second order kinetics and (c) B-M-G kinetics for MP degradation by Fenton oxidation. (Initial MP concentration = 11.4×10^{-5} M, Fe^{2+} = 8.99×10^{-3} M, H_2O_2 = 3.36 – 8.16×10^{-1} M , pH = 3, time = 0 − 60 min, temperature = 25 ºC).

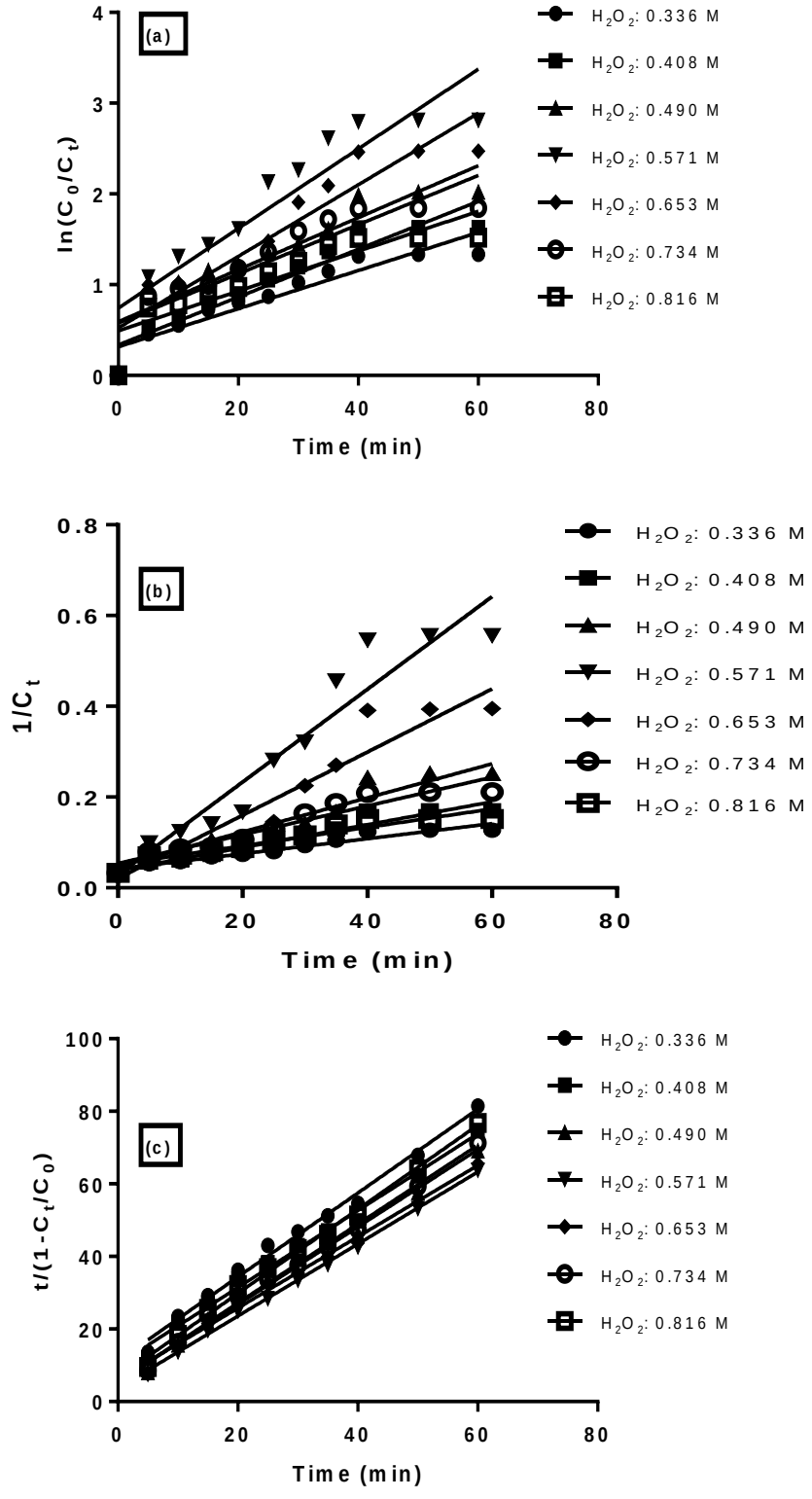

Figure 6.46: (a) First order kinetics, (b) second order kinetics and (c) B-M-G kinetics for CPF degradation by Fenton oxidation. (Initial CPF concentration = 8.65×10^{-5} M, Fe^{2+} = 8.99×10^{-3} M, H_2O_2 = 3.36 – 8.16×10^{-1} M , pH = 3, time = 0 − 60 min, temperature = 25 ºC).

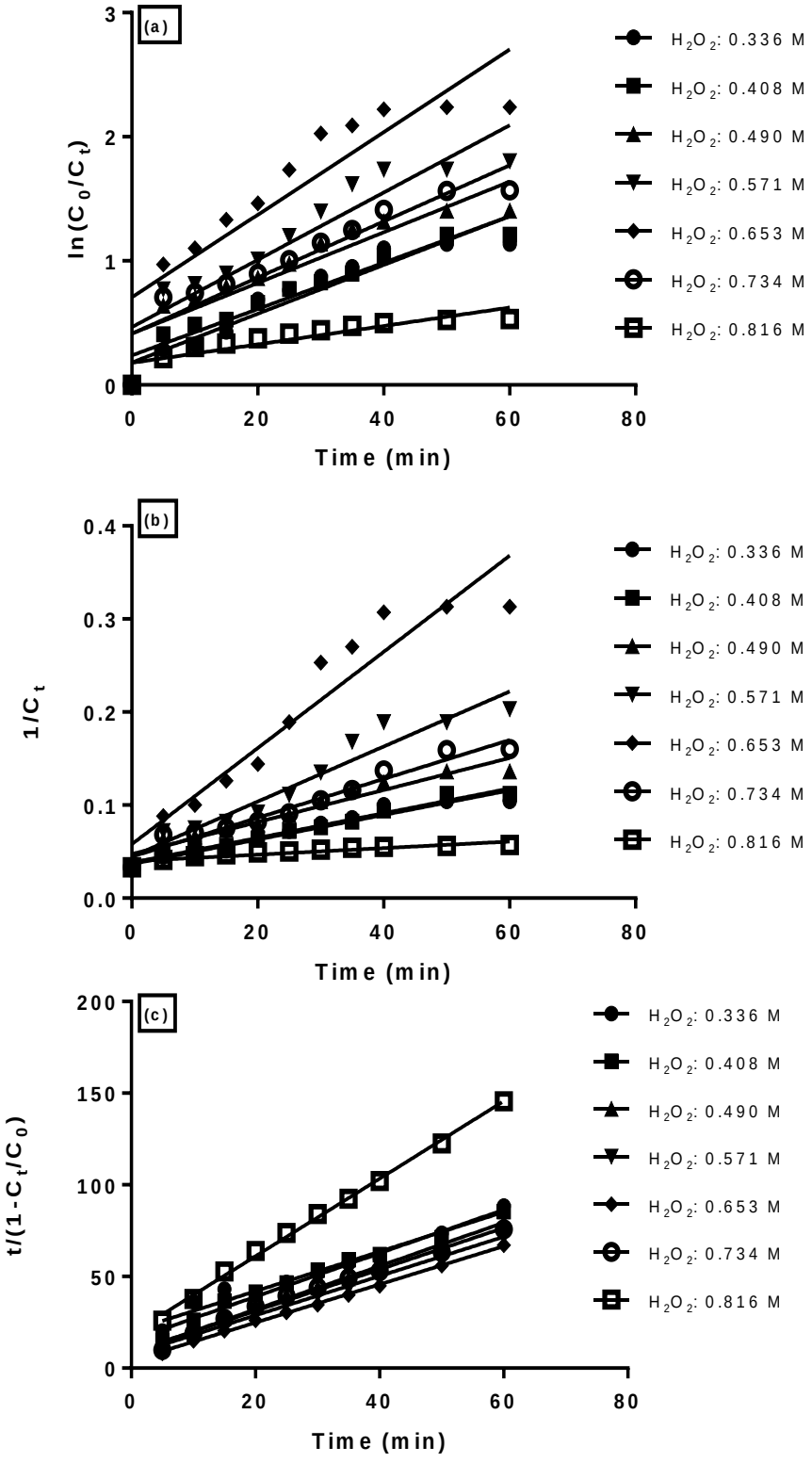

Figure 6.47: (a) First order kinetics, (b) second order kinetics and (c) B-M-G kinetics for CF degradation by Fenton oxidation. (Initial CF concentration = 13.5×10^{-5} M, Fe^{2+} = 8.99×10^{-3} M, H_2O_2 = 3.36 – 8.16×10^{-1} M, pH = 3, time = 0 − 60 min, temperature = 25 ºC).

6.3 Coupled Fenton and Coagulation Process

The aim of this study has been to remove pesticide contaminants from simulated wastewater up to a concentration level having the lowest or no toxicity to the living beings. The residual concentration of MP, CPF and CF in the solution after either coagulation alone or Fenton process alone does not come in the range of permissible limit, set by various regulatory organisations. Therefore, experiments using coupled Fenton and coagulation process were performed to achieve the permissible limit of these pesticides in the treated solution.

Experiments were conducted in series, Fenton oxidation followed by coagulation under the respective optimum conditions. The maximum COD reduction obtained was 96.36, 96.42 and 96.27% for MP, CPF, and CF, respectively. The corresponding residual concentrations were 0.009, 0.003 and 0.066 mg/L for MP, CPF and CF, respectively (Figure 6.48). The residual concentration values are well within the range of maximum acceptable concentration (MAC), thus coupled Fenton and coagulation process can be successfully applied for the treatment of pesticide bearing wastewater.

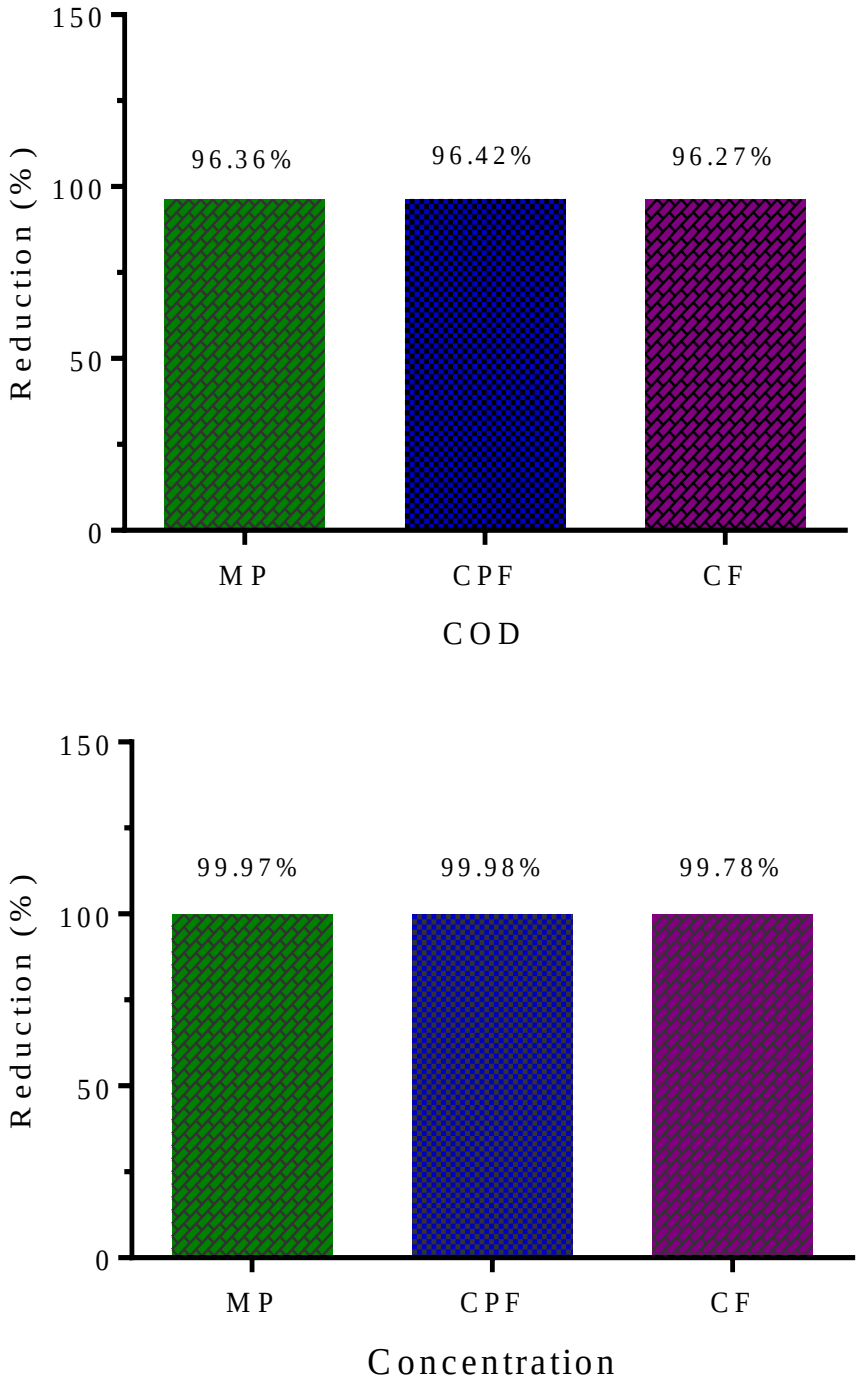

Figure 6.48: Effect on MP, CPF, and CF reduction using coupled coagulation and Fenton process.

6.4 Toxicity Analysis of Pre- and Post- Fenton Oxidation

6.4.1 Improved proliferation of U-87 cells following Fenton oxidation

Each tissue and organ in the body are composed of vast populations of cells, total $>10^{14}$ cells. An astonishing 10^{12} cells die in the normal course of each day and must be replaced to sustain life. The process by which cells grow and divide to replenish (refill) the lost cells is termed as ***cell proliferation***. The term ***cytotoxicity*** is the characteristic of being toxic to cells or any agent or process that kills cells.

In this study effect of several concentrations (1-16 µM) of MP, CPF and CF and their corresponding Fenton oxidation derivatives against U-87 cells were tested. MP, CPF and CF individually restricted the proliferation of U-87 cells in a concentration dependent manner (Figure 6.49A). In contrast, Fenton oxidation of the above compounds significantly reversed the growth inhibition of U-87 cells (Figure 6.49A). Similar results were also observed for percent cytotoxicity of the U-87 cells (Figure 6.49B). Fenton oxidation of MP, CPF and CF significantly improved the percent proliferation of U-87 cells at all the concentrations tested. The above results demonstrate that the Fenton oxidation improves the proliferation suggesting that it enhances the tolerance index of the above compounds.

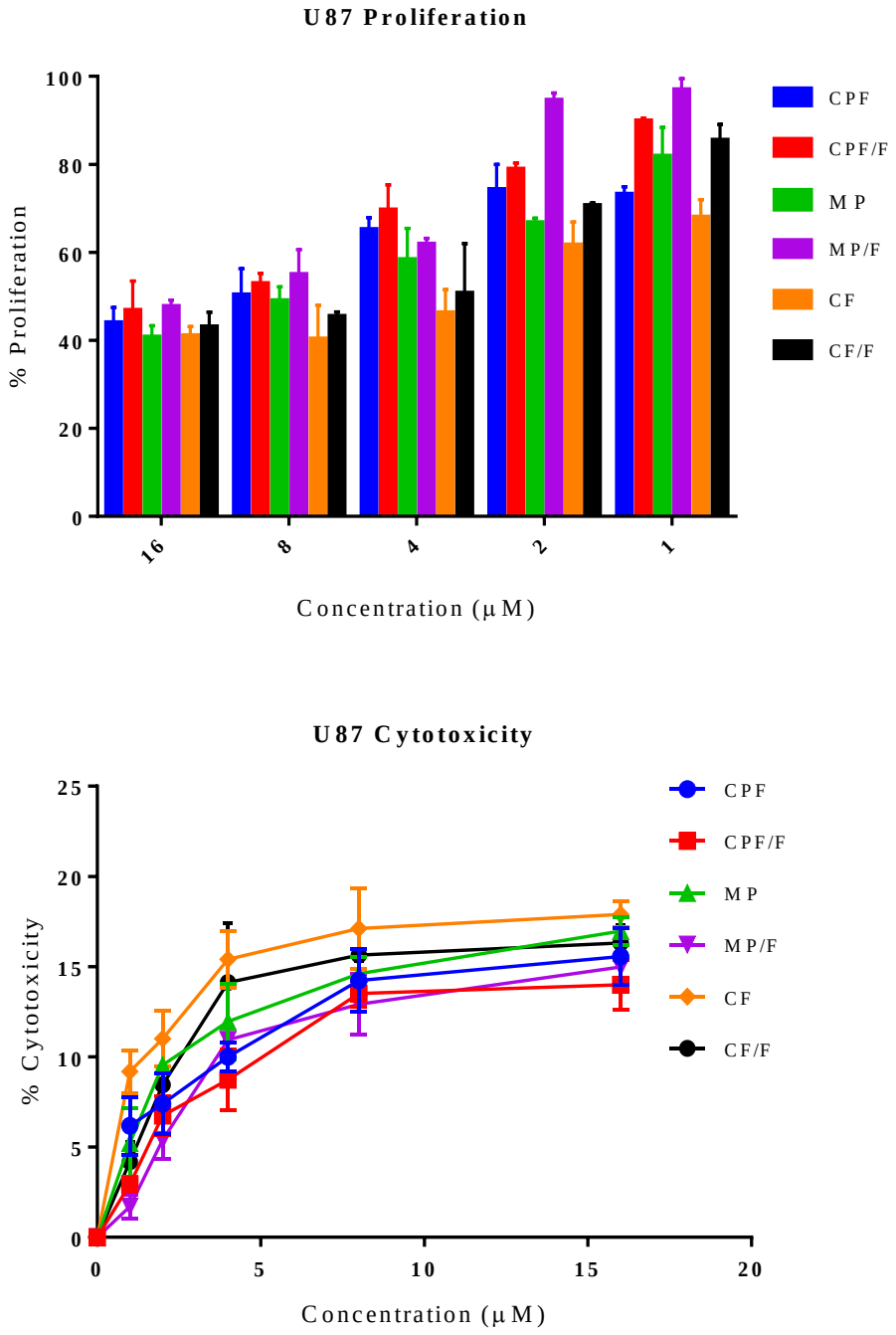

Figure 6.49: Effect of Fenton oxidation on proliferation and cytotoxicity of U-87 cells. (A) U-87 cells (5×10^3) were plated in 96 well tissue culture plate and allowed to become confluent. The cells were treated with increasing concentrations of MP, CPF and CF and their Fenton oxidation derivatives and were incubated for 48 h at 37 °C in 5% CO_2. Data has been presented as % proliferation of cells as described in materials and methods. (B) Direct cytotoxicity of the above compounds against the U-87 cells was determined as described in materials and methods. Mean ± SD triplicate determination. n=3.

6.4.2 Tolerance DC and Lymphocytes

Cell viability is the determination of living cells, based on a total cell sample. Human DC and PBMC (lymphocytes) tolerate the Fenton oxidation derivatives of MP, CPF and CF significantly well compared to the parent compounds themselves (Figure 6.50A). Thus, compared to influet MP, CPF and CF, their Fenton oxidation derivatives are relatively less toxic to the human DC and lymphocytes (Figure 6.50A). The comparative analysis suggests that viability of DC is relatively unaffected by the compounds even at the highest concentration with or without Fenton oxidation (Figure 6.50A). Lymphocytes on the other hand suffered a moderate loss in viability at the highest concentration (10 µM). However, at lower concentration the lymphocytes tolerate better with little or no significant loss in the cell viability (Figure 6.50B).

6.4.3 Toxicity to RBC

Hemolysis is the rupturing (lysis) of red blood cells (erythrocytes) and the release of their contents (hemoglobin) into the surrounding fluid (i.e. blood plasma). The Fenton oxidation of MP, CPF and CF improved the survival of RBC by preventing hemolysis (Figure 6.51 A). At higher concentrations CF is relatively more toxic to RBC compared to other two compounds tested (Figure 6.51A). Treatment of RBC at a fixed concentration of the compounds with or without the Fenton oxidation demonstrates the prevention of hemolysis following Fenton oxidation. Hemolysis of RBC were also performed at a fixed concentration (5 µM) of the compounds and found significant reduction in hemolysis (Figure 6.51A).

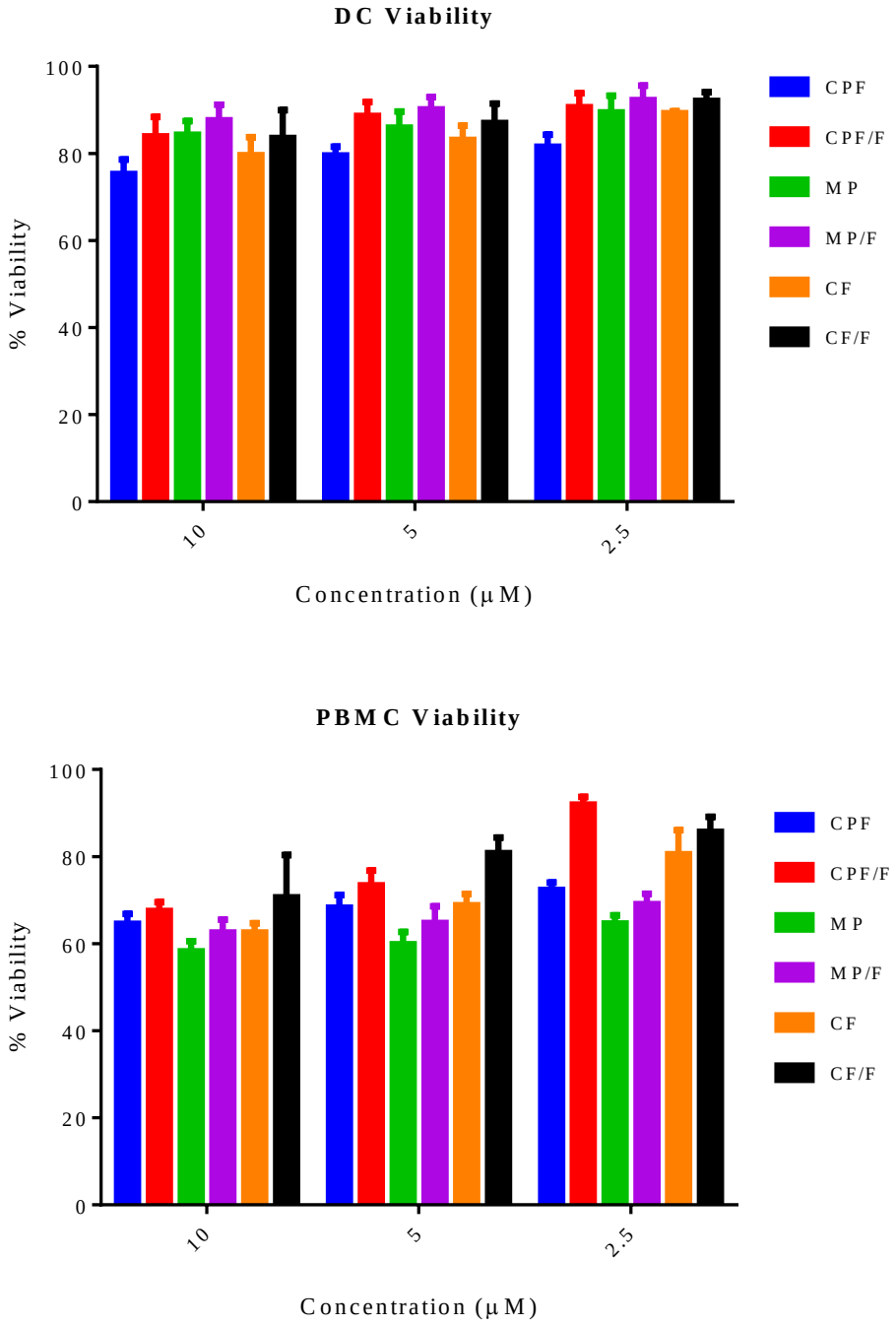

Figure 6.50: Effect of Fenton oxidation on viability of monocytes and lymphocytes. Viability of DC (A) and PBMC (B) in the presence of MP, CPF and CF and their Fenton oxidation derivatives. Mean ± SD with triplicate determination. n=3.

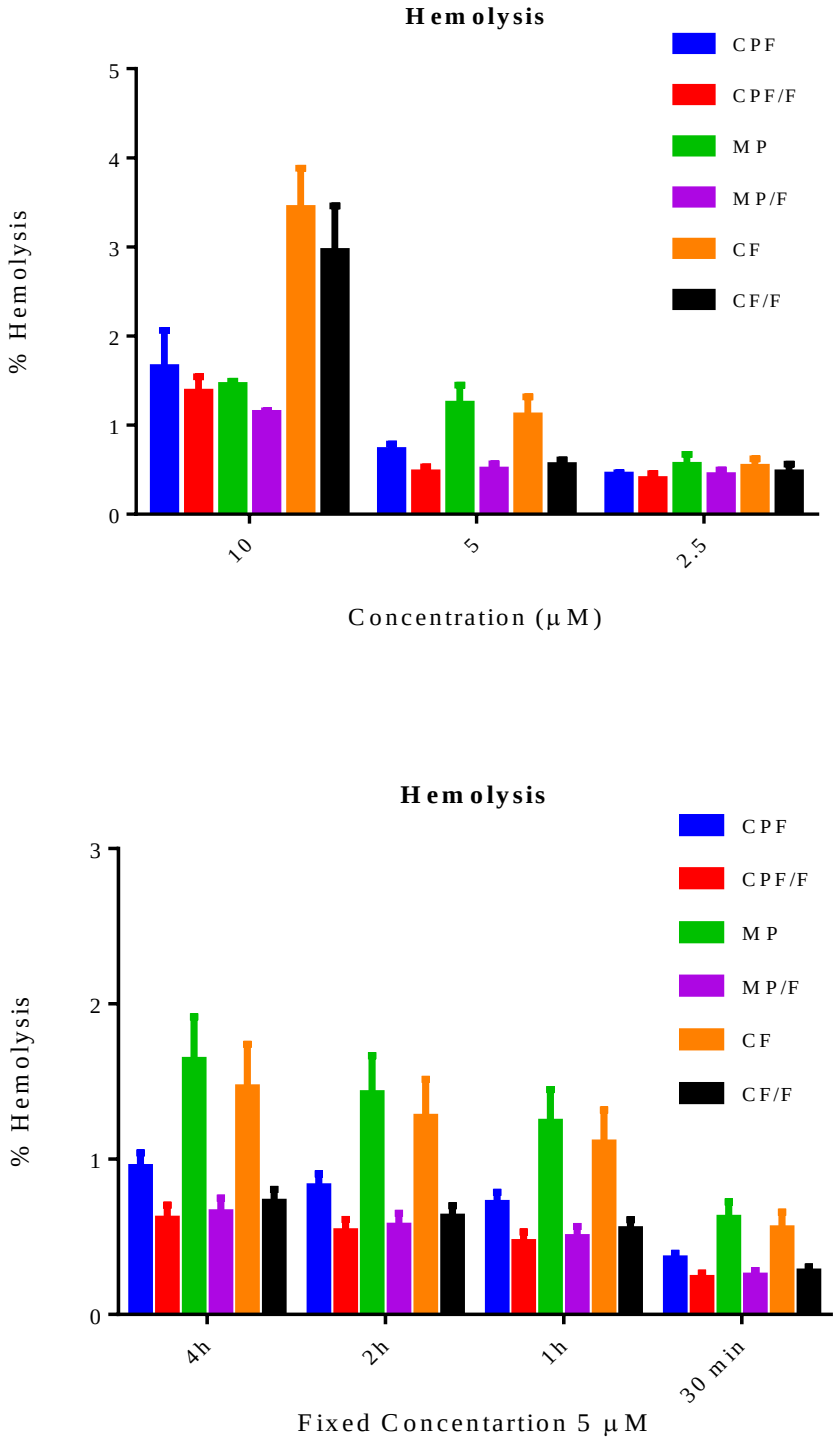

Figure 6.51: Hemolysis study. Concentration (A) and time dependent (fixed concentration) (B) hemolysis of RBC were performed in presence of carbofuran, methyl parathion and chlorpyrifos and their Fenton oxidation derivatives. Data presented as Mean ± SD with triplicate determination, n=3.